

ISSN: 2220-9506 (Print)
ISSN: 2414-0473 (Online)

ПРИБОРЫ И МЕТОДЫ ИЗМЕРЕНИЙ

DEVICES AND METHODS
OF MEASUREMENTS

Том 11

№ 3

Vol. 11

100 ЛЕТ



ХРАНИМ ТРАДИЦИИ, ЖИВЕМ НАСТОЯЩИМ, СОЗДАЕМ БУДУЩЕЕ!

2020

ПРИБОРЫ И МЕТОДЫ ИЗМЕРЕНИЙ

Научно-технический журнал

Основан в 2010 г.

Учредитель

Белорусский национальный технический университет

Выходит 4 раза в год

Журнал включен в базы данных:
Web of Science Core Collection (ESCI),
EBSCO, DOAJ, WorldCat, OpenAIRE, Google Scholar, РИНЦ,
ЭБС «Лань», НЭБ «КиберЛенинка», Соционет

Том 11

№ 3

2020

ГЛАВНЫЙ РЕДАКТОР

Гусев О.К., д.т.н., профессор, проректор Белорусского национального технического университета
(г. Минск, Беларусь)

ЗАМЕСТИТЕЛЬ ГЛАВНОГО РЕДАКТОРА

Маляревич А.М., член-корреспондент НАН Беларуси, д.ф.-м.н., профессор, проректор Белорусского национального технического университета (г. Минск, Беларусь)

РЕДАКЦИОННАЯ КОЛЛЕГИЯ

Алексеев В.А., д.т.н., профессор, ученый секретарь Ижевского государственного технического университета имени М.Т. Калашникова (г. Ижевск, Россия)

Анищик В.М., д.ф.-м.н., профессор, профессор кафедры физики твёрдого тела Белорусского государственного университета (г. Минск, Беларусь)

Бубулис А., д.т.н., профессор, главный научный сотрудник Научного центра мехатроники Каунасского технологического университета (г. Каунас, Литва)

Вайн А.А., д.т.н., профессор Тартуского университета (г. Тарту, Эстония)

Виба Я., д.т.н., профессор, директор Института механики Рижского технического университета (г. Рига, Латвия)

Гуттен М., д.т.н., заведующий кафедрой метрологии и прикладной электротехники Жилинского университета (г. Жилина, Словакия)

Дмитриев С.М., д.т.н., профессор, ректор Нижегородского государственного технического университета имени Р.Е. Алексеева (г. Нижний Новгород, Россия)

Дэнилак С., профессор Производственно-исследовательского центра Технологического института штата Джорджия (г. Атланта, США)

Жарин А.Л., д.т.н., профессор, профессор кафедры «Информационно-измерительная техника и технологии» Белорусского национального технического университета (г. Минск, Беларусь)

Жуковский П., д.т.н., профессор, заведующий кафедрой электрических аппаратов и техники высоких напряжений Люблинского технического университета (г. Люблин, Польша)

Колтунович Т.Н., д.т.н., профессор, Люблинский технический университет (г. Люблин, Польша)

Комаров Ф.Ф., член-корреспондент НАН Беларуси, д.ф.-м.н., профессор, заведующий лабораторией элионики Института прикладных физических проблем имени А.Н. Севченко Белорусского государственного университета (г. Минск, Беларусь)

- Кулешов Н.В.**, д.ф.-м.н., профессор, заведующий кафедрой «Лазерная техника и технология» Белорусского национального технического университета (г. Минск, Беларусь)
- Кучинский П.В.**, д.ф.-м.н., доцент, директор Института прикладных физических проблем имени А.Н. Севченко Белорусского государственного университета (г. Минск, Беларусь)
- Кэмп А.**, профессор Института фотоники Страсклайдского университета (г. Глазго, Великобритания)
- Матеос Х.**, к.ф.-м.н., доцент, университет Ровира и Вирхилий (г. Таррагона, Испания)
- Пилипенко В.А.**, член-корреспондент НАН Беларуси, д.т.н., профессор, заместитель директора ГЦ «Белмикроанализ» НТЦ «Белмикросистемы» ОАО «ИНТЕГРАЛ» – управляющая компания холдинга «ИНТЕГРАЛ» (г. Минск, Беларусь)
- Плескачевский Ю.М.**, член-корреспондент НАН Беларуси, д.т.н., профессор, заведующий кафедрой «Микро- и нанотехника» Белорусского национального технического университета (г. Минск, Беларусь)
- Погребняк А.Д.**, д.ф.-м.н., профессор, заведующий кафедрой нанoeлектроники Сумского государственного университета (г. Сумы, Украина)
- Распопов В.Я.**, д.т.н., профессор, заведующий кафедрой «Приборы управления» Тульского государственного университета (г. Тула, Россия)
- Тимчик Г.С.**, д.т.н., профессор, декан приборостроительного факультета, Национальный технический университет Украины «Киевский политехнический институт имени Игоря Сикорского» (г. Киев, Украина)
- Це Ли**, заместитель директора Северо-Восточного НИИ техники датчиков (г. Харбин, КНР)
- Чижик С.А.**, академик НАН Беларуси, д.т.н., профессор, Первый заместитель Председателя Президиума НАН Беларуси (г. Минск, Беларусь)
- Шкадаревич А.П.**, академик НАН Беларуси, д.ф.-м.н., профессор, директор НТЦ «ЛЭМТ» Белорусского оптико-механического объединения (г. Минск, Беларусь)
- Юмашев К.В.**, д.ф.-м.н., профессор, заведующий кафедрой «Экспериментальная и теоретическая физика» Белорусского национального технического университета (г. Минск, Беларусь)

**Издание зарегистрировано в Министерстве информации Республики Беларусь 25 июня 2010 г.
Регистрационный номер 1372**

В соответствии с решением ВАК от 8 июля 2011 г. №13/1 журнал включен в Перечень научных изданий для опубликования результатов диссертационных исследований; научное направление: «Средства и методы измерений, контроля, диагностики и оценки качества объектов и процессов» (технические и физико-математические науки)

ISSN 2220-9506

Подписка осуществляется через почтовые отделения связи по «Каталогу газет и журналов Республики Беларусь».

Подписные индексы – 74835; 748352.

Ответственный секретарь редакции: Шахлевич Л.Н.

Редактор: Чабарова О.Л.

Набор и верстка выполнены в редакции журнала «Приборы и методы измерений».

Подписано в печать 15.09.2020. Формат бумаги 60×84 1/8. Бумага мелованная.

Гарнитура Times New Roman. Печать цифровая. Усл. печ. л. 10,70. Уч.-изд. л. 4,18. Тираж 120 экз.

Дата выхода в свет 23.09.2020. Заказ № 569.

Отпечатано в Белорусском национальном техническом университете. ЛП № 02330/74 от 03.03.2014. Пр. Независимости, 65, 220013, г. Минск

АДРЕС РЕДАКЦИИ:

Белорусский национальный технический университет
пр. Независимости, 65, 220013, г. Минск, Республика Беларусь,
тел.: +375 (17) 293 96 67, факс: +375 (17) 292 67 94
e-mail: pimi@bntu.by
<http://pimi.bntu.by>

DEVICES AND METHODS OF MEASUREMENTS

Scientific and Engineering Journal

Founded in 2010

Founder
Belarusian National Technical University

Issued four times a year

The Journal is included in the following databases:
Web of Science Core Collection (ESCI),
EBSCO, DOAJ, WorldCat, OpenAIRE, Google Scholar,
RISC, Lan, CyberLeninka, Socionet

Volume 11

№ 3

2020

EDITOR-IN-CHIEF

Oleg K. Gusev, *Doctor of Science (Engineering), Professor, Vice-Rector of Belarusian National Technical University (Minsk, Belarus)*

DEPUTY EDITOR-IN-CHIEF

Aliaksandr M. Malyarevich, *Corresponding Member of the National Academy of Sciences of Belarus, Doctor of Science (Physics and Mathematics), Professor, Vice-Rector of Belarusian National Technical University (Minsk, Belarus)*

EDITORIAL BOARD

Vladimir A. Alekseev, *Doctor of Science (Engineering), Professor, Scientific Secretary of M.T. Kalashnikov Izhevsk State Technical University (Izhevsk, Russia)*

Victor M. Anishchik, *Doctor of Science (Physics and Mathematics), Professor, Department of Solid State Physics, Belarusian State University (Minsk, Belarus)*

Algimantas Bubulis, *Doctor of Science (Engineering), Professor, Kaunas University of Technology (Kaunas, Lithuania)*

Arvid A. Vain, *Doctor of Science (Engineering), Professor, University of Tartu (Tartu, Estonia)*

Janis Viba, *Doctor of Science (Engineering), Professor, Director of Institute of Mechanics, Riga Technical University (Riga, Latvia)*

Miroslav Gutten, *Doctor of Science (Engineering), Head of Department of Metrology and Applied Electrical Engineering, University of Žilina (Žilina, Slovakia)*

Sergei M. Dmitriev, *Doctor of Science (Engineering), Professor, Rector of R.E. Alekseev Nizhny Novgorod State Technical University (Nizhny Novgorod, Russia)*

Steven Danyluk, *PhD, Professor, Production and Research Center, Georgia Institute of Technology (Atlanta, USA)*

Anatoly L. Zharin, *Doctor of Science (Engineering), Professor, Information and Measuring Technologies Department, Belarusian National Technical University (Minsk, Belarus)*

Pawel Żukowski, *Doctor of Science (Engineering), Professor, Head of Department of Electrical Devices and High Voltages Technology, Lublin University of Technology (Lublin, Poland)*

Tomasz N. Koltunowicz, *Doctor of Science (Engineering), Professor, Lublin University of Technology (Lublin, Poland)*

Fadey F. Komarov, *Corresponding Member of the National Academy of Sciences of Belarus, Doctor of Science (Physics and Mathematics), Professor, Head of the Elionics Laboratory, A.N. Sevchenko Institute of Applied Physical Problems, Belarusian State University (Minsk, Belarus)*

Nikolay V. Kuleshov, Doctor of Science (Physics and Mathematics), Professor, Head of Laser Equipment and Technology Department, Belarusian National Technical University (Minsk, Belarus)

Petr V. Kuchynski, Doctor of Science (Physics and Mathematics), Director of A.N. Sevchenko Institute of Applied Physical Problems, Belarusian State University (Minsk, Belarus)

Alan Kemp, PhD, Professor, Institute of Photonics, University of Strathclyde (Glasgow, United Kingdom)

Xavier Mateos, PhD, Associate Professor, Rovira i Virgili University (Tarragona, Spain)

Vladimir A. Pilipenko, Corresponding Member of the National Academy of Sciences of Belarus, Doctor of Science (Engineering), Professor, Deputy Director of the State Center «Belmicroanalysis», Branch of the Scientific-Technical Center «Belmicrosystems» of JSC «INTEGRAL» – «INTEGRAL» Holding Managing Company (Minsk, Belarus)

Yuriy M. Pleskachevsky, Corresponding Member of the National Academy of Sciences of Belarus, Doctor of Science (Engineering), Professor, Head of Micro- and Nanotechnics Department, Belarusian National Technical University (Minsk, Belarus)

Alexander D. Pogrebnyak, Doctor of Science (Physics and Mathematics), Professor, Head of Department of Nanoelectronic, Sumy State University (Sumy, Ukraine)

Vladimir Ya. Raspopov, Doctor of Science (Engineering), Professor, Head of Control Devices Department, Tula State University (Tula, Russia)

Gryhoriy S. Tymchyk, Doctor of Science (Engineering), Professor, Dean of the Faculty of Instrumentation Engineering, National Technical University of Ukraine «Igor Sikorsky Kyiv Polytechnic Institute» (Kyiv, Ukraine)

Tse Li, Deputy Director of Northeast Scientific Research Institute of Sensor Technology (Harbin, China)

Sergei A. Chizhik, Academician of National Academy of Sciences of Belarus, Professor, Doctor of Science (Engineering), the First Vice Chairman of the Presidium of the National Academy of Sciences of Belarus (Minsk, Belarus)

Alexey P. Shkadarevich, Academician of the National Academy of Sciences of Belarus, Doctor of Science (Physics and Mathematics), Professor, Director of the Scientific and Technical Center «LEMT» of the BelOMO (Minsk, Belarus)

Konstantin V. Yumashev, Doctor of Science (Physics and Mathematics), Professor, Head of Experimental and Theoretical Physics Department, Belarusian National Technical University (Minsk, Belarus)

ADDRESS:

Belarusian National Technical University
Nezavisimosty Ave., 65, Minsk 220013, Belarus
Tel.: +375 (17) 293 96 67, fax: +375 (17) 292 67 94
e-mail: pimi@bntu.by
<http://pimi.bntu.by>

СОДЕРЖАНИЕ

Средства измерений

P. Okal

Measuring Setup for Investigation and Visualization of the Percolation Phenomenon in Non-Ordered Models of Metal-Dielectric Nanocomposites 171

Alexander Rudenkov, Viktor Kisel, Anatol Yasukevich, Karine Hovhannesyanyan, Ashot Petrosyan, Nikolai Kuleshov

High Power SESAM Mode-Locked Laser Based on Yb³⁺:YAIO₃ Bulk Crystal 179

P. Rogalski

Measurement Stand, Method and Results of Composite Electrotechnical Pressboard-Mineral Oil Electrical Measurements..... 187

Методы измерений, контроля, диагностики

I.A. Konovalov, A.E. Khrobostov, M.A. Legchanov, D.N. Solncev, A.A. Barinov, A.V. Ryazanov, A.A. Chesnokov, M.A. Makarov

Application of the Correlation Velocity Measurements for Hydrodynamic Investigations of Turbulent Coolant Flow in Nuclear Reactor Elements..... 196

T. Reader, V.A. Tenenev, A.A. Chernova

Determination of Flow Characteristics in Technological Processes with Controlled Pressure..... 204

A.V. Skazochkin, G.G. Bondarenko, P. Żukowski

Features of Measuring the Hardness of a Metal Surface Modified with Ultrafine Particles of Minerals..... 212

D.P. Ilyaschenko, A.V. Kryukov, E.V. Lavrova, M.A. Kuznetsov, E.V. Verkhoturouva

Determination of Parameters of Electrode Metal Transported Drops by Simulation and Visualization..... 222

V.N. Nesterov, A.R. Li

Application of Two-Channel Principle in Measuring Devices to Compensate for Disturbing Influences of Unknown Physical Nature..... 228

S.G. Sandomirski

Analysis of Requirements and the Feasible Limit for Error Reduction in Two-Parameter Magnetic Determination of Steels' Hardness 236

A.И. Куцак

Контраст изображения объекта, наблюдаемого в условиях задымления, при поляризационной фильтрации излучения, рассеянного частицами дыма..... 245

CONTENTS

Measuring Instruments

P. Okal

Measuring Setup for Investigation and Visualization of the Percolation Phenomenon in Non-Ordered Models of Metal-Dielectric Nanocomposites	171
---	------------

Alexander Rudenkov, Viktor Kisel, Anatol Yasukevich, Karine Hovhannesian, Ashot Petrosyan, Nikolai Kuleshov

High Power SESAM Mode-Locked Laser Based on Yb³⁺:YAIO₃ Bulk Crystal	179
--	------------

P. Rogalski

Measurement Stand, Method and Results of Composite Electrotechnical Pressboard-Mineral Oil Electrical Measurements.....	187
--	------------

Methods of Measurements, Monitoring, Diagnostics

I.A. Konovalov, A.E. Khrobostov, M.A. Legchanov, D.N. Solncev, A.A. Barinov, A.V. Ryazanov, A.A. Chesnokov, M.A. Makarov

Application of the Correlation Velocity Measurements for Hydrodynamic Investigations of Turbulent Coolant Flow in Nuclear Reactor Elements.....	196
--	------------

T. Reader, V.A. Tenenev, A.A. Chernova

Determination of Flow Characteristics in Technological Processes with Controlled Pressure.....	204
---	------------

A.V. Skazochkin, G.G. Bondarenko, P. Żukowski

Features of Measuring the Hardness of a Metal Surface Modified with Ultrafine Particles of Minerals.....	212
---	------------

D.P. Ilyaschenko, A.V. Kryukov, E.V. Lavrova, M.A. Kuznetsov, E.V. Verkhoturova

Determination of Parameters of Electrode Metal Transported Drops by Simulation and Visualization.....	222
--	------------

V.N. Nesterov, A.R. Li

Application of Two-Channel Principle in Measuring Devices to Compensate for Disturbing Influences of Unknown Physical Nature.....	228
--	------------

S.G. Sandomirski

Analysis of Requirements and the Feasible Limit for Error Reduction in Two-Parameter Magnetic Determination of Steels' Hardness	236
--	------------

A.I. Kitsak

Contrast of Image of an Object Observed in Smoke Conditions using Polarizing Filtering of Radiation Scattered by Smoke Particles.....	245
--	------------

Measuring Setup for Investigation and Visualization of the Percolation Phenomenon in Non-Ordered Models of Metal-Dielectric Nanocomposites

P. Okal

Lublin University of Technology,
Nadbystrzycka str., 38A, Lublin 20-618, Poland

Received 05.06.2020

Accepted for publication 27.08.2020

Abstract

The study uses the phenomenon of high voltage partial discharge to investigate the phenomenon of percolation and visualisation of the percolation channel. The phenomenon of partial discharges is very similar to the quantum tunneling phenomenon observed in metal-dielectric nanocomposites. In both cases the flow of alternating current occurs in the absence of direct contact between the metallic phase particles.

A measuring stand was developed and constructed to test models of metal dielectric nanocomposites using high voltage partial discharge. The stand consists of a 110 kV high voltage transformer, a voltage regulator protecting the constant rate of high voltage rise, a measuring system consisting of a measuring probe, voltmeters and a computer. The communication between the measuring probe and the voltmeter was made in digital technology with the use of fiber optic technology, which allowed the meter to communicate with the computer without any errors and eliminated the interference caused by a strong electromagnetic field resulting from the use of high voltage.

Systems modelling metal-dielectric composites were built, consisting of metallic elements in the form of disks, randomly distributed on the surface of the dielectric matrix. The number of disks was increased in series of 40 in each. The maximum number of disks was 1520. The dependence was determined of one of the important parameters characterising an partial discharge, i. e. the initial voltage, at which an electric current starts to flow between electrodes, on the concentration of the metallic phase. On the basis of these results, a percolation threshold was established for a matrix with a random distribution of metallic phase elements, the value of which is about 50 %. Films and pictures of partial discharges with visible percolation channels were taken with the camera with which the stand was equipped.

Keywords: percolation, nanocomposites, partial discharge, high voltage.

DOI: 10.21122/2220-9506-2020-11-3-171-178

Адрес для переписки:

P. Okal
Lublin University of Technology,
Nadbystrzycka str., 38A, Lublin 20-618, Poland
e-mail: p.okal@pollub.pl

Address for correspondence:

P. Okal
Lublin University of Technology,
Nadbystrzycka str., 38A, Lublin 20-618, Poland
e-mail: p.okal@pollub.pl

Для цитирования:

P. Okal.
Measuring Setup for Investigation and Visualization of the Percolation Phenomenon in Non-Ordered Models of Metal-Dielectric Nanocomposites.
Приборы и методы измерений.
2020. – Т. 11, № 3. – С. 171–178.
DOI: 10.21122/2220-9506-2020-11-3-171-178

For citation:

P. Okal.
Measuring Setup for Investigation and Visualization of the Percolation Phenomenon in Non-Ordered Models of Metal-Dielectric Nanocomposites.
Devices and Methods of Measurements.
2020, vol. 11, no. 3, pp. 171–178.
DOI: 10.21122/2220-9506-2020-11-3-171-178

Измерительная установка для исследования и визуализации явления перколяции в неупорядоченных моделях нанокompозитов металл-диэлектрик

П. Окаль

Люблинский технический университет,
ул. Надбыстрицкая, 38А, Люблин 20-618, Польша

Поступила 05.06.2020

Принята к печати 27.08.2020

В статье для исследования явления перколяции и визуализации каналов перколяции использован высоковольтный частичный пробой. Частичный пробой очень похож на квантовое явление туннелирования, наблюдаемое в нанокompозитах металл-диэлектрик. Как в первом, так и во втором случаях для протекания электрического тока не требуется контакт между частицами металлической фазы.

Разработана и изготовлена измерительная установка, предназначенная для измерений моделей нанокompозитов металл-диэлектрик с использованием высоковольтного частичного пробоя. В состав установки входят: высоковольтный трансформатор с максимальным напряжением до 110 кВ, регулятор напряжения первичной обмотки высоковольтного трансформатора, обеспечивающий постоянную скорость увеличения напряжения, измерительный зонд, вольтметры и компьютер. Сигналы от зонда и вольтметра с целью ограничения помех, связанных с сильным электрическим полем, передаются с использованием оптоэлектронного кабеля.

Разработаны и изготовлены двумерные модели нанокompозитов, в которых частицы металлической фазы в форме металлических дисков размещены случайным образом на поверхности диэлектрической матрицы. Число металлических дисков во время измерений увеличивалось по 40 штук в серии до максимальной величины 1520.

Определена зависимость от концентрации металлической фазы одного из существенных параметров высоковольтного частичного пробоя – пороговое напряжение, выше которого между электродами начинает течь ток. На основании этих измерений определён порог перколяции для матрицы со случайным распределением элементов металлической фазы.

С помощью фотоаппарата, входящего в состав установки, зарегистрированы фильмы и фотографии явления частичного пробоя между элементами металлической фазы моделей, на которых видны каналы перколяции.

Ключевые слова: перколяция, нанокompозиты, частичный пробой, высокие напряжения.

DOI: 10.21122/2220-9506-2020-11-3-171-178

Адрес для переписки:

P. Okal
Lublin University of Technology,
Nadbystrzycka str., 38A, Lublin 20-618, Poland
e-mail: p.okal@pollub.pl

Address for correspondence:

P. Okal
Lublin University of Technology,
Nadbystrzycka str., 38A, Lublin 20-618, Poland
e-mail: p.okal@pollub.pl

Для цитирования:

P. Okal.
Measuring Setup for Investigation and Visualization of the Percolation Phenomenon in Non-Ordered Models of Metal-Dielectric Nanocomposites.
Приборы и методы измерений.
2020. – Т. 11, № 3. – С. 171–178.
DOI: 10.21122/2220-9506-2020-11-3-171-178

For citation:

P. Okal.
Measuring Setup for Investigation and Visualization of the Percolation Phenomenon in Non-Ordered Models of Metal-Dielectric Nanocomposites.
Devices and Methods of Measurements.
2020, vol. 11, no. 3, pp. 171–178.
DOI: 10.21122/2220-9506-2020-11-3-171-178

Introduction

There are currently more and more studies and applications of nanocomposites and nanomaterials which are characterised by a number of interesting chemical, optical, mechanical and electrical properties [1]. These are materials that consist of at least two phases with at least one component less than 10^{-7} m in size [2]. Their special properties are related to the influence of surface energy, much higher than that of solid materials, and to quantum phenomena that occur in nanocomposites. One of the types of nanocomposites are metal-dielectric nanocomposites. Such material has special electrical properties related to conductivity. Metallic nanoparticles are so small that they should be considered as wells of potential. Then all phenomena must be described on the principles of quantum physics.

In such materials, which are characterised by high resistivity, there may be a type of conductivity, based on step exchange (tunnelling) of electrons [3]. The condition of its observation is the weakening to the lowest possible level of ionic conductivity in dielectrics and electron or hole conductivity in semiconductors. The basis for the occurrence of the quantum effect of electron tunnelling between potential wells is that the wave function of the electron in a potential well of nanometre dimensions or smaller has a non-zero probability beyond the potential barrier. The probability of finding a valence electron at a distance r outside a three-dimensional potential well is given by the formula [3]:

$$\Psi^2 = \exp(-2\alpha r), \quad (1)$$

where: α – inverse of the radius of the location of the electron; r – distance from the well of potential in which the electron is located.

$$\alpha^{-1} \cong R_B, \quad (2)$$

where R_B – Bohr's radius.

In the absence of an external electric field, the direction of electron tunnelling is random. After applying an electric field to the semiconductor, there is a partial ordering of electron jumps, related to the Debye factor [3]:

$$\exp\left(\pm \frac{e \cdot r \cdot E}{k \cdot T}\right) = \sinh\left(\frac{e \cdot r \cdot E}{k \cdot T}\right), \quad (3)$$

where: e – electron charge; r – distance between the well of potential from which the electron is tunnelling and the well to which it is jumping (tunnelling);

E – electric field strength; k – Boltzman constant; T – temperature.

According to the precursor of the theory of electron tunnelling in disordered semiconductors and dielectrics [3] electron tunnelling between potential wells can take place in two ways. The first one occurs in the case of weak location of electrons and temperature, close to the temperature of liquid helium. The second mechanism occurs in the case of strong electron localisation and high temperatures. Then electron tunnelling occurs between the closest adjacent potential wells. The conductivity formula for the case of tunnelling between the closest neighbours [3]:

$$\sigma = \sigma_0 \exp\left(-2\alpha r - \frac{\Delta W}{kT}\right), \quad (4)$$

where: r – distance between wells between which the electron is tunnelled; k – Boltzman constant; T – temperature; ΔW – activation energy.

As can be seen from formula (4), in the mechanism of electron tunnelling between the closest adjacent potential wells there is a strong temperature dependence of conductivity. The activation energy entering the formula is related to the fact that the tunnelling electron, as a rule, jumps from a lower energy level in the first well to a higher level in the second well. The distance between the potentials wells to be seen in formula (4) is a function of their concentration N :

$$r \approx N^{-\frac{1}{3}}. \quad (5)$$

Formulas (4) and (5) demonstrate that conductivity increases faster than linearly as the concentration of potential wells increases. Mott's calculations [3] show that when the distance between potentials wells decreases to a value two-and-a-half times greater than Bohr's radius R_B , as the concentration of potentials wells increases:

$$r \cong 2,5R_B, \quad (6)$$

there will be a transition from dielectric type conduction with a positive temperature coefficient of conductivity $d\sigma/dT > 0$ to metallic type conduction with $d\sigma/dT < 0$.

The transition from dielectric type conductivity at low contents to metallic type conductivity in the area of high potential well contents is associated with percolation [4]. Below the percolation threshold there is a rapid increase in the conductivity of the nanocomposite with an increase in the metallic phase

content, while above the percolation threshold the increase in conductivity significantly slows down and the transition to metallic type conductivity occurs.

Percolation phenomena cover a wide range of issues related to the flow of current in spatial networks, self-generated in metal-dielectric nanomaterials. Networks composed of resistive (R), resistive and capacitive (RC) and resistive, capacitive and inductive (RLC) elements are used to model such phenomena [5]. The network consists of nodes connected to each other by sections consisting of these elements [6]. When the network is continuous, there is a current flow channel from one side of the network (contact) to the opposite through the elements forming the network. After it is connected to a power source, current flows through the network. When more than one damage is introduced into the network, at some point the current stops flowing from one contact to another. It is said that the percolation threshold has been reached [7]. Such a state can be achieved in networks consisting of passive elements in two ways. In the first one, randomly determined nodes are eliminated. In the second one, the sections connecting the nodes are randomly cut. There are also other ways of modelling the percolation phenomenon, for example testing the current conduction by randomly mixed balls of identical dimensions, one of which is made of metal and the other of insulating material. Gradually increasing the content of metallic balls, we achieve a rapid increase in current intensity practically from zero, which corresponds to passing through the percolation threshold. Nowadays, the phenomenon of percolation has been analysed using the Monte Carlo method. The most common models studied were two-dimensional networks with translational symmetry. Such networks were damaged by eliminating nodes or crossing bonds with statistically independent probability p . Depending on the method of network damage, they formed models of bond percolation or node percolation. In the last few decades a huge amount of work has been put into finding precise and approximate ways to determine the values of percolation thresholds for different networks [8]. Exact thresholds are only known for some two-dimensional networks such as square or triangular.

Unfortunately, both in the grating, ball and Monte Carlo models below the percolation threshold, the conductivity of the investigated grating is zero, which is not observed in real nanocomposites. The models do not take into account the fact that in nanocomposites the current conductivity is also

below the percolation threshold through electron tunnelling, and with the increase of metallic phase content the conductivity of the material increases [9]. Real nanocomposites are characterised, first of all, by random distribution of metallic phase elements in dielectric matrix, secondly, the flow of direct or alternating current occurs also in the absence of direct contact between adjacent nanoparticles. This is due to the quantum tunnelling phenomenon. Another problem related to both the network and ball models is that these models do not allow to determine the route of the percolation channel.

Comparing the voltage behaviour in the case of high voltage partial discharge (HVPD) and conductivity behaviour in the case of electron tunnelling in the nanocomposite we can state that they are similar. For both phenomena, HVPD and tunnelling, the resistance decreases with the decrease of distance. The application of an partial high voltage discharge does not require direct contact of the metallic phase elements to the current flow between the electrodes. Of course the scale of these phenomena is completely different. Tunnelling occurs on a nanometer scale, while the phenomenon of high voltage discharge – on a macroscopic scale. Due to the similarity of both phenomena, the phenomenon of high voltage discharge was used in the study to model the percolation phenomenon in metal-to-electric nanocomposites. The aim of this work was to develop and build a stand for research of the phenomenon of percolation and visualisation of percolation channels in disordered systems modelling metal dielectric nanocomposites, make models and define the percolation threshold for them and determine the route of percolation channels.

Measuring stand

In order to investigate the phenomenon of percolation in metal-to-dielectric nanocomposites based on an partial high voltage discharge, a measuring stand was developed and made, the block diagram of which is shown in Figure 1. A dielectric matrix 3 was used as a model of a two-dimensional metal-to-dielectric composite. In the model, the dielectric phase is modelled by air, while the metallic phase is represented by metal disks. The base of the matrix is XPS extruded polystyrene. The primary winding of the single-phase high voltage transformer 2, whose gearbox was 110 kV/220 V, was powered by autotransformer 1, which was used to control the voltage. It was a specially designed autotransformer

with a stepper motor drive. Such a solution allowed precise regulation of the voltage increase at a constant speed. This is very important due to changes in the strength of the system depending on the rate of voltage increase. The stepper motor is controlled by an electronic system based on a sixteen-bit Atmega microcontroller. The program that has been written and imported to the microcontroller supports the motor controller in such a way that the value of voltage increase is digitally regulated in the range from 1 to 2 kV/s. On the surface of matrix 3 there are flat electrodes between which, as a result of the voltage increase, an partial discharge is created. The essence of the work was to register the changes in the HVPD current value along with the voltage increase for different concentration of metallic phase. Due to the very high values of the electromagnetic field it was significantly difficult.

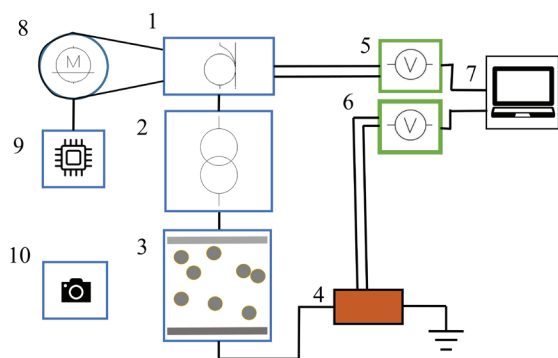


Figure 1 – Block diagram of the measuring station: 1 – autotransformer; 2 – high voltage transformer; 3 – percolation model; 4 – measuring probe; 5, 6 – voltmeters; 7 – computer; 8 – stepper motor; 9 – stepper motor control electronics; 10 – camera

The first and fundamental problem was the measurement of the current intensity. Due to the use of high voltage it was not possible to make direct measurements. In order to measure the current in the grounding branch, resistance was incorporated into the system. Two resistors of 50 Ω each were used. The voltage on the resistor did not exceed 4 V. The tests showed the presence of residual inductance in the measuring circuit, which significantly deformed the course making it impossible to obtain reliable measurements. This problem was solved by using specialised non-inductive resistors. For smaller voltage values, i. e. up to 80 kV, the system met the requirements. For larger values, the electromagnetic field induced a voltage in the cables and resistors, which resulted in a very noisy signal. In order to limit

the influence of the field, a Faraday cage was used, in which both resistors to which the test leads were connected were placed. It was a 1 mm thick copper cuboid, earthed, which allowed the wires to be earthed. Figure 2 shows a diagram of the measuring probe used in the model.

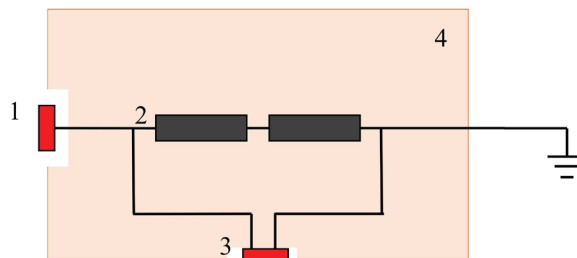


Figure 2 – Diagram of the measuring probe: 1 – BNC connector; 2 – resistors; 3 – measuring BNC output; 4 – copper casing

An additional element used to reduce electromagnetic field interference was the use of BNC RG213 50 Ω coaxial cables, double-insulated with braid. These cables were used in the branch between the model output and the probe in order not to interfere with the input current and in the branch that provided the measuring signal to the meter. Thanks to this solution, the measuring system was not exposed to a strong field and the received signal was free of noise resulting from its operation.

Then, a computer program with a graphical interface was created, communicating via a computer with two electronic meters 5 and 6, which had digital outputs. The communication was created in accordance with the RS-232 standard. This allowed the computer to receive 7 synchronised items of data from the two meters. One indicated the voltage value on non-inductive measuring resistors. The other was connected to an autotransformer supplying a high voltage transformer and was used to read the voltage given to the model. The program supported data recording at a frequency of 32 per second in a CSV format file. Such a resolution of measurements is sufficient to be able to plot characteristics such as the value of the voltage on the measuring resistors or changes in the current of the exhaust depending on the voltage supplied by the test transformer. As it turned out, such measurement method was effective only for HVPD registration. When the stand was applied in the full range, i. e. until the moment of a full discharge, the electromagnetic field of the resulting electric arc caused a disturbance of the digital signal between the meters and the computer,

which made it impossible to read the downloaded data. Therefore Universal Serial Bus cables were replaced by TOSLINK type optical fibre cables. This procedure reduced transmission errors to zero, thanks to which the created measuring station was used in the full measuring range.

Test results and their analysis

In order to measure the changes in the current intensity value as a function of the supply voltage depending on the concentration of the diffuse phase, it was necessary, in the first step, to place the metal disks in the dielectric matrix in strictly defined quantities depending on the series being tested. The matrices with the coordinates of points were generated by means of a computer program created. This program was based on a random number generator. The model of the matrix was generated for the smallest possible distances equal to 0 mm and the diameters of points were the same and amounted to 6 mm. The matrix generated in this way leaves the freedom to choose the number of disks in a series. The whole matrix was composed of 1520 points, randomly distributed on the matrix surface. Such a large number of disks was selected due to the fact that errors, resulting from the statistics, for sets over 1000 do not exceed 2 %. The matrix was divided into 38 series which contained 40 discs each [10]. It was not a continuum type because the program did not allow disk overlapping. The concentration of disks modelling metallic phase molecules is defined as the ratio of the metal surface area of the disks to the surface area of the matrix. Figure 3 shows a matrix for four concentration values of metallic phase as an example.

For testing, another series of metal discs, 40 in each, were placed on the matrix. When each series was mounted on the model, a program was run to connect to the meters and initiate the download of measurement data from them. A microcontroller-controlled stepper motor was started, driving an autotransformer to control the test transformer voltage. The rate of voltage increase was 2 kV/s in the range from 0 V to jump voltage. An electric field was generated between the electrodes on the matrix. Voltages on the test transformer and on the probe were read by electronic voltmeters and their values were stored in the computer memory. In this way, for a specific concentration value of the metallic phase, the course of voltage changes on the resistors in the probe depending on the model supply voltage was

obtained. The voltage measured on the measuring probe was proportional to the current of the partial discharge, formed on the model of nanocomposite metal dielectric. The diagram for one of the series of measurements is shown in Figure 4.

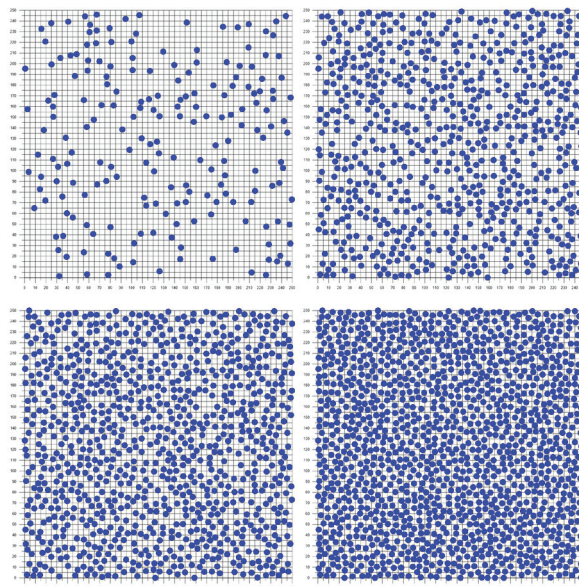


Figure 3 – Coordinates of discs of computer-generated dielectric matrix for 12 %, 30 %, 42 %, 58 % concentration

One of the basic parameters of the partial discharge is the initial voltage. Only when this voltage is exceeded will an partial discharge be initiated and a current start to flow between the electrodes. From Figure 4 it can be seen that for a concentration of the metallic phase of 42 % the partial discharge starts at an initial voltage of about 35 kV.

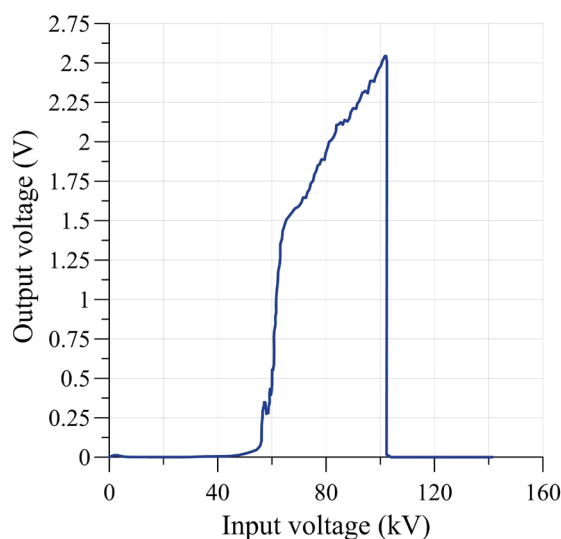


Figure 4 – The course of the voltage value on the measuring probe depending on the model supply voltage for concentration of metallic phase 42 %

After exceeding this voltage, the current flowing through the model starts to rise faster and faster. After reaching the voltage value of about 45 kV, the increase of the current intensity is clearly slowing down. When a voltage of about 72 kV is reached, an electric arc is ignited and the overcurrent protection switches off the power supply. This can be seen on a vertical drop to zero current.

The most important feature of the partial discharge applied in the test is the flow of electric current through the matrix below the percolation threshold. This is due to the similarity of the partial discharge and quantum tunnelling of electrons. Metallic phase elements, exactly as in real nanocomposites, do not need any direct contact current for the flow of current and the flow of current between them depends on the value of probability of jumps as a function of distance. By comparing the waveforms for individual concentrations of the metallic phase shown in Figure 5, it is possible to determine the initial voltage at which a partially discharged current appears. Figure 5 shows that for the concentration of the metallic phase $X \leq 42\%$ the initial voltage of partial discharges appears at a voltage of about 36 kV. An increase in concentration up to 50% causes the initial voltage of partial discharges to decrease rapidly to about 15 kV.

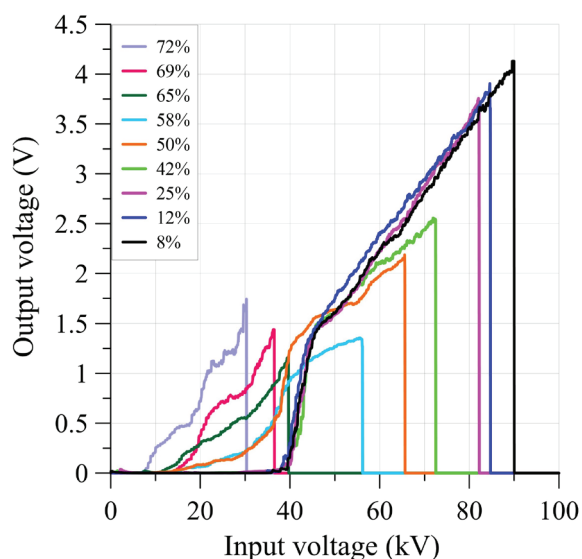


Figure 5 – Diagram of the voltage waveforms on the measuring probe depending on the supply voltage for different concentration of metallic phase

Such a leap change can be interpreted as reaching the percolation threshold. Its value is $(46 \pm 4)\%$. The conductivity of the system suddenly changes, which

means that a small change of concentration between 42% and 50% significantly affects the properties of the whole system.

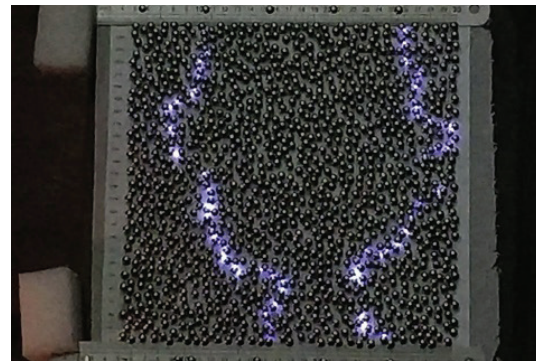


Figure 6 – Example picture of percolation channel

During partial discharges radiation is generated in the areas of visible light and ultraviolet. One of the elements of the station equipment is a camera. Its application allows the visualisation of percolation channels which are recorded in the form of films and photographs. Figure 6 shows a picture of a partial discharge, on which percolation channels and disks modelling the metallic phase are visible. In the picture, the light is visible in places where there is no direct contact with the metallic elements of the model and a partial discharge occurs. The photos taken during the research show that in the matrix, similarly as in nanocomposites, a number of percolation channels may occur.

Conclusion

A measurement stand was developed and built to study the percolation phenomenon and visualise the percolation channel using a high voltage partial discharge. The phenomenon of partial discharge applied in the work is very similar to the quantum tunnelling phenomenon. In both cases the current flow occurs in the absence of direct contact between elements of the metallic phase.

The measuring equipment, i. e. the measuring probe and connecting cables, were made in such a way as to eliminate the interference caused by a strong alternating electromagnetic field resulting from the use of high voltage. The communication between the measuring probe and the voltmeter was made in digital technology with the use of optical fibre technology, which allowed the meter to communicate with a computer without errors.

Models of nanocomposites of metal dielectric type were used for the tests. Modelling systems

consisting of metallic elements in the form of disks with concentration varying from 0 % to 72 % randomly distributed in the dielectric matrix were generated by computer and built. During the research, the concentration of the metallic phase was gradually increased by placing successive series of discs, 40 in each. The maximum number of discs was 1520 at 72 % concentration. The initial voltages of the exhaust were determined, at which the electric current starts to flow through the model, depending on the concentration of the metallic phase. Based on the obtained dependencies, a percolation threshold was determined, the value of which for the random distribution of the metallic phase elements is about $(46 \pm 4)\%$. The radiation generated during partial discharges in the visible light area was used to visualise the percolation channels. Photographs of partial discharges, on which percolation channels are visible, were taken during the tests. The photos taken during the study show that the matrix, similarly to nanocomposites, may contain a number of percolation channels.

Acknowledgments

This research was partially funded from the Polish Ministry of Science and Higher Education from science fund of the Lublin University of Technology, at the Faculty of Electrical Engineering and Computer Science FN-28/E/EE/2019, entitled "Researches of electrical, magnetic, thermal and mechanical properties of modern electrotechnical and electronic materials, including nanomaterials and diagnostic of electrical devices and their components".

References

1. Czarnacka K., Koltunowicz T.N., Żukowski P., Fedotov A.K. Dielectric properties of multi-layer nanocomposites $\text{SiO}_x/\text{ZrO}_2$ after high temperature

annealing. *Ceram. Int.*, 2019, vol. 45, no. 5, pp. 6499–6502. DOI: 10.1016/j.ceramint.2018.12.139

2. Larkin A.V., Fedotov A.K., Fedotova J.A., Koltunowicz T.N., Żukowski P. Temperature and frequency dependences of real part of impedance in the FeCoZr-doped PZT nanogranular composites. *Mater. Sci. Pol.*, 2012, vol. 30, no. 2, pp. 75–81.

DOI: 10.2478/s13536-012-0015-2

3. Nevill F. Mott and Edward A. Davis. *Electronic Processes in Non-Crystalline Materials*. Oxford University Press, 2012.

4. Okal P. Modeling of the percolation phenomenon of disordered two-dimensional systems. In *Photonics Applications in Astronomy, Communications, Industry, and High-Energy Physics Experiments*, 2019, vol. 11176, p. 90. DOI: 10.1117/12.2536741

5. Wang P., Zhang X., Lu X., Zheng W., Liu Q. A dual percolation model for predicting the connectivity of fractured porous media. *Water Resour.*, 2016, vol. 43, no 1, pp. 95–110. DOI: 10.1134/S0097807816120095

6. Gold J. Isoperimetry in supercritical bond percolation in dimensions three and higher. *Ann. l'institut Henri Poincaré Probab. Stat.*, 2018, vol. 54, no. 4, pp. 2092–2158. DOI: 10.1214/17-AIHP866

7. Okal P., Rogalski P., Żukowski P. Visualization of the percolation phenomenon in two-dimensional arrangement of metallic spherical particles. In *Proceedings of SPIE – The International Society for Optical Engineering*, 2017, vol. 10445.

DOI: 10.1117/12.2280152

8. Jacobsen J.L. High-precision percolation thresholds and Potts-model critical manifolds from graph polynomials. *J. Phys. A Math. Theor.*, 2014, vol. 47, no. 13, p. 135001. DOI: 10.1088/1751-8113/47/13/135001

9. Hassan M.K., Rahman M.M. Percolation on a multifractal scale-free planar stochastic lattice and its universality class. *Phys. Rev. E – Stat. Nonlinear, Soft Matter Phys.*, 2015, vol. 92, no. 4, pp. 040101-1– 040101-6. DOI: 10.1103/PhysRevE.92.040101

10. Torquato S., Jiao Y. Effect of dimensionality on the continuum percolation of overlapping hyperspheres and hypercubes. II. Simulation results and analyses. *J. Chem. Phys.*, 2012, vol. 137, no. 7. DOI: 10.1063/1.4742750

High Power SESAM Mode-Locked Laser Based on $\text{Yb}^{3+}:\text{YAlO}_3$ Bulk Crystal

Alexander Rudenkov¹, Viktor Kisel¹, Anatol Yasukevich¹, Karine Hovhannesian², Ashot Petrosyan², Nikolai Kuleshov¹

¹Center for Optical Materials and Technologies, Belarusian National Technical University, Nezavisimosty Ave., 65, Minsk 220013, Belarus

²Institute for Physical Research, National Academy of Sciences of Armenia, 0203, Ashtarak-2, Armenia

Received 04.08.2020

Accepted for publication 15.09.2020

Abstract

Yttrium aluminium perovskite YAlO_3 (YAP) crystal, doped with rare-earth ions, has been extensively studied as a diode-pumped laser host material. The wide interest to rare-earth ions doped YAP crystals is explained by its good thermal and mechanical properties, high natural birefringence, widely used Czochralski growth method. The aim of this work was to study the $\text{Yb}^{3+}:\text{YAlO}_3$ crystal as an active medium for high power mode-locked laser.

Yb^{3+} -doped perovskite-like aluminate crystals have unique spectroscopic and thermo-optical properties that allowed using these crystals as an active medium of high power continuous wave (CW) and mode-locked (ML) bulk lasers with diode pumping.

In our work spectroscopic properties of $\text{Yb}:\text{YAP}$ crystal and laser characteristics in CW and ML regimes are investigated. Maximum output power of 4 W with optical-to-optical efficiency of 16.3 % and 140 fs pulse duration have been obtained for $\text{Yb}:\text{YAP}$ $E//c$ -polarization with 10 % output coupler transmittance. Tunability range as wide as 67 nm confirms high promise of using $\text{Yb}:\text{YAP}$ crystal for lasers working in wide spectral range.

Keywords: mode-locked laser, ytterbium ions, diode pumping, yttrium aluminate crystals.

DOI: 10.21122/2220-9506-2020-11-3-179-186

Адрес для переписки:

Александр Руденков
Центр оптических материалов и технологий,
Белорусский национальный технический университет,
пр-т Независимости, 65, г. Минск 220013, Беларусь
e-mail: a.rudenkov@bntu.by

Address for correspondence:

Alexander Rudenkov
Center for Optical Materials and Technologies,
Belarusian National Technical University,
Nezavisimosty Ave., 65, Minsk 220013, Belarus
e-mail: a.rudenkov@bntu.by

Для цитирования:

Alexander Rudenkov, Viktor Kisel, Anatol Yasukevich,
Karine Hovhannesian, Ashot Petrosyan, Nikolai Kuleshov.
High Power SESAM Mode-Locked Laser Based
on $\text{Yb}^{3+}:\text{YAlO}_3$ Bulk Crystal.
Приборы и методы измерений.
2020. – Т. 11, № 3. – С. 179–186.
DOI: 10.21122/2220-9506-2020-11-3-179-186

For citation:

Alexander Rudenkov, Viktor Kisel, Anatol Yasukevich,
Karine Hovhannesian, Ashot Petrosyan, Nikolai Kuleshov.
High Power SESAM Mode-Locked Laser Based
on $\text{Yb}^{3+}:\text{YAlO}_3$ Bulk Crystal.
Devices and Methods of Measurements.
2020, vol. 11, no. 3, pp. 179–186.
DOI: 10.21122/2220-9506-2020-11-3-179-186

УДК 621.373.826

Высокомощный лазер на кристалле $\text{Yb}^{3+}:\text{YAlO}_3$, работающий в режиме синхронизации мод на основе полупроводниковых зеркал с насыщающимся поглотителем

Александр Руденков¹, Виктор Кисель¹, Анатолий Ясюкевич¹, Карин Ованесьян², Ашот Петросян², Николай Кулешов¹

¹Центр оптических материалов и технологий, Белорусский национальный технический университет, пр-т Независимости, 65, Минск 220013, Беларусь

²Институт физических исследований Национальной академии наук Армении, 0203, Аштарак-2, Армения

Поступила 04.08.2020

Принята к печати 15.09.2020

Кристаллы иттрий-алюминиевого перовскита YAlO_3 (YAP), легированные ионами редкоземельных элементов интенсивно изучались в качестве активных сред лазеров с диодной накачкой. Интерес к данным кристаллам обусловлен их высокими теплофизическими и механическими свойствами, высоким двулучепреломлением, возможностью роста по широко распространённому методу Чохральского. Целью данной работы было изучение кристалла $\text{Yb}^{3+}:\text{YAlO}_3$ в качестве активной среды лазера с высокой средней выходной мощностью, работающего в режиме синхронизации мод.

Кристаллы YAlO_3 , легированные трёхвалентными ионами иттербия имеют уникальные спектроскопические и теплофизические свойства, что позволяет использовать данные кристаллы в качестве активных сред лазеров с высокой средней выходной мощностью и диодной накачкой, работающих в режимах непрерывной генерации и пассивной синхронизации мод.

В работе исследованы спектроскопические характеристики кристалла $\text{Yb}:\text{YAP}$, а также выходные характеристики лазеров на основе данного кристалла, работающих в режимах непрерывной генерации и пассивной синхронизации мод. Средняя выходная мощность 4 Вт с оптической эффективностью 16.3 % и длительностью импульса 140 фс получена для $E//c$ -поляризации при пропускании выходного зеркала 10 %. Диапазон перестройки 67 нм подтверждает высокие перспективы использования кристалла $\text{Yb}:\text{YAP}$ в качестве активной среды лазеров, работающих в широком спектральном диапазоне.

Ключевые слова: лазер с синхронизацией мод, ионы иттербия, диодная накачка, кристаллы иттриевого алюмината.

DOI: 10.21122/2220-9506-2020-11-3-179-186

Адрес для переписки:

Александр Руденков
Центр оптических материалов и технологий,
Белорусский национальный технический университет,
пр-т Независимости, 65, г. Минск 220013, Беларусь
e-mail: a.rudenkov@bntu.by

Address for correspondence:

Alexander Rudenkov
Center for Optical Materials and Technologies,
Belarusian National Technical University,
Nezavisimosty Ave., 65, Minsk 220013, Belarus
e-mail: a.rudenkov@bntu.by

Для цитирования:

Alexander Rudenkov, Viktor Kisel, Anatol Yasukevich,
Karine Hovhannesian, Ashot Petrosyan, Nikolai Kuleshov.
High Power SESAM Mode-Locked Laser Based
on $\text{Yb}^{3+}:\text{YAlO}_3$ Bulk Crystal.
Приборы и методы измерений.
2020. – Т. 11, № 3. – С. 179–186.
DOI: 10.21122/2220-9506-2020-11-3-179-186

For citation:

Alexander Rudenkov, Viktor Kisel, Anatol Yasukevich,
Karine Hovhannesian, Ashot Petrosyan, Nikolai Kuleshov.
High Power SESAM Mode-Locked Laser Based
on $\text{Yb}^{3+}:\text{YAlO}_3$ Bulk Crystal.
Devices and Methods of Measurements.
2020, vol. 11, no. 3, pp. 179–186.
DOI: 10.21122/2220-9506-2020-11-3-179-186

Introduction

Yttrium aluminium perovskite (YAP) crystal, $YAlO_3$, doped with rare-earth ions, has been extensively studied as a diode-pumped laser host material. Numerous impressive results were reported for Nd^{3+} -doped YAP crystal. Among them 100 W output power at 1079 nm and 18.3 W at 1341 nm were obtained in diode-side-pump module [1]. 6.2 W laser output with a slope efficiency as high as 27.2 % at 1341.4 nm were demonstrated in a compact plane-concave cavity [2]. Laser emitting at 1378 and 1385 nm with power of 800 mW was reported in a folded cavity with prism inserted [3] and second harmonic generation at 536 nm was obtained with an LBO crystal inside the cavity [4]. Intensive studies were also made with Tm^{3+} and Ho^{3+} -doping. 730 mW of laser output power with 40.3 % slope efficiency were obtained over the range 1965–2020 nm with singly Tm-doped aluminate [5] and as high as 8.36 W at 2120 nm [6] and 9.3 W at 2044 nm [7] with slope efficiencies 35.7 % and 42.5 %, correspondingly, were demonstrated in Tm and Ho co-doped YAP crystal. Furthermore efficient Pr-doped $YAlO_3$ laser operation under diode pumping was recently reported emitting in the near-infrared spectral range [8].

The wide interest to rare-earth ions doped YAP crystals is explained by its good thermal and mechanical properties similar to those of YAG, but growing faster and anisotropic [9]. Previously thermal conductivity of undoped YAP crystal was reported to be close to 11 W/[m·K] [9, 10]. Lately more modest values of 7–8 W/[m·K] were published [11]. Nevertheless they remain two times higher than those of tungstate crystals [12]. $YAlO_3$ is a biaxial crystal and belongs to orthorhombic space group [9]. Its high natural birefringence dominates thermally induced one in lasers and leads to overcoming depolarization losses at high average powers [13]. It results in a very high polarization degree of the laser emission under different levels of pump power which is advantageous for non-linear frequency conversion [14], efficient modulation loss in Q-switch lasers [6] and other applications where linearly polarized light is necessary.

In this work we present the experimental study results of high power passively mode-locked laser based on yttrium aluminium perovskite crystal doped with Yb^{3+} ions.

Crystal growth

Single crystals of Yb:YAP can be grown by several growth techniques [15–20] among

which Czochralski is the most usable for practical applications.

For this study Yb:YAP crystals were grown by Czochralski method using Y_2O_3 , Yb_2O_3 and crystalline sapphire as starting oxides of at least 99.99 % purity and seeds oriented along the b axis. The melts were corresponding to stoichiometric compositions $Y_{1-x}Yb_xAlO_3$ ($x=0-0.03$). The growth melts ($x=0-0.03$) were held in iridium crucibles ($40 \times 5 \times 40$ mm³) and inductively heated under a pure Ar atmosphere. The pulling and rotation rates were 2.5 mm/h and 35 rpm. The grown boules are 15 mm in diameter and 30–40 mm long, transparent but some of them of a yellow-brown shade.

Spectroscopy

Polarized absorption spectra of Yb^{3+} (2 at.%) :YAP (corresponding ytterbium concentration was 4.02×10^{20} cm⁻³) at room temperature were registered by a Varian CARY-5000 spectrophotometer. Absorption cross-section spectra for three light polarizations parallel to the a, b and c crystallographic axes are shown in Figure 1.

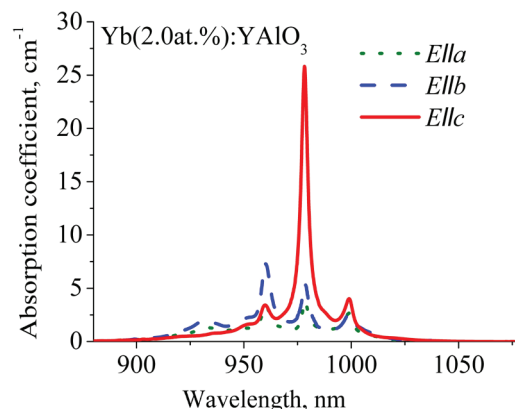
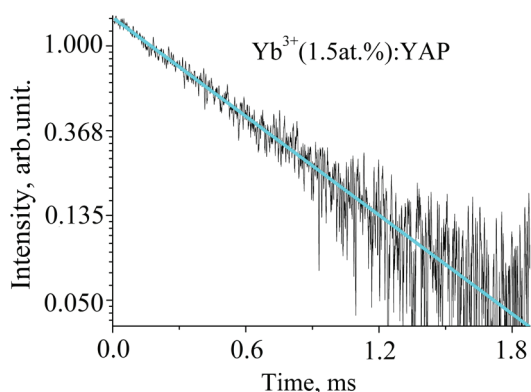


Figure 1 – Polarized absorption spectra of Yb^{3+} :YAP crystal (the spectra were obtained for Yb^{3+} (2 at.%) :YAP)

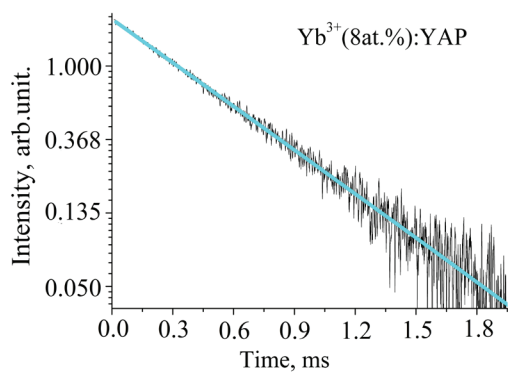
Strong absorption is found for $E//c$ light polarization with the peak absorption at 978.2 nm of about 25 cm⁻¹ and spectral bandwidth FWHM of 4 nm.

It is well known that radiation trapping strongly affects the measured lifetime of Yb-doped materials because of significant overlap of the absorption and emission bands [21, 22]. The comparatively high index of refraction of YAP ($n_c = 1.914$ for $\lambda = 1040$ nm) also increases the probability of reabsorption even in optically thin samples because of the total internal reflection. Thus the special methods discussed in the literature [21, 22] should be used to determine the

luminescence lifetime accurately. In our experiments we used a fine powder of Yb:YAP crystal immersed in glycerin. The diameter of the powder particles was measured to be approximately 30–40 μm , several times lower than absorption length of the most heavily doped Yb³⁺ (8 at.%):YAP crystal (97 μm at 978.2 nm). The Yb ions contents in the samples were 1.5, 2, 3 and 8 at.%. The samples were excited by 20 ns pulses at wavelength of about 978 nm and luminescence kinetics were registered with the use of a 0.3-m monochromator, fast Ge-photodiode with a rise time of < 20 ns and a 500 MHz digital storage oscilloscope. All the samples exhibited single exponential decays (see Figure 2).



a



b

Figure 2 – Kinetics of luminescence decay for Yb(1.5 at.%):YAP (a) and Yb(8 at.%):YAP (b)

Starting from certain powder content, the lifetime remained constant despite further dilution (Figure 3), thus indicating that reabsorption effects became negligible. Emission lifetime for 8, 3, 2 and 1.5 at.% Yb-doped crystals was measured to be about $510 \pm 20 \mu\text{s}$ that indicates a weak influence of the luminescence concentration quenching. Presented values are in good agreement with the previously obtained data [23].

The stimulated-emission (SE) cross sections were calculated by use of the modified reciprocity

method in which it is not necessary to know the Stark level structure of the Yb³⁺ manifolds (²F_{5/2} and ²F_{7/2}) [24]:

$$\sigma_{SE}^{\alpha}(\lambda) = \frac{3 \cdot \exp(-hc/(kT\lambda))}{8\pi n^2 \tau_{rad} \cdot c \cdot \sum_{\beta} \int \lambda^{-4} \sigma_{ABS}^{\beta}(\lambda) \exp(-hc/(kT\lambda)) d\lambda} \sigma_{ABS}^{\alpha}(\lambda), \quad (1)$$

where τ_{rad} is the radiation lifetime of an active center; c is the light velocity; h and k are Planck and Boltzmann constants, respectively; T is the crystal temperature; n is the refractive index of a crystal; α and β denote the polarization state; and σ_{ABS} is the ground-state absorption cross section.

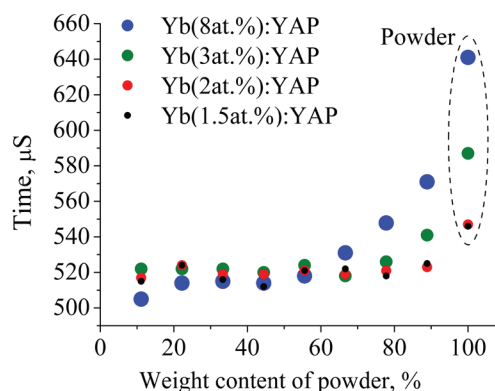


Figure 3 – Measured lifetime for different weight content of Yb:YAP crystalline powder in glycerin suspension for YAP with different Yb³⁺ concentrations

The SE cross section spectra calculated with this method are presented in Figure 4.

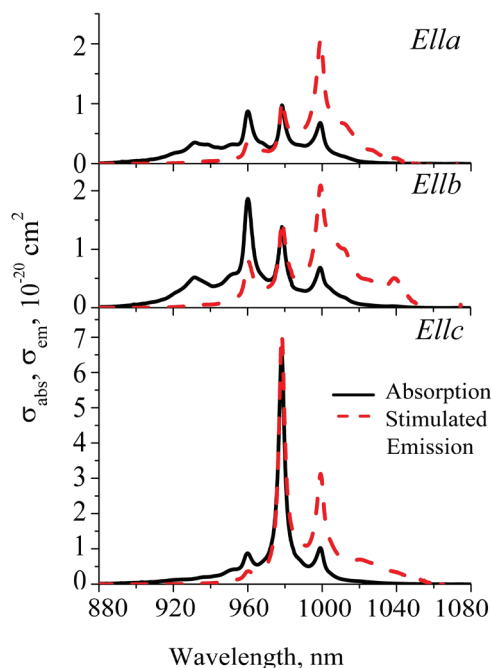


Figure 4 – Polarized absorption and stimulated emission cross-section spectra of Yb³⁺:YAlO₃ crystal

The most intensive SE cross-section band at 999.2 nm has peak value of about $3.13 \times 10^{-20} \text{ cm}^2$ for $E//c$ -polarization. Such a high value is very suitable for mode-locked and actively Q-switched laser operation.

Moderate SE cross-section values ($0.4\text{--}1.1 \times 10^{-20} \text{ cm}^2$) are observed for $E//b$ - and $E//c$ -polarizations in wavelength range 1005–1030 nm where the spectra are smooth.

Continuous wave laser experiment

For laser operation the most interesting polarization states in the crystal are $E//c$ and $E//b$ (c and b are crystallographic axes) due to high stimulated-emission cross sections values.

For a continuous wave laser experiments a set up with X-folded cavity design was used (see Figure 5). It consisted of two curved mirrors M1 and M2 and two plane mirrors: OC and HR.

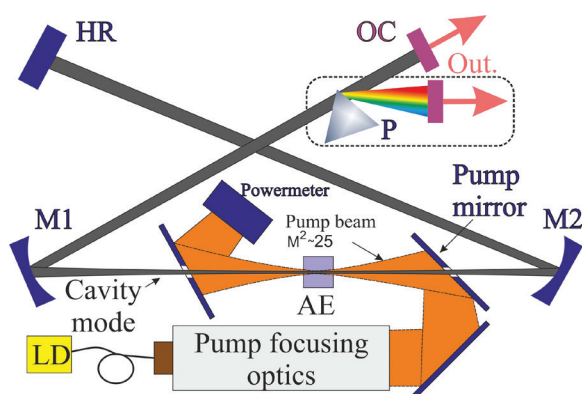


Figure 5 – Experimental setup of continuous wave diode-pumped Yb:YAP laser: HR – highly reflective mirror; OC – output coupler; P – prism; M1, M2 – concave mirrors; AE – active element; LD – laser diode

The calculated TEM_{00} mode diameter in the crystal was about 100 μm . As a pump source, a multiple single emitter InGaAs fiber-coupled laser diode ($\varnothing 105 \mu\text{m}$, $NA = 0.15$) with a maximum output power of about 25 W was used. An "off-axis" pump layout was used for longitudinal pumping of the active element (see Figure 5). This pump arrangement was successfully tested in our previous work [25–26] and the main advantage of such a pump scheme is that all the cavity mirrors have highly reflecting coating at 900–1100 nm. The pump light was formed by a set of lenses into the spot with a diameter of about 100 μm ($1/e^2$). A 2 mm long $\text{Yb}^{3+}(2 \text{ at.}\%)\text{:YAlO}_3$ crystal was used as a gain medium. The crystal was a-cut to provide $E//b$ and $E//c$ polarized laser output. It was a slab with dimensions $2(a) \times 5(b) \times 1.5(c) \text{ mm}^3$;

both $5 \times 2 \text{ mm}^2$ lateral faces were maintained at 15 °C by means of copper plates (indium foil was used to improve thermal contact) and thermo-electrical cooling elements with water-cooled heat sink, while $1.5 \times 5 \text{ mm}^2$ working faces were antireflection coated for pump and laser radiation.

The dependencies of the laser output power on the absorbed pump power for $E//b$ - and $E//c$ -polarized outputs and different OCs are shown in Figure 6. Absorbed pump power was real-time measured during the laser action.

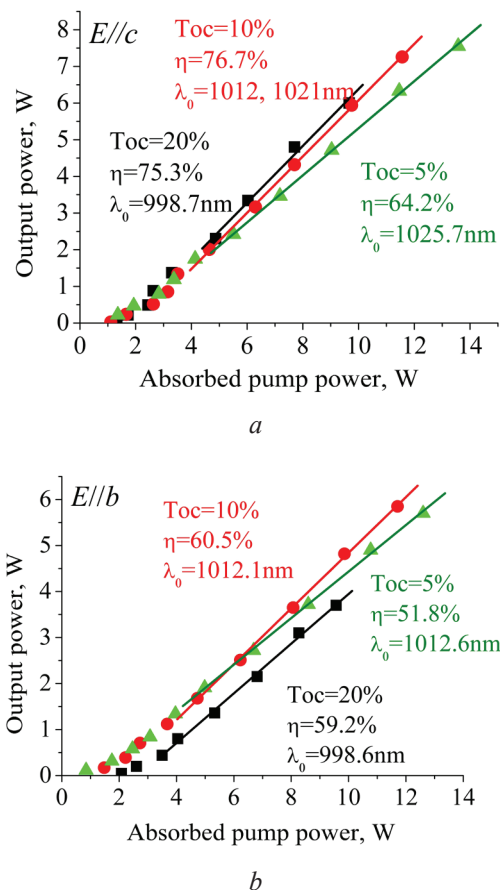


Figure 6 – CW laser performance of Yb:YAP crystal for different polarizations and output coupler transmittances

The maximum CW output power of 7.6 W at absorbed pump power of 13.6 W with slope efficiency of 64.2 % was demonstrated for $E//c$ polarization with 5 % OC transmittance (Figure 6a). With output coupler transmission of 10 % and 20 % the laser output power slightly decreased to 7.3 W and 6.0 W, respectively, while the corresponding slope efficiencies increased to 76.7 % and 75.3 %. Similar output powers were demonstrated for $E//b$ laser output (Figure 6b). With 10 % output coupler transmittance 5.9 W of output power was obtained at 11.7 W of absorbed pump power with 60.5 %

slope efficiency. Output powers of 5.7 W and 3.7 W with slope efficiencies of 51.8 % and 59.2 % were obtained for 5 % and 20 % OCs, respectively.

Wavelength tunability of the Yb:YAP laser was investigated during CW laser experiments. For this purpose prism was inserted into the cavity. The dependency of average output power (in normalized units) from the central wavelength of the Yb:YAP laser is shown in the Figure 7.

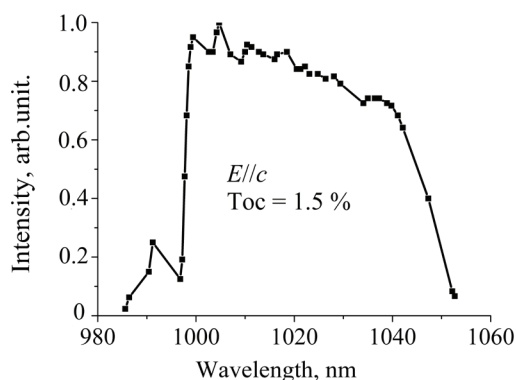


Figure 7 – Tunability curve of Yb:YAP laser with output coupler transmittance 1.5 % for $E//c$ -polarization

Tunability range as wide as 67 nm (985.6–1052.7 nm) was demonstrated with output coupler transmittance of 1.5 %.

Mode-locked laser experiment

For the mode-locked laser experiment the same crystal was used as for CW one. Schematic of the experimental setup is shown in Figure 8.

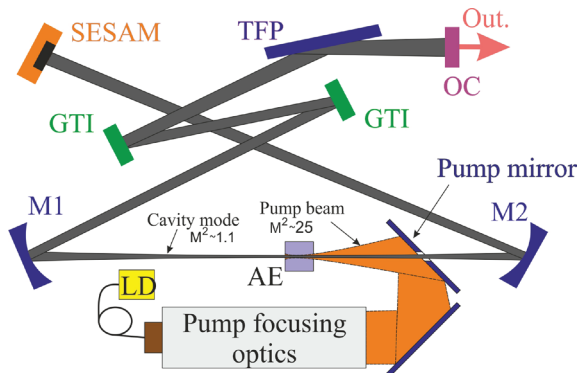


Figure 8 – Schematic of the Yb:YAP mode-locked laser: SESAM – semiconductor saturable absorber mirror; TFP – thin film polarizer; OC – output coupler; GTI – chirped mirrors; M1, M2 – concave mirrors; AE – active element; LD – laser diode

InGaAs-based SESAM with modulation depth of about 4.0 % was used in the experiments. The SESAM based on quantum wells separated by nano-

structured barriers was grown by molecular beam epitaxy (MBE) technique over the semi-insulating GaAs substrate of (001) orientation. The crystallinity of each layer was controlled via reflection of high energy electrons diffraction (RHEED technique). The number of quantum wells, their thickness and the concentration of the ternary alloy were chosen to match the requirement on the saturable absorption modulation depth. The recovery time shortening was performed by the barriers separation into the thinner layers via the insertion narrow band gap material. The design of the SESAM described in [27]. The measured reflectivity spectrum of the SESAM is presented in Figure 9. Used SESAM enabled to support mode-locking in the spectral range from 1000 nm to about 1050 nm. The result of the pump-probe testing of the SESAM with modulation depth of 4 % is shown in Figure 10. The saturation energy fluence of the SESAM was measured to be about 70–120 $\mu\text{J}/\text{cm}^2$.

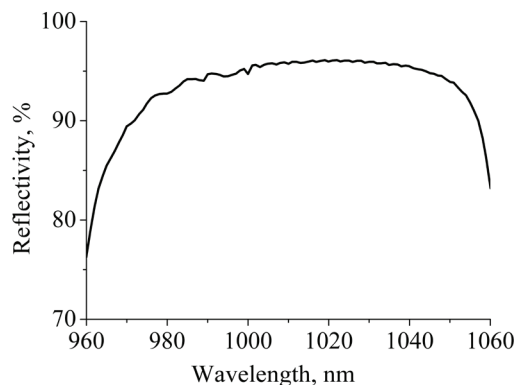


Figure 9 – SESAM reflectivity spectrum with modulation depth 4 %

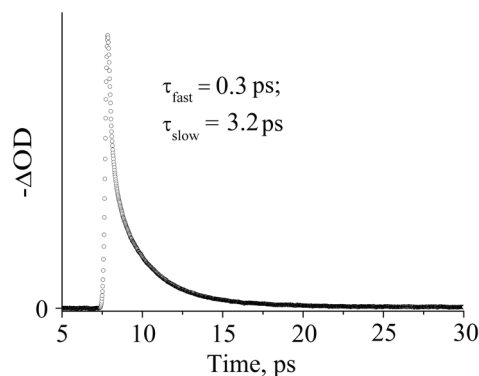


Figure 10 – "Fast" (0.3 ps) and "slow" (3.2 ps) recovery times of the SESAM

Stable mode-locked operation of Yb³⁺ (2 at.%) :YAP laser was obtained only for OCs with 5 % and 10 % transmittance. The maximum output power of 4 W with optical-to-optical efficiency of 16.3 % was obtained with 10 % OC for $E//c$ -polarization.

Pulses with 8 nm (see Figure 11) full width at half maximum (FWHM) obtained at 1009.7 nm central wavelength resulting in 140 fs pulse duration (see Figure 12) with time-bandwidth product of about 0.32 assuming Sech^2 pulse shape.

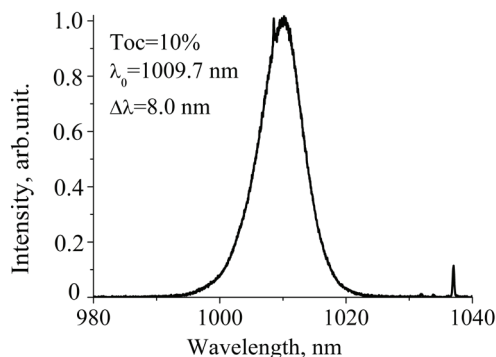


Figure 11 – Spectrum of the Yb:YAP (*E//c*) mode-locked laser for 10 % OC

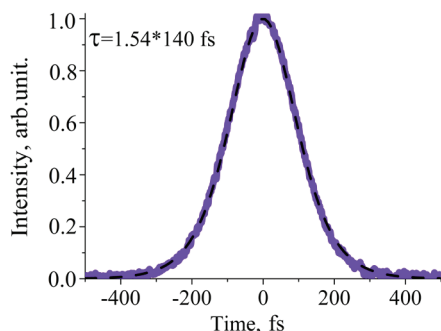


Figure 12 – Autocorrelation trace of the Yb:YAP (*E//c*) mode-locked laser pulses for 10 % OC

Output power of 2.4 W with optical-to-optical efficiency of 10.7 % obtained with 5 % OC transmittance. Spectral width of 7.6 nm at 1021.9 nm central wavelength (Figure 13) was demonstrated resulting in about 150 fs pulse duration (Figure 14) with time-bandwidth product of about 0.33 assuming Sech^2 pulse shape. The pulse repetition frequency was around 70 MHz.

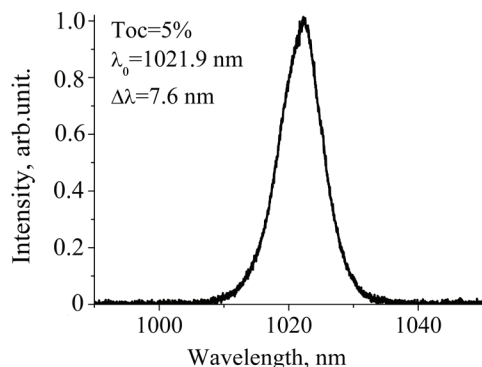


Figure 13 – Spectrum of the Yb:YAP (*E//c*) mode-locked laser for 5 % OC

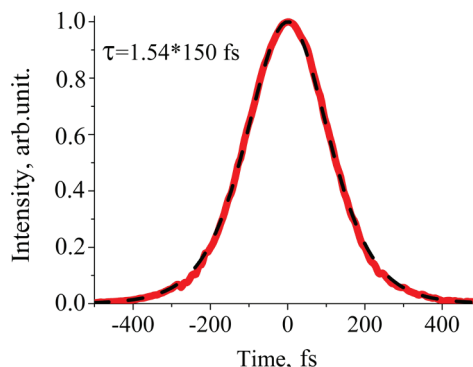


Figure 14 – Autocorrelation trace of the Yb:YAP (*E//c*) mode-locked laser pulses for 5 % OC

Conclusion

In conclusion, Yb:YAP bulk crystal as a gain medium for high power mode-locked lasers was investigated in our work. Maximum output power of 4 W with optical-to-optical efficiency of 16.3 % and 140 fs pulse duration have been obtained for Yb:YAP *E//c*-polarization with 10 % output coupler transmittance. Tunability range as wide as 67 nm confirms high promise of using Yb:YAP crystal for lasers working in wide spectral range.

References

1. Ruifen Wu, Poh Boon Phua, Kin Seng Lai. Linearly Polarized 100-W Output From a Diode-Pumped Nd:YAlO Laser. *Applied Optics*, 2000, vol. 39, iss. 3, pp. 431–434.
DOI: 10.1364/AO.39.000431
2. Zhu H.Y., Zhang G., Huang C.H., Wei Y., Duan Y.M., Chen W.D., Zhuang F.J. 6.2 W laser-diode end-pumped continuous-wave Nd:YAlO₃ laser at 1.34 μm . *Optics Communications*, 2011, vol. 284, pp. 2985–2987.
DOI: 10.1016/j.optcom.2011.01.080
3. Yiou S., Balembois F., Georges P., Brun A. High-power continuous-wave diode-pumped Nd:YAlO₃ laser that emits on low-gain 1378- and 1385-nm transitions. *Applied Optics*, 2001, vol. 20, iss. 18, pp. 3019–3022.
DOI: 10.1364/AO.40.003019
4. Fu X.H., Li Y.L., Tao Z.H., Zeng Y.H. Diode pumped CW Nd³⁺:YAlO₃ laser at 1339 nm. *Laser Physics*, 2011, vol. 21, no. 5, pp. 877–879.
DOI: 10.1134/S1054660X1109009X
5. Elder I.F., Payne M.J. YAP versus YAG as a diode-pumped host for thulium. *Optics Communications*, 1998, vol. 148, iss. 4–6, pp. 265–269.
DOI: 10.1016/S0030-4018(97)00714-1
6. Li L.J., Yao B.Q., Wu D.Y., Wang J., Gang L., Wang Y.Z., Zhang Z.G. High Efficient Double End-Pumped b-cut Tm,Ho:YAlO₃ Laser. *Laser Physics*, 2011,

vol. 21, no. 3, pp. 446–449.

DOI: 10.1134/S1054660X11050148

7. Li L.J., Yao B.Q., Qin J.P., Wu D.Y., Wang Y.M., Wang J., He Z.L., Liu W.Y., Chen J.J., Wang Y.Z., Zhang Z.G., Li A.H. High Power and Efficiency of a 2044-nm c-cut Tm, Ho:YAlO₃ Laser. *Laser Physics*, 2011, vol. 21, no. 3, pp. 489–492.

DOI: 10.1134/S1054660X11050173

8. Fibrich M., Jelínková H., Šulc J., Nejezchleb K., Škoda V. Diode-pumped Pr:YAP lasers. *Laser physics letters*, 2011, vol. 8, p. 559–568.

DOI: 10.1134/S1054660X11050173

9. Weber M.J., Bass M., Andringa K., Monchamp R.R., Comperchio E. Czochralski growth and properties of YAlO₃ laser crystals. *Applied Physics Letters*, 1969, vol. 15, no. 10, p. 342.

DOI: 10.1063/1.1652851

10. Aggarwal R.L., Ripin D.J., Ochoa J.R., Fan T.Y. Measurement of thermo-optic properties of Y₃Al₅O₁₂, Lu₃Al₅O₁₂, YAlO₃, LiYF₄, LiLuF₄, BaY₂F₈, KGd(WO₄)₂, and KY(WO₄)₂ laser crystals in the 80–300 K temperature range. *J. Appl. Phys.*, 2005, vol. 98, p. 103514.

DOI: 10.1063/1.2128696

11. Petit Johan, Viana Bruno, Goldner Philippe, Roger Jean-Paul, Fournier Danièle. Thermomechanical properties of Yb³⁺ doped laser crystals: Experiments and modeling. *J. Appl. Phys.*, 2010, vol. 108, p. 123108.

DOI: 10.1063/1.3520216

12. Lagatsky A.A., Abdolvand A., Kuleshov N.V. Passively Q switched and self-frequency Raman conversion in a diode-pumped Yb:KGd(WO₄)₂ laser. *Optics Letters*, 2000, vol. 25, no. 9, p. 616.

DOI: 10.1364/OL.25.000616

13. Massey G.A. Criterion for selection of CW laser host materials to increase available power in the fundamental mode. *Applied Physics Letters*, 1970, vol. 17, no. 5, p. 213. **DOI:** 10.1063/1.1653370

14. Shen H.Y., Zhou Y.P., Lin W.X., Zeng Z.D., Zeng R.R., Yu G.F., Huang C.H., Jiang A.D., Jia S.Q., Shen D.Z. Second harmonic generation and sum frequency mixing of dual wavelength Nd:YAlO₃ laser in flux grown KTiOPO₄ crystal. *IEEE Journal of Quantum Electronics*, 1992, vol. 28, iss. 1, p. 48–51. **DOI:** 10.1109/3.119494

15. Sugak D., Matkovskii A., Savitskii D., Durygin A., Suchocki A., Zhydachevskii Y., Solskii I., Stefaniuk I., Wallrafen F. Growth and Induced Color Centers in YAlO₃-Nd Single Crystals. *Phys. Status Solidi A*, 2001, vol. 184, p. 239.

DOI: 10.1002/1521-396X(200103)184:1<239::AID-PSSA239>3.0.CO;2-I

16. Kvapil J., Perner B., Manek B., Blazek K., Hendrich Z. Nonstoichiometric Defects in YAG and YAP. *Cryst. Res. Technol.*, 1985, vol. 20, p. 473.

DOI: 10.1002/crat.2170200410

17. Petit P.O., Petit J., Goldner Ph., Viana B. Colour centre-free perovskite single crystals. *J. Lumin.*, 2009, vol. 129, p. 1586. **DOI:** 10.1016/j.jlumin.2009.04.056

18. Antonov V.A., Arsenev P.A., Linda I.G., Farshendiker V.L. Studies of Some Point Defects in YAlO₃ and GdAlO Single Crystals. *Phys. Status Solidi A*, 1973, vol. 15, p. K63. **DOI:** 10.1002/pssa.2210150158

19. Kovaleva N.S., Mochalov I.V. Formation of color centers in yttrium orthoaluminate crystals. *J. Quantum Electron.*, 1978, vol. 8, no. 12, p. 1427.

DOI: 10.1070/QE1978v008n12ABEH011380

20. Kvapil J., Kvapil, J., Kubelka, J., and Autrata, R. The Role of Iron Ions in YAG and YAP. *Cryst. Res. Technol.*, 1983, vol. 18, pp. 127–131.

DOI: 10.1002/crat.2170180120

21. Kühn Henning, Fredrich-Thornton Susanne T., Kränkel Christian, Peters Rigo, Petermann Klaus. Model for the calculation of radiation trapping and description of the pinhole method. *Opt. Lett.*, 2007, vol. 32, pp. 1908–1910. **DOI:** 10.1364/OL.32.001908

22. Sumida D.S., Fan T.Y. Effect of radiation trapping on fluorescence lifetime and emission cross section measurements in solid-state laser media. *Opt. Lett.*, 1994, vol. 19, pp. 1343–1345. **DOI:** 10.1364/OL.19.001343

23. Kisel V.E., Kurilchik S.V., Yasukevich A.S., Grigoriev S.V., Smirnova S.A., Kuleshov N.V. Spectroscopy and femtosecond laser performance of Yb³⁺:YAlO₃ crystal. *Opt. Lett.*, 2008, vol. 33, p. 2194.

DOI: 10.1364/OL.33.002194

24. Yasyukevich A.S., Shcherbitskii V.G., Kisel V.E., Mandrik A.V., Kuleshov N.V. Integral method of reciprocity in the spectroscopy of laser crystals with impurity centers. *Journal of Applied Spectroscopy*, 2004, vol. 71, no. 2, pp. 202–208.

DOI: 10.1023/B:JAPS.0000032875.04400.a0

25. Alexander Rudenkov, Viktor Kisel, Anatol Yasukevich, Karine Hovhannesian, Ashot Petrosyan, Nikolay Kuleshov. Spectroscopy and continuous wave laser performance of Yb³⁺:LuAlO₃ crystal. *Opt. Lett.*, 2016, vol. 41, pp. 5805–5808.

DOI: 10.1364/OL.41.005805

26. Alexander Rudenkov, Viktor Kisel, Anatol Yasukevich, Karine Hovhannesian, Ashot Petrosyan, Nikolay Kuleshov. Yb³⁺:LuAlO₃ crystal as a gain medium for efficient broadband chirped pulse regenerative amplification, *Opt. Lett.*, 2017, vol. 42, pp. 2415–2418.

DOI: 10.1364/OL.42.002415

27. Rubtsova N.N., Borisov G.M., Ledovskikh D.V., Kovalyov A.A., Preobrazhenskii V.V., Putyato M.A., Semyagin B.R., Kisel V.E., Rudenkov A.S., Kuleshov N.V., Pavlyuk A.A. Fast mirrors for femtosecond passive mode-locked near-infrared lasers. *Laser Phys.*, 2016, vol. 26, p. 125001.

DOI: 10.1088/1054-660X/26/12/125001

Measurement Stand, Method and Results of Composite Electrotechnical Pressboard-Mineral Oil Electrical Measurements

P. Rogalski

Lublin University of Technology,
Nadbystrzycka str., 38A, Lublin 20-618, Poland

Received 21.07.2020

Accepted for publication 03.09.2020

Abstract

The paper presents a measuring stand designed and built for testing direct and alternating current properties of power transformers basic insulation component i.e. electrotechnical pressboard impregnated with transformer oil. Measurements of direct and alternating current parameters are performed using the frequency domain spectroscopy and polarization depolarization current methods.

The measuring station includes a specially developed climatic chamber which is characterized by high accuracy of temperature stabilization and maintenance during several dozen hours of measurements. The uncertainty of temperature maintaining during several dozen hours of measurements does not exceed ± 0.01 °C. The computer software developed to control the station allows for remote measurements, changes in supply voltage and temperature settings and acquisition of the obtained results. A new type of measuring capacitor was developed and manufactured, the structure of which significantly reduces the chance of samples contamination during measurements. By increasing the accuracy of temperature stabilization during measurements, the resolution of measurement temperatures was increased, at which it is possible to perform measurements with the frequency domain spectroscopy and polarization depolarization current methods. This allowed to reduce the step of measurement temperature change and thus to increase the accuracy of determining the activation energy of the measured parameters.

The article also contains basic information on the analysis of the direct and alternating current electrical parameters of the composite electrotechnical pressboard-mineral oil-water nanoparticles. The results of several direct and alternating current parameters measurements of a transformer oil impregnated pressboard sample with a moisture content of (5.2 ± 0.1) % by weight obtained by the use of a measuring stand are presented as examples.

Keywords: AC and DC measurements by FDS and PDC methods, electrotechnical pressboard, insulating oil.

DOI: 10.21122/2220-9506-2020-11-3-187-195

Адрес для переписки:

P. Rogalski
Lublin University of Technology,
Nadbystrzycka str., 38A, Lublin 20-618, Poland
e-mail: p.rogalski@pollub.pl

Address for correspondence:

P. Rogalski
Lublin University of Technology,
Nadbystrzycka str., 38A, Lublin 20-618, Poland
e-mail: p.rogalski@pollub.pl

Для цитирования:

P. Rogalski.
Measurement Stand, Method and Results of Composite Electrotechnical Pressboard-Mineral Oil Electrical Measurements.
Приборы и методы измерений.
2020. – Т. 11, № 3. – С. 187–195.
DOI: 10.21122/2220-9506-2020-11-3-187-195

For citation:

P. Rogalski.
Measurement Stand, Method and Results of Composite Electrotechnical Pressboard-Mineral Oil Electrical Measurements.
Devices and Methods of Measurements.
2020, vol. 11, no. 3, pp. 187–195.
DOI: 10.21122/2220-9506-2020-11-3-187-195

Установка, методика и результаты измерений электрических параметров композита электротехнический картон-трансформаторное масло

П. Рогальски

Люблинский технический университет,
ул. Надбыстрицкая, 38А, Люблин 20-618, Польша

Поступила 21.07.2020

Принята к печати 03.09.2020

В работе представлена разработанная и изготовленная установка для исследования одной из главных составляющих изоляции энергетических трансформаторов – электротехнического картона, пропитанного трансформаторным маслом.

В состав установки входит специально разработанная климатическая камера с высокой точностью измерения, стабилизации и поддержания в течение длительного времени температуры. Точность поддержания и измерения температуры в течение нескольких десятков часов измерений не превосходит $\pm 0,01$ °С. Электрические измерения на постоянном токе выполнены с использованием метода токов поляризации и депольаризации (англ. *Polarization Depolarization Current*, сокр. *PDC*), а на переменном токе – методом импедансной спектроскопии (англ. *Frequency Domain Spectroscopy*, сокр. *FDS*). Управление работой установки и процессом измерений осуществляется с помощью разработанной компьютерной программы, которая позволяет дистанционно проводить измерения, изменять вид измерений, величины напряжения и температуры, а также регистрировать результаты измерений.

Разработан и изготовлен измерительный конденсатор нового типа, конструкция которого значительно уменьшает вероятность загрязнения образцов в процессе измерений. Благодаря увеличению точности стабилизации и поддержания температуры во время измерений уменьшен шаг изменения температуры при измерениях методами *FDS* и *PDC*. Это позволило увеличить точность определения энергии активации измеряемых параметров.

Представлена также основная информация по анализу результатов измерений на постоянном и переменном токе композита – электротехнический картон, пропитанный трансформаторным маслом, содержащим нанокapли воды. В качестве примера представлены результаты нескольких измерений основных параметров электротехнического картона, пропитанного трансформаторным маслом, содержащим нанокapли воды в концентрации $(5,2 \pm 0,1)$ % вес., полученные на установке.

Ключевые слова: измерения на постоянном и переменном токе методами *FDS* и *PDC*, электротехнический картон, трансформаторное масло.

DOI: 10.21122/2220-9506-2020-11-3-187-195

Адрес для переписки:

P. Rogalski
Lublin University of Technology,
Nadbystrzycka str., 38A, Lublin 20-618, Poland
e-mail: p.rogalski@pollub.pl

Address for correspondence:

P. Rogalski
Lublin University of Technology,
Nadbystrzycka str., 38A, Lublin 20-618, Poland
e-mail: p.rogalski@pollub.pl

Для цитирования:

P. Rogalski.
Measurement Stand, Method and Results of Composite Electrotechnical Pressboard-Mineral Oil Electrical Measurements.

Приборы и методы измерений.

2020. – Т. 11, № 3. – С. 187–195.

DOI: 10.21122/2220-9506-2020-11-3-187-195

For citation:

P. Rogalski.
Measurement Stand, Method and Results of Composite Electrotechnical Pressboard-Mineral Oil Electrical Measurements.

Devices and Methods of Measurements.

2020, vol. 11, no. 3, pp. 187–195.

DOI: 10.21122/2220-9506-2020-11-3-187-195

Introduction

For over a century cellulose in form of paper and pressboard impregnated with mineral oil is a mainly used material for power transformers insulation. It is related to good electrical parameters and cost efficiency of cellulose-mineral oil composite. This kind of insulation is usually called paper-oil or liquid-solid insulation. The main source of this type of insulation malfunction is increase of cellulose water content. At the beginning of transformer operation water level of cellulose is usually lower than 0.8 %. With years of the device operation water penetrates seals of transformer, solutes in oil and then is transported by it to the solid component of insulation. After exceeding 5 % of water content in pressboard or paper the catastrophic breakdown of transformer is only a matter of time. Recently it was discovered that water in cellulose insulation occurs in form of nanodrops [1] creating cellulose-mineral oil-water nanodrops composite.

Due to the fact that transformers are hermetic devices extraction of insulation sample is impossible. Because of that reason nowadays a lot of effort is made to develop non-destructive methods of paper and pressboard moisture level determination [2]. The most popular are electrical methods. They can be classified into two basic group. The first one includes methods based on measurements in the time domain like the return voltage measurement (RVM) [3, 4] and polarization-depolarization current (PDC) measurement [5], [6] while in the second one there are methods based on measurements using frequency-domain spectroscopy (FDS) [7, 8].

Presented in this article measurement stand enables usage of FDS and PDC method. Due to the low accuracy of temperature stabilization, so far in research of temperature impact on solid-liquid electrical parameters it was necessary to use results for a large temperature differences, for example $\Delta T = 30\text{ }^{\circ}\text{C}$ [9]. By increase of thermal stabilization accuracy during the FDS and PDC measurements of composite cellulose-mineral oil-water nanodrops, it became possible to increase the concentration of the measurements performed in a function of temperature to $\Delta T = 8\text{ }^{\circ}\text{C}$. Usually FDS measurements are made in frequency range from 100 μHz to 5 kHz, with 3 points per decade resolution. A further rise in accuracy was obtained by increasing the number of measurement points per decade to 10 for the frequency range from 1 MHz to 5 kHz and 5 for the frequency range from 100 μHz to 1 MHz.

The aim of this study was to develop a new measurement stand for precise tests of direct and alternating current parameters of the composite electrotechnical pressboard-transformer oil-water nanodrops in a wide range of measurement temperatures, the maintenance accuracy of which is below $\pm 0.01\text{ }^{\circ}\text{C}$. And to present selected measurement results for a sample with a moisture content of 5.2 % by wt.

The new polarization depolarization current and frequency domain spectroscopy measurement stand

Figure 1 shows a diagram with basic elements of the measuring stand. The stand includes: climatic chamber, measuring capacitor with a sample in glass vessel, Omicron Dirana FDS Analyzer, Agilent data acquisition unit with a PT100 temperature sensor, a computer with control and recording software.

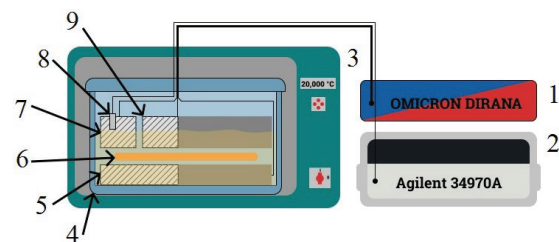


Figure 1 – Diagram of the stand for the measurements of direct and alternating current electrical properties of liquid-solid insulation: 1 – Dielectric Response Analyzer Omicron Dirana; 2 – Agilent 34970a data acquisition unit; 3 – climatic chamber; 4 – glass vessel; 5 – measuring electrode; 6 – sample of oil-impregnated pressboard; 7 – guard electrode; 8 – PT100 temperature sensor; 9 – voltage electrode

The measurement of dielectric response analysis is made by Omicron Dirana FDS meter. The device is equipped with voltage source with maximum output voltage amplitude of 200 V and maximum output current of 50 mA. The voltage source is capable of outputting direct voltage and alternating voltage in frequency range 10 μHz –5 kHz. The meter can measure dissipation factor value up to 100, with accuracy $1\% \pm 3 \cdot 10^{-4}$ and capacitance in range from 10 pF to 100 μF , with accuracy of $0.5\% \pm 1\text{ pF}$. Furthermore, the device is capable of direct current measurement in range of $\pm 10\text{ mA}$, with accuracy of $0.5\% \pm 1\text{ pA}$, which is used in PDC measurements. The meter work is fully supervised by computer software. The Dirana FDS meter is

capable of performing in field measurements on number of devices such as: power transformers, autotransformers, bushings, cables, current and voltage transformers and electric motors, by using predefined setups. Due to high electromagnetic interference in case of infield measurements, the meter is equipped in advance noise suppression functions. Which facilitates measurements both in the laboratory and in the field conditions.

For the need of the measuring station, a three-electrode measuring capacitor was designed and manufactured. It was built only of aluminum, and as an insulator in between guarded and unguarded electrode air gap was used. Before measurement, capacitor is placed in glass cylindrical vessel, which dimensions are few millimeters bigger than capacitor itself. Small volume of oil in the vessel reduces chances of moisture migration between oil and pressboard during measurements performed in different temperatures, due to changes of water solubility in oil. After putting a sample of oil impregnated pressboard into the capacitor, air gap is filled with oil in which the sample was stored. All electrical connections are made of silver plated copper wire without any insulation. This approach is to eliminate potential measured sample contamination. At the end the vessel with the capacitor is hermetically closed.

Temperature value is measured by Agilent 34970a data acquisition unit with use of PT100 sensor in time intervals of 1 s.

The specificity of the measurements requires high accuracy of temperature stabilization during the measurement. In order to obtain this objective, it was decided to build a climate chamber. For this purpose, it was decided to modernize an old stove that was once used for material testing. The housing and heating elements have remained from the old device. The electronic control system was redesigned and made. The new control system includes: the LCD display that allows to monitor the current parameters of the chamber, the keyboard for entering settings, the solid state relay (SRT) as an executive element, the 12 V DC stabilized power supply and the main controller board. Electronic circuit, printed circuit board and software of controller was made. The heart of the controller is the ATMEGA368 microcontroller. The temperature is measured using the four-wire method with use of a PT1000 sensor. The MCP3550-50 Single-Channel 22-Bit Delta-Sigma ADC chip is responsible for the conversion of the analog voltage signal representing temperature to digital form, and then sending its value to the

microcontroller via SPI bus 11 times per minute. Based on the obtained temperature value and using PID algorithm, the microcontroller controls SRT to regulate the power of the heater inside the chamber. For precise control of the heater's power, phase control was used. To make its realization possible, the controller board is equipped with a mains voltage zero crossing detection circuit. Inside the chamber five small fans were used for fast and even heat distribution. In order to achieve temperatures lower than the ambient temperature, it was necessary to use a cold air source. For this purpose, a small freezer was used, which was connected to the climate chamber with two thermally insulated pipes. One of them is equipped with a fan forcing cold air to flow into the chamber. The rotational speed of the fan is supervised by the main controller. The operation of the freezer is steered by a relay located on the controller board. The device is equipped with three independent thermal fuses. One software and two physical in two different circuits. The overheating protections will react selectively after exceeding the temperature of 100 °C. This threshold level was selected due to the flammability of measured mineral oils. The climatic chamber can be controlled via the USB bus by a computer. For this purpose, a Windows Forms Application software was developed, which enables the display of the current temperature and settings. It also provides the settings entering. In addition, the software allows to program any two actions with a given date and time, for example, in order to switch off or change the chamber settings. Measurements of capacitor temperature in time of FDS and PDC measurements are shown in Figure 2.

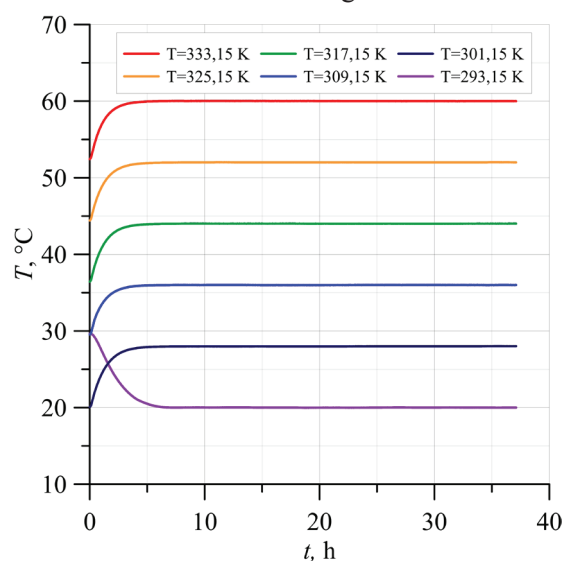


Figure 2 – Time dependence of the measuring capacitor temperature

In order to estimate uncertainty of a temperature stabilization, standard deviation of measured temperatures was calculated (Figure 3). As can be seen in Figure 3, all values of standard deviation are lower than ± 0.01 °C. Higher values of standard deviation for temperature 20 °C and 28 °C than for the rest of temperatures, are caused by on-off cycle of cooling device operation, which is used in this measurements.

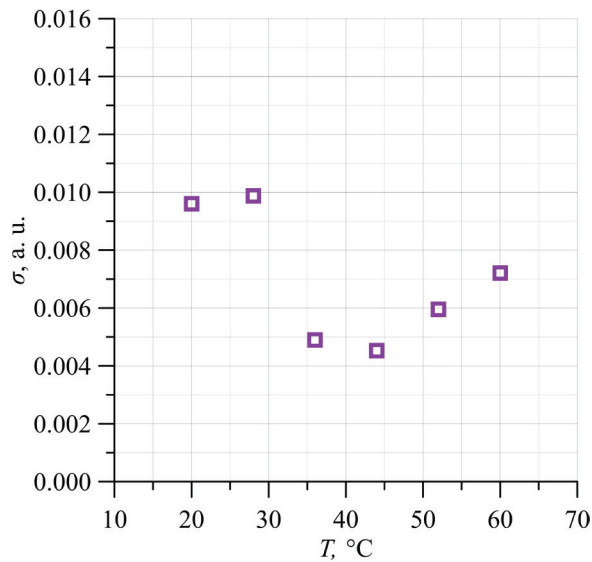


Figure 3 – Measurement uncertainty of temperature stabilization

Fundamentals of the direct and alternating current material parameters analysis of the composite cellulose-transformer oil-water nanoparticles

Direct current conductivity measurements of the composite cellulose-transformer oil-water nanoparticles take place in a three-electrode system [5], in which two electrodes, measuring and voltage, are used to determine the conductivity. The third electrode is designed to conduct the surface current to the ground, characteristic in high-resistance systems. Due to high values of relaxation times in the tested materials, measurements within several hours are necessary to achieve the value of the set current. After obtaining the value of the set current I , the direct current conductivity is determined by the formula:

$$\sigma_{DC} = \frac{I \cdot d}{U \cdot S}, \quad (1)$$

where: I – steady value of current; U – applied voltage; d – pressboard thickness; S – electrode area.

Measurements of the alternating current insulation characteristics of power transformers are performed with FDS meters in a parallel equivalent circuit, shown in the Figure 4a. The phasor diagram for the parallel equivalent circuit is shown in Figure 4b.

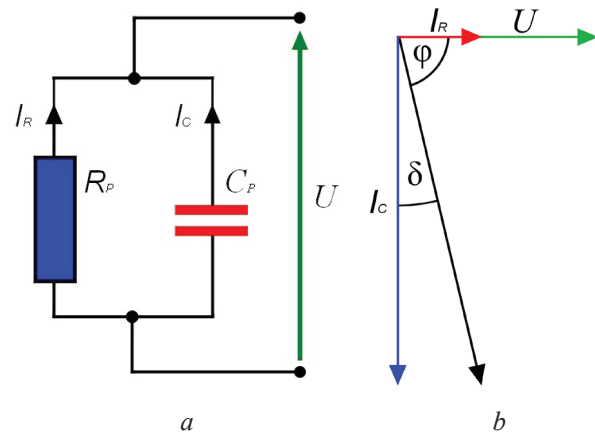


Figure 4 – Parallel equivalent diagram of the insulating material (a): U – supply voltage amplitude; I_R – conduction current amplitude; I_C – displacement current amplitude; R_p – resistance; C_p – capacitance and phasor diagram for the parallel equivalent diagram (b): φ – phase shift angle; δ – loss angle

The second Maxwell equation (generalized Ampere's law) shows that in real dielectric materials a conduction current flows with a density \mathbf{j}_R and a displacement current with a density \mathbf{j}_C , so that [7]:

$$\Delta \times \mathbf{H} = \mathbf{j}_R + \mathbf{j}_C, \quad (2)$$

where: \mathbf{H} – vector of the magnetic field strength; \mathbf{j}_R – conduction current density; \mathbf{j}_C – displacement current density.

In FDS measurements, a sinusoidal forcing electric field with a circular frequency ω is used:

$$\mathbf{E} = \mathbf{E}_0 \sin(\omega t), \quad (3)$$

where: \mathbf{E} – electric field strength; \mathbf{E}_0 – electric field amplitude; ω – circular frequency; t – time.

The conduction current density, falling into the second Maxwell equation, is described by the formula:

$$\mathbf{j}_R(\omega) = \sigma(\omega) \mathbf{E} = \sigma(\omega) \mathbf{E}_0 \sin(\omega t), \quad (4)$$

where $\sigma(\omega)$ – conductivity.

Displacement current density, falling into the second Maxwell equation:

$$j_c(\omega) = \frac{\partial \mathbf{D}}{\partial t} = (\mathbf{D} = \varepsilon_0 \varepsilon' \mathbf{E}) = \omega \varepsilon' \varepsilon_0 \mathbf{E}_0 \sin(\omega t - \frac{\pi}{2}), \quad (5)$$

where: ε' – relative dielectric permittivity; ε_0 – dielectric permittivity of vacuum; \mathbf{D} – electric field induction vector.

The conductivity in equation (4) describes the material's ability to conduct an electric current. The dielectric permittivity ε' in the formula (5) describes the ability of the dielectric to polarize. In impregnated pressboard occurs dependencies of conductivity and permeability on temperature, frequency and moisture. In real dielectrics, the phase shift angle φ ranges from 0° to -90° (Figure 4). Meters designed to measure alternating current parameters of electrical systems, the so-called impedance (admittance) meters measure two basic values characteristic for systems containing passive elements. In the parallel equivalent scheme, these are the values of the phase shift angle φ and the admittance Y :

$$Y = \frac{i}{V}, \quad (6)$$

where: Y – admittance; V – voltage amplitude; i – current amplitude.

Parameters such as conductance G_p and capacitance C_p in a parallel equivalent circuit and the tangent of the loss angle $\tan \delta$ are most often used to analyze the results of in power transformers insulation measurements. The FDS meter calculates these parameters using formulas:

$$G_p = |Y \cos \varphi|; \quad (7)$$

$$C_p = \frac{|Y \sin \varphi|}{\omega}; \quad (8)$$

$$\tan \delta = \frac{1}{|\tan \varphi|} = |\cotan \varphi|. \quad (9)$$

Based on the G_p and C_p values, taking into account the geometrical dimensions of the dielectric material, such as the thickness of the pressboard d and the surface area of the measuring electrode S , the material parameters are calculated using appropriate formulas – conductivity and relative dielectric permittivity, which are included in the second Maxwell equation:

$$\sigma = \frac{G_p d}{S} = \frac{|Y \cos \varphi| d}{S}, \quad (10)$$

where: σ – conductivity; G_p – conductance; d – dielectric thickness; S – voltage electrode surface area.

$$\varepsilon' = \frac{C_p d}{\omega \varepsilon_0 S} = \frac{|Y \sin \varphi| d}{\omega \varepsilon_0 S}, \quad (11)$$

where: C_p – capacitance; ε_0 – dielectric permittivity of vacuum; d – dielectric thickness; S – voltage electrode surface area.

$$\varepsilon'' = \frac{\sigma}{\omega \varepsilon_0} = \frac{|Y \cos \varphi| d}{\omega \varepsilon_0 S}. \quad (12)$$

For the analysis of relaxation processes, the power loss value ε'' , calculated as:

The power loss value is used to develop its dependence on the permeability value, so-called Cole-Cole plots $\varepsilon''(\varepsilon')$. The shape of the Cole-Cole charts is related to the mechanisms of relaxation [10].

The analysis of formulas (4)–(12) shows that the admittance and phase shift angle are the basic measurement parameters determined in the FDS method. On the basis of these values, using the formulas (7)–(12), it is possible to calculate the electrical parameters of cellulose-mineral oil-water nanoparticles composite.

Measurements results of the cellulose-mineral oil-water nanoparticles composite

In the work electrotechnical pressboard and transformer oil with a moisture content of several ppm produced by the world's leading companies, dedicated to the construction for power transformers insulation, were used. A pressboard sample with a moisture content of $5.2 \pm 0.1\%$ by weight was prepared for the tests. The work includes measurements of basic direct and alternating current parameters:

- time dependence of the polarization and depolarization currents and their difference, determining the strength of the resistive current (Figure 5);

- frequency dependence of admittance Y (Figure 6);

- frequency dependence of the phase shift angle φ (Figure 7).

Based on measurements of admittance and phase angle, using the formulas (10)–(12) frequency dependencies of the loss angle tangent $\tan \delta$ (Figure 8), alternating current conductivity σ (Figure 9), permittivity ε' (Figure 10) and power loss value ε'' (Figure 11), were calculated.

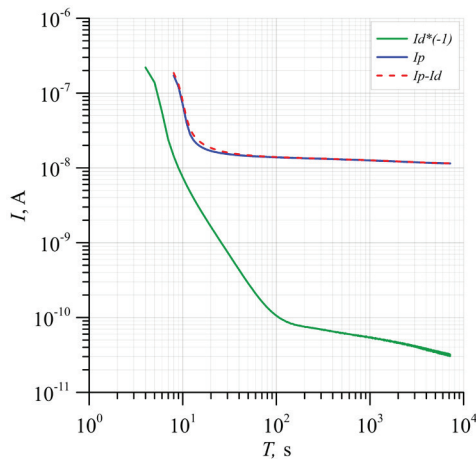


Figure 5 – Time relationships of the polarization current I_p , depolarization current $-I_d$ and their difference $-I_p - I_d$ of the electrotechnical pressboard impregnated with transformer oil with a moisture content of 5.2 % by weight measured at 293.15 K

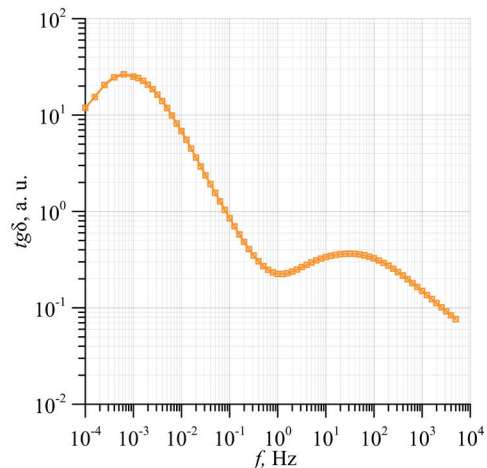


Figure 8 – Frequency dependence of the loss angle tangent of electrotechnical pressboard impregnated with transformer oil with a moisture content of 5.2 % by weight measured at 325.15 K

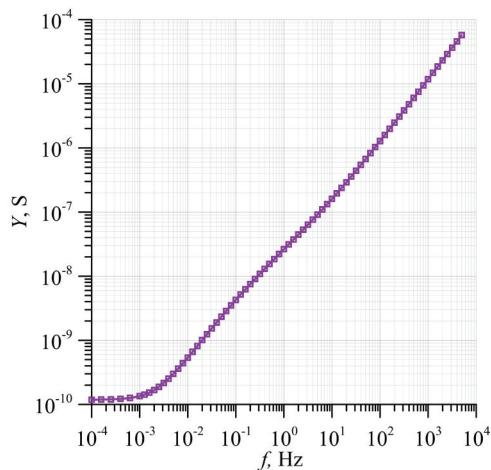


Figure 6 – Frequency dependence of the admittance of electrotechnical pressboard impregnated with transformer oil with a moisture content of 5.2 % by weight measured at 293.15 K

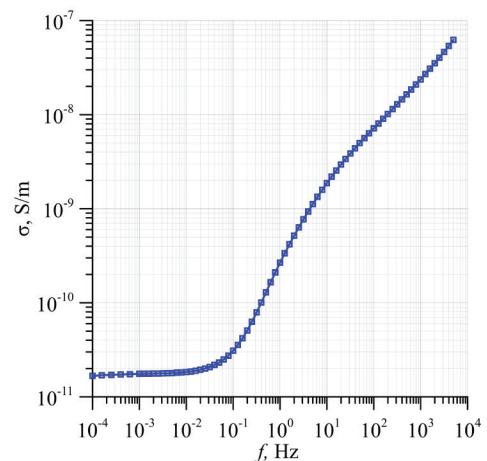


Figure 9 – Frequency dependence of the loss angle tangent of electrotechnical pressboard impregnated with transformer oil with a moisture content of 5.2 % by weight measured at 309.15 K

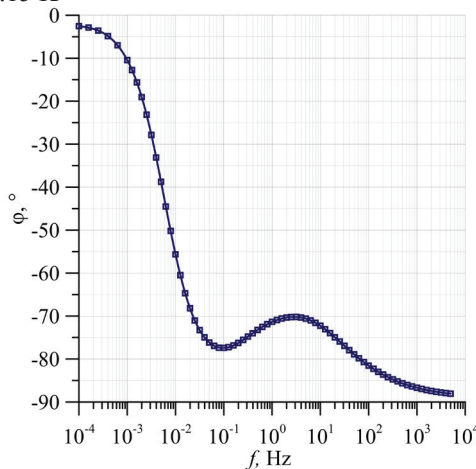


Figure 7 – Frequency dependence of the phase shift angle of electrotechnical pressboard impregnated with transformer oil with a moisture content of 5.2 % by weight measured at 301.15 K

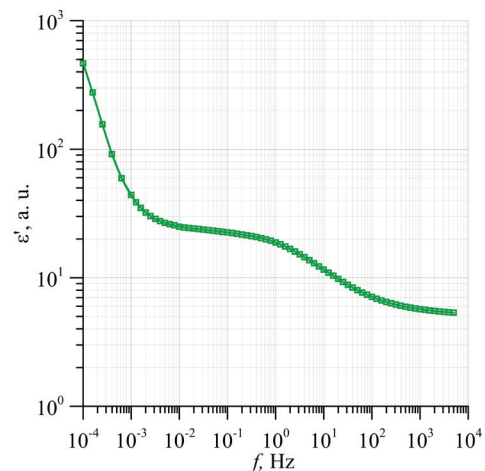


Figure 10 – Frequency dependence of the permittivity of electrotechnical pressboard impregnated with transformer oil with a moisture content of 5.2 % by weight measured at 317.15 K

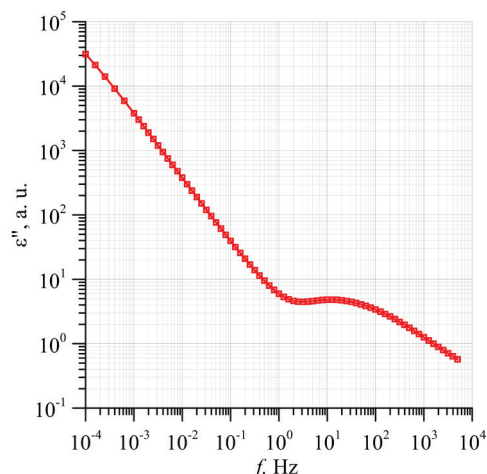


Figure 11 – Frequency dependence of the power loss coefficient of electrotechnical pressboard impregnated with transformer oil with a moisture content of 5.2 % by weight measured at 333.15 K

The shape of the polarization and depolarization current waveforms (Figure 5) is caused by the presence of the sum of two components. The first is the capacitive current that decreases with time, the second is the resistive current that is constant over time. During polarization, after charging is complete, the resistive current that is constant over time can be used to calculate the direct current conductivity. The large changes in the low frequency range visible in the phase shift angle φ (Figure 7), loss angle tangent $\text{tg}\delta$ (Figure 8), permittivity ϵ' (Figure 10) and power loss value ϵ'' (Figure 11) waveforms are caused by the relaxation processes occurring in the water nanoparticles present in the composite electrotechnical pressboard-transformer oil-water nanodrops. The reason for the significant changes in electrical parameters such as admittance Y (Figure 6) and alternating current conductivity σ (Figure 9) in the high frequency range is the phenomenon of hopping conductivity occurring between adjacent potential wells formed by water nanoparticles. The occurrence of water in the composite electrotechnical pressboard-transformer oil-water nanodrops significantly affects the direct and alternating current parameters of the material, thanks to which it is possible to determine its moisture content.

Conclusion

In the paper a new measurement stand for frequency-domain spectroscopy and polarization-depolarization current measurements of oil impregnated pressboard for different temperatures was

presented. The stand includes: climatic chamber; three electrode measuring capacitor with a sample; Omicron Dirana Frequency Domain Spectroscopy and Polarization Depolarization Current Analyzer; Agilent temperature meter with a PT100 temperature sensor; a computer with control and recording software. For the purpose of the stand a new climatic chamber was developed and made. The device allows long term temperature stabilization in range of 0 °C to 100 °C with high accuracy ± 0.01 °C. The use of three independent thermal fuses results in safety operation of the device even without on-site supervision. Equipping the chamber in USB communication with computer and by development of computer software, in combination with meters computer software, enabled fully remote control of the measuring stand. Application of new hermetical three electrode measuring capacitor lowered the chance for sample contamination.

Article presents basics of direct and alternating current material parameters analysis of composite cellulose-transformer oil-water nanodrops based on frequency-domain spectroscopy and polarization-depolarization current measurements. The use of a new climatic chamber with a higher accuracy of temperature stabilization resulted in the possibility of reducing the difference between successive measurement temperatures. Which resulted in the possibility of increasing the number of measurements in the scope of measuring temperatures. Additionally, increasing the number of measurement points per decade increased the accuracy of the measurements. Additionally, by increasing number of measurement points per decade to 10 for the frequency range from 1 mHz to 5 kHz and 5 for the frequency range from 100 uHz to 1 mHz, resulted in increase of measurements accuracy.

The paper presents results of electrical parameters measurements of the composite electrotechnical pressboard-mineral oil-water nanoparticles. The measurements were made on a sample of oil-impregnated pressboard with a moisture content of 5.2 ± 0.1 % by weight.

Acknowledgments

This research was partially supported by the Polish Ministry of Science and Higher Education as a science fund of the Lublin University of Technology, FN-28/E/EE/2020 – Researches of electrical, magnetic, thermal and mechanical

properties of modern electrotechnical and electronic materials, including nanomaterials and diagnostic of electrical devices and their components.

References

1. Żukowski P., Kołtunowicz T.N., Kierczyński K., Subocz J., Szrot M. Formation of water nanodrops in cellulose impregnated with insulating oil. *Cellulose*, 2015, vol. 22, no. 1, pp. 861–866. DOI: 10.1007/s10570-015-0543-0
2. Zhang M., Liu J., Lv J., Chen Q., Qi P., Sun Y., Jia H., Chen X. Improved method for measuring moisture content of mineral-oil-impregnated cellulose pressboard based on dielectric response. *Cellulose*, 2018, vol. 25, no. 10, pp. 5611–5622. DOI: 10.1007/s10570-018-1988-8
3. Zhang T., Li X., Lv H., Tan X. Parameter Identification and Calculation of Return Voltage Curve Based on FDS Data. *IEEE Trans. Appl. Supercond.*, 2014, vol. 24, no. 5, pp. 1–5. DOI: 10.1109/TASC.2014.2344763
4. Żukowski P., Kołtunowicz T.N., Gutten M., Janura R., Korenciak D., Sebok M. Diagnostics of transformer with insulation oil-paper. *Przegląd Elektrotechniczny*, 2015, vol. 91, no. 8, pp. 69–72 [Online]. Available: <http://pe.org.pl/articles/2015/8/18.pdf>
5. Żukowski P., Kołtunowicz T.N., Kierczyński K., Subocz J., Szrot M., Gutten M. Assessment of water content in an impregnated pressboard based on DC conductivity measurements. Theoretical assumptions. *IEEE Trans. Dielectr. Electr. Insul.*, 2014, vol. 21, no. 3, pp. 1268–1275. DOI: 10.1109/TDEI.2014.6832274
6. Zenker M., Kierczyński K. The influence of electric field intensity on the activation energy of the DC conductivity the electrical pressboard of impregnated with synthetic ester. In *Photonics Applications in Astronomy, Communications, Industry, and High Energy Physics Experiments*, 2017, vol. 10445, p. 104455Q. DOI: 10.1117/12.2280735
7. Żukowski P., Kołtunowicz T.N., Kierczyński K., Rogalski P., Subocz J., Szrot M., Gutten M., Sebok M., Jurcik J. Permittivity of a composite of cellulose, mineral oil, and water nanoparticles: theoretical assumptions. *Cellulose*, 2016, vol. 23, no. 1, pp. 175–183. DOI: 10.1007/s10570-015-0797-6
8. Żukowski P., Kołtunowicz T.N., Kierczyński K., Rogalski P., Subocz J., Szrot M., Gutten M., Sebok M. Dielectric losses in the composite cellulose-mineral oil-water nanoparticles: theoretical assumptions. *Cellulose*, 2016, vol. 23, no. 3, pp. 1609–1616. DOI: 10.1007/s10570-016-0934-x
9. Żukowski P., Kołtunowicz T.N., Kierczyński K., Subocz J., Szrot M., Gutten M., Sebok M., Jurcik J. An analysis of AC conductivity in moist oil-impregnated insulation pressboard. *IEEE Trans. Dielectr. Electr. Insul.*, 2015, vol. 22, no. 4, pp. 2156–2164. DOI: 10.1109/TDEI.2015.004606
10. Seifert J.M., Stietzel U., Kaerner H.C. Ageing of composite insulating materials – new possibilities to detect and to classify ageing phenomena with dielectric diagnostic tools. In *Conference Record of IEEE International Symposium on Electrical Insulation*, 1998, vol. 2, pp. 373–377. DOI: 10.1109/elinsl.1998.694812

Application of the Correlation Velocity Measurements for Hydrodynamic Investigations of Turbulent Coolant Flow in Nuclear Reactor Elements

I.A. Konovalov, A.E. Khrobostov, M.A. Legchanov, D.N. Solncev, A.A. Barinov, A.V. Ryazanov, A.A. Chesnokov, M.A. Makarov

Nizhny Novgorod State Technical University n.a. R.E. Alekseev,
Minin str., 24, Nizhny Novgorod 603950, Russia

Received 29.06.2020

Accepted for publication 28.08.2020

Abstract

The method of correlation measurement of the coolant flow rate, widely used for operational diagnostics of nuclear power plants, can be extensively used in research practice. The aim of this work was to apply a correlation method based on the conductometric measurement system with wire-mesh sensors for measuring a coolant flow rate.

Insignificant concentration of a salt solution (NaCl or Na₂SO₄) creates a gradient of the conductivity in the flow, which is used as a passive scalar measured by the system. Authors used turbulent pulsations at the interface of two concurrent flows with identical velocities in a square channel as a signal source for the correlation method. The paper presents the methodology of the tests, test facility description, signal-to-noise ratio estimation, the results of digital signal processing and comparison of the measured velocities in the model with the flowrate-averaged velocity determined by the use of flowmeters. The measured velocity values give acceptable agreement for the turbulent flow modes. It was shown that the measurement accuracy drops sharply for low-Reynolds flows.

The obtained results were used for flowrate measurements in core-imitator channels of the nuclear reactor test model.

The presented paper is an approbation of this approach for its application as part of a test model of a nuclear reactor in order to determine the each duct flow rates in the channels of the core simulator using wire mesh sensors.

Keywords: measuring system, correlation flowmeter, spatial conductometry, modeling of processes in the elements of nuclear power units.

DOI: 10.21122/2220-9506-2020-11-3-196-203

Адрес для переписки:

И.А. Коновалов
Нижегородский государственный технический университет,
ул. Минина, 24, г. Нижний Новгород 603950, Россия
e-mail: iliakonowaloff@yandex.ru

Address for correspondence:

I.A. Konovalov
Nizhny Novgorod State Technical University,
Minin str., 24, Nizhny Novgorod 603950, Russia
e-mail: iliakonowaloff@yandex.ru

Для цитирования:

I.A. Konovalov, A.E. Khrobostov, M.A. Legchanov, D.N. Solncev, A.A. Barinov, A.V. Ryazanov, A.A. Chesnokov, M.A. Makarov.
Application of the Correlation Velocity Measurements for Hydrodynamic Investigations of Turbulent Coolant Flow in Nuclear Reactor Elements.
Приборы и методы измерений.
2020. – Т. 11, № 3. – С. 196–203.
DOI: 10.21122/2220-9506-2020-11-3-196-203

For citation:

I.A. Konovalov, A.E. Khrobostov, M.A. Legchanov, D.N. Solncev, A.A. Barinov, A.V. Ryazanov, A.A. Chesnokov, M.A. Makarov.
Application of the Correlation Velocity Measurements for Hydrodynamic Investigations of Turbulent Coolant Flow in Nuclear Reactor Elements.
Devices and Methods of Measurements.
2020, vol. 11, no. 3, pp. 196–203.
DOI: 10.21122/2220-9506-2020-11-3-196-203

УДК 621.039

Применение корреляционного метода определения скорости потока теплоносителя при исследованиях гидродинамики турбулентных потоков в элементах ядерных реакторов

И.А. Коновалов, А.Е. Хробостов, М.А. Легчанов, Д.Н. Солнцев, А.А. Баринов,
А.В. Рязанов, А.А. Чесноков, М.А. Макаров

Нижегородский государственный технический университет имени Р.Е. Алексеева,
ул. Минина, 24, г. Нижний Новгород 603950, Россия

Поступила 29.06.2020

Принята к печати 28.08.2020

Корреляционный метод измерения расхода теплоносителя, широко применяемый для эксплуатационной диагностики ядерных энергетических установок, может находить широкое применение в том числе и в исследовательской практике. Целью данной работы являлась отработка корреляционного метода измерения расхода теплоносителя с применением кондуктометрических систем.

В работе представлен вариант применения корреляционного метода для исследования турбулентных потоков на основе кондуктометрической измерительной системы – пространственных кондуктометров сетчатой конструкции. В качестве пассивной примеси используется незначительная концентрация раствора соли (NaCl или Na₂SO₄), создающей градиент проводимости среды, регистрируемый кондуктометрической системой. В качестве переносимых возмущений в работе используются турбулентные пульсации на границе раздела двух спутных струй с одинаковыми скоростями в канале квадратного сечения. Представлена методика проведения исследований на лабораторном стенде, результаты оценки отношения сигнал–шум измерительной системы, проведена обработка сигналов пространственных датчиков и сравнение измеренной скорости в модели со среднерасходной скоростью, определяемой с помощью показаний расходомеров стенда.

Результаты измерений дают приемлемое согласие с показаниями штатных расходомеров для характерных турбулентных режимов течения (погрешность измерения скорости потока при помощи кондуктометров составляет менее 5 %). Показано, что точность измерений резко падает для потоков с низким числом Рейнольдса.

Представленная работа является апробацией данного подхода для его применения в составе экспериментальной модели ядерного реактора с целью определения поканальных расходов в каналах имитатора активной зоны при помощи сетчатых кондуктометрических датчиков.

Ключевые слова: измерительная система, корреляционный расходомер, пространственная кондуктометрия, моделирование процессов в элементах ЯЭУ.

DOI: 10.21122/2220-9506-2020-11-3-196-203

Адрес для переписки:

И.А. Коновалов
Нижегородский государственный технический университет,
ул. Минина, 24, г. Нижний Новгород 603950, Россия
e-mail: iliakonowaloff@yandex.ru

Address for correspondence:

I.A. Konovalov
Nizhny Novgorod State Technical University,
Minin str., 24, Nizhny Novgorod 603950, Russia
e-mail: iliakonowaloff@yandex.ru

Для цитирования:

I.A. Konovalov, A.E. Khrobostov, M.A. Legchanov, D.N. Solncev,
A.A. Barinov, A.V. Ryazanov, A.A. Chesnokov, M.A. Makarov.
Application of the Correlation Velocity Measurements
for Hydrodynamic Investigations of Turbulent Coolant
Flow in Nuclear Reactor Elements.
Приборы и методы измерений.
2020. – Т. 11, № 3. – С. 196–203.
DOI: 10.21122/2220-9506-2020-11-3-196-203

For citation:

I.A. Konovalov, A.E. Khrobostov, M.A. Legchanov, D.N. Solncev,
A.A. Barinov, A.V. Ryazanov, A.A. Chesnokov, M.A. Makarov.
Application of the Correlation Velocity Measurements
for Hydrodynamic Investigations of Turbulent Coolant
Flow in Nuclear Reactor Elements.
Devices and Methods of Measurements.
2020, vol. 11, no. 3, pp. 196–203.
DOI: 10.21122/2220-9506-2020-11-3-196-203

Introduction

In the modern designs of nuclear power plants a special attention is paid to improve the reliability, safety and economy of the operation. These requirements dictate the need for experimental studies on large-scale models of elements of nuclear power plants [1], which in turn raises the question of the development of new control systems for the most important parameters of the reactor plant (RP) which include the flow rate of the coolant in various elements of nuclear power plants.

Currently known is the correlation method for measuring the flow rate of the coolant, the main requirement of which is the presence of some passive scalar flow function, convectively transferred along with the current mass. It allows one to implement correlation measurements using various methods for measuring flow properties: temperature, content of radioactive isotopes, optically distinguishable impurities, etc. [2].

In nuclear power, the correlation method is used to determine the flow rates in the loops of a reactor plant. It is based on the analysis of the readings of detectors of gamma radiation caused by the activation of the O^{16} isotope in the neutron field

of the core [3]. In the Russian nuclear power industry, this method was first applied to measure the flow rate of the primary circuit of a channel reactor [4]. Later in the prototype of the system for correlation control of the coolant flow rate of the pressure vessel reactor installed reactor at the Kalinin nuclear power plant [5], [6].

However, this method cannot be applied for laboratory studies of the reactor thermohydraulics, since there are no necessary radionuclides in the simulated flow. This problem can be solved by a measuring system based on the conductometric sensors widely used in research practice with a hydrodynamically passive admixture protruding as a tracer.

The purpose of this work was to develop a correlation method for measuring the flow rate of a heating agent using conductometric systems.

Test facility

The general circuit of the TF (Figure 1) allows to perform experiments with isothermal mixing in an open circulation loop (with the use of flows with different concentrations of impurities) and non-isothermal mixing when using flows with different temperatures.

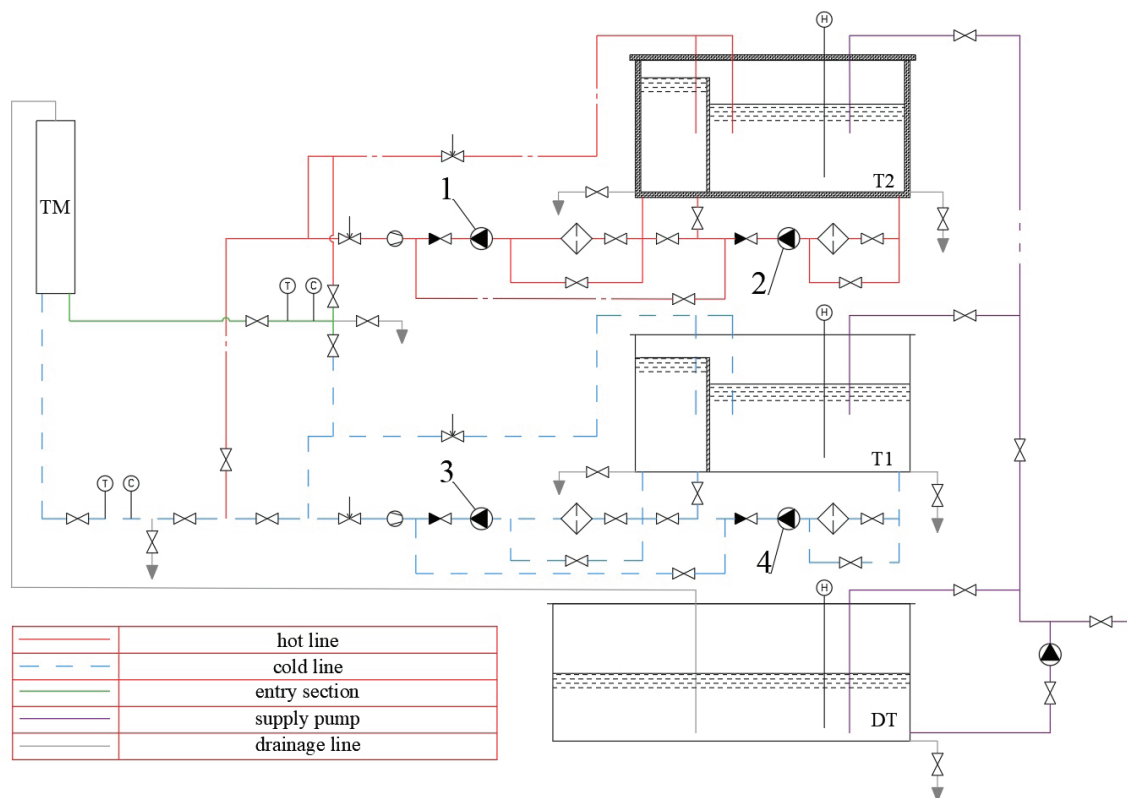


Figure 1 – Hydraulic diagram of the test facility: 1 – hot line circulation pump; 2 – hot line supply pump; 3 – cold line circulation pump; 4 – cold line supply pump; T1 – cold tank; T2 – hot tank; DT – drainage tank; TM – test model

The mixed streams are supplied by the boost pumps (2 and 4) to the constant level tank volumes, from which they are fed to the suction side of the circulation pumps (1 and 3). This solution provides a constant hydrostatic pressure at the suction of the pumps, which is one of the main criteria to maintain the stationary mixing process. Further, the streams are pumped along the supply lines through the test model and enter the drainage tank. The valves of the supply line assumes the possibility of the fluid from each tank to enter the upper or lower branch pipes of the model, or to direct a fluid from one of the tanks to both branch pipes.

The equipment of the TF makes it possible to create both laminar and turbulent flow mode (with Re from 900 to $12 \cdot 10^3$) at different temperatures, flow rates and concentration of impurities in the coolant flow. The main characteristics of the TF are shown in Table 1.

Table 1

Main parameters of the test facility

Parameter	Value
The total power of the heaters, kW	12
Flow through test model, m ³ /hr	up to 2.9
Temperature of the mixing flows, °C	10–60

The measuring system of the TF consists of a technological part, which is necessary to control the mode parameters of the installation, and the research part, which is necessary for measuring the physical characteristics in the zone of turbulent flow mixing [7].

The measurements were carried out by method of conductometry using two wire mesh sensors (WMS) with location of cells 8×8 and a step between the centers of adjacent cells of 5 mm [8].

The output current of the measuring system is proportional to the electrical conductivity, which depends on the salt content in the measuring cells of the WMS. Before the measurements, the WMS cells were calibrated to eliminate common and systematic errors in measuring electrical conductivity.

Measuring principle

The measurements were carried out in a test model with a square cross section of 50×50 mm, the general view of which is shown in Figure 2. The WMSs were installed in a zone of intensive mixing at axial distance of 500 mm.

The mass flow rate measurements were performed in the range from $0.173 \text{ m}^3/\text{h}$ ($Re = 900$) to $2.64 \text{ m}^3/\text{h}$ ($Re = 12 \cdot 10^3$). The actual flow rate was recorded using individually calibrated flow meters [4].

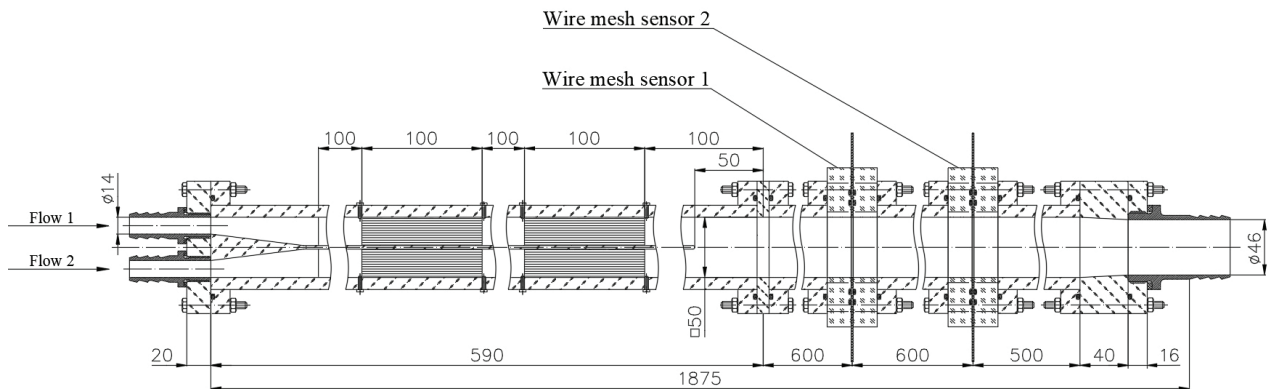


Figure 2 – Test model

The basis of the used flow measurement method is to determine the time of transport of the turbulent fluctuations between two WMS. For this purpose, an algorithm of cross-correlation (CCF) between the electric conductivities $X(t)$ and $Y(t)$, determined by the WMS was used. The discrete CCF of time sequences $X(t)$ and $Y(t)$ was calculated as follows:

$$R_k(X, Y) = \frac{1}{\sqrt{R_{xx}(0)R_{yy}(0)}} \cdot \frac{1}{N} \sum_{t=0}^{N-k-1} x_t \cdot y_{t+k}, \quad (1)$$

where: $\frac{1}{\sqrt{R_{xx}(0)R_{yy}(0)}}$ – CCF normalization parameter;
 x_t – electrical conductivity obtained from the first WMS;
 y_{t+k} – electrical conductivity obtained from the second WMS ($t+k$); k – shift by time

axis; N – number of counting in implementation; $k = 0, 1, \dots, N - 1$ – sample numbers.

Because of the measurements were carried out using WMS, after applying the specified algorithm, an array of velocities in the measuring cells of the WMS was obtained. The cell numbering is shown in Figure 3.

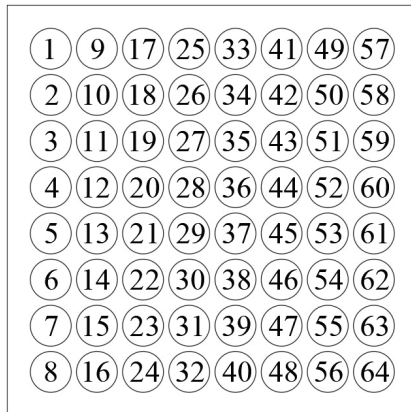


Figure 3 – Measuring cells of WMS

The obtained velocity values depend on the position of the measuring cells in the channel section. This happened because the intensity of the turbulent pulsations in the center of the channel is greater than at the periphery, as a result of which the cross-correlation between the readings of electrical conductivity between the central cells of the sensors is much stronger than between the peripheral ones.

By this reason, the assessment of the integral characteristic of the velocity over the channel section of the test model was carried out using weight coefficients:

$$w = \frac{\sum \omega_i \cdot w_i}{\sum \omega_i}, \quad (2)$$

where: i – WMS cell number; ω_i – weight coefficient of i -th cell; w_i – flow rate in the i -th measuring cell.

In this case, the contribution of a particular cell to the integral estimate of the velocity will be proportional to the variance and the correlation coefficient between the readings of the electrical conductivity of the first and second WMSs in the i -th measuring cell. Based on this, the weight coefficients for each cell were calculated as follows:

$$\omega_i = (\sigma_i^2) \cdot \rho_i, \quad (3)$$

where: σ_i^2 – variance of readings in the i -th measuring cell; $\rho_i = \max(|R_k(X, Y)|)$ – correlation coefficient between the readings in the i -th measuring cell of the first and second WMS.

Measurement results

As a result of the measurements, instantaneous and averaged values of electrical conductivity at the cells of the sensors were obtained. Figure 4 shows an example of the measured conductivity in test with $Re = 12 \cdot 10^3$.

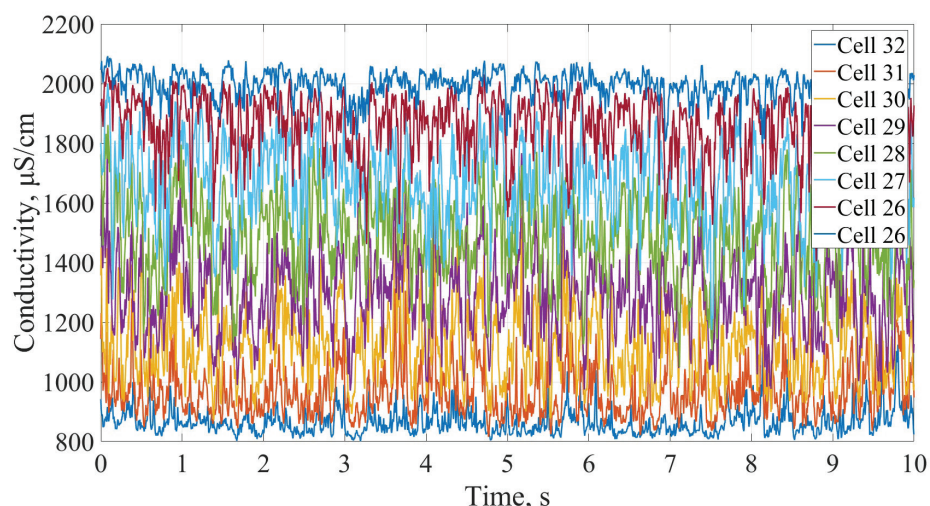


Figure 4 – Example of the electrical conductivity data in test with $Re = 12 \cdot 10^3$

Figure 5 shows the distribution of the averaged electrical conductivity over the measuring cells for the data in test $Re = 12 \cdot 10^3$ and $Re = 900$.

The presence of a sharp leap in the conductivity for $Re = 900$ indicates the absence of mixing of

flows in this test. Conversely, the smooth distribution of conductivity over the cells with a simultaneous shift of the maximum readings to the center indicates a significant intensity of turbulent pulsations in the test with $Re = 12 \cdot 10^3$.

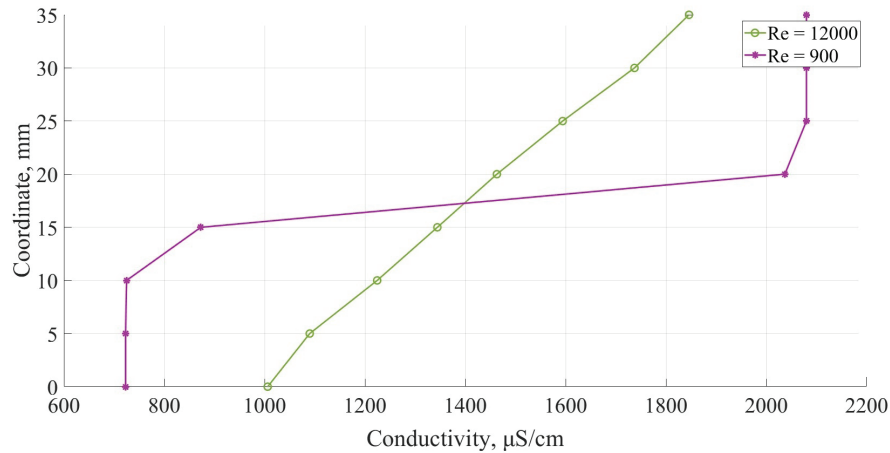


Figure 5 – Averaged electrical conductivity in measuring cells in tests with $Re = 12 \cdot 10^3$ and $Re = 900$

The first objective was to assess the effect of noise on the measurement results. To obtain this estimate the electrical conductivity in a flow without a tracer was measured. Further, based on the analysis of the power spectral density (PSD) and the estimation of the main vortex frequencies noise intensity and its frequency band were obtained. In this case, the assessment noise frequency band was $f_{noise} = 61$ Hz.

The resulting periodograms are shown in Figure 6.

Further correlation measurements were carried out using a digital low-pass filter with a passband $f_{stop} = 40$ Hz.

Figure 7 shows a view of the wire mesh sensor realization after passing through a low-pass filter. The signal shape for the central cells shows a high level of their correlation.

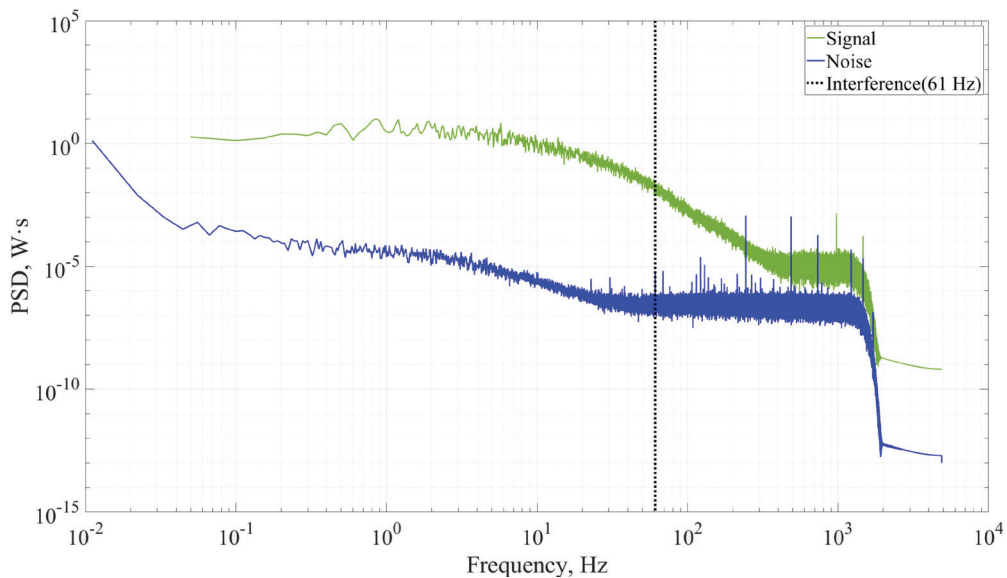


Figure 6 – Periodograms of power spectrum density (PSD) during "contrast mixing" (signal) and "non-contrast" mixing (noise)

A high level of correlation for the central cells ($\rho = 0.63$) provides good accuracy in determining the time shift ($\tau = 4.78$ c).

Table 2 shows the data on the flow rate obtained by the correlation method in comparison with the readings from the flow meters of the TF.

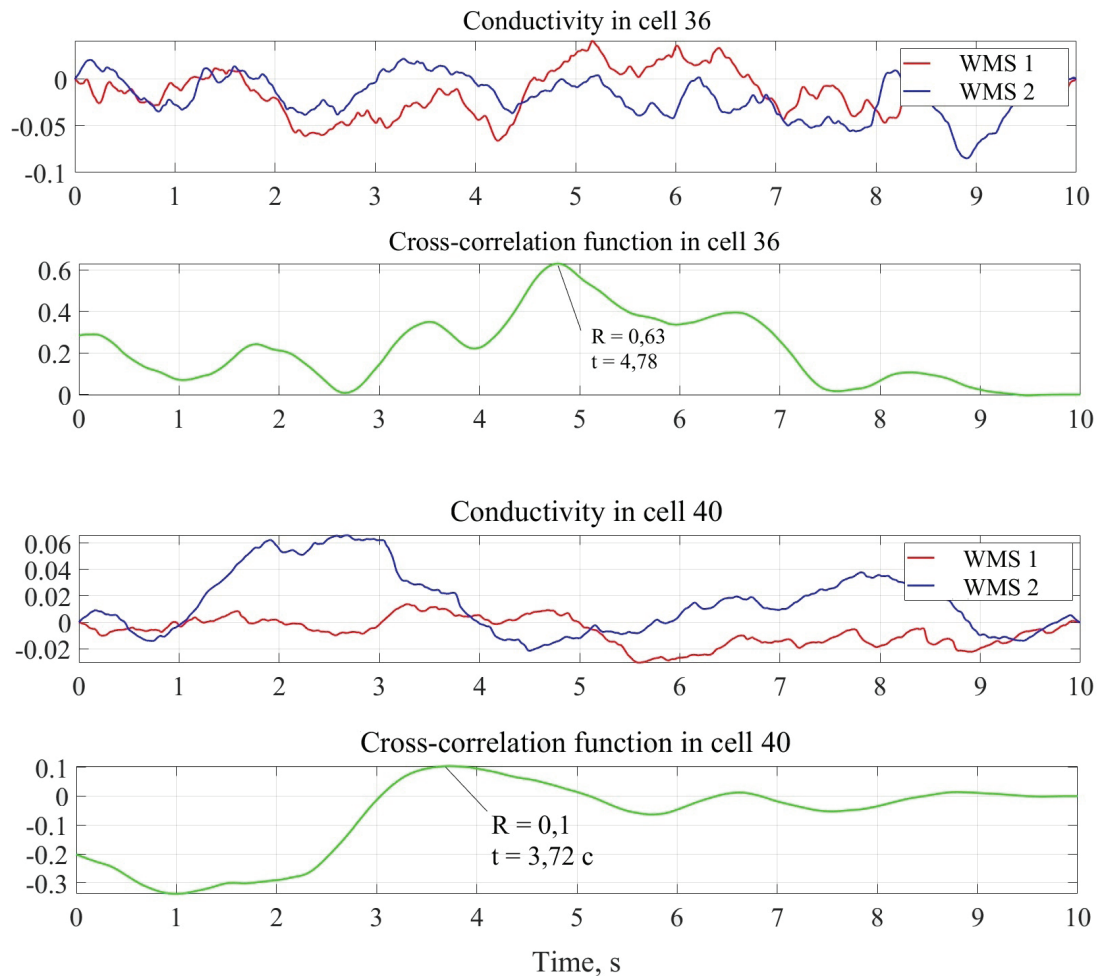


Figure 7 – Electrical conductivities and cross-correlation functions in test with $Re = 6.3 \cdot 10^3$ for central and peripheral cells

Table 2

Comparative analysis of values

Parameter	Reynolds		
	Re = 900	Re = 6300	Re = 12000
Flow according to standard flowmeters, l/min	2.88	22.38	43.92
Correlation flow, l/min	110.25	23.25	44.7
Relative error	3719 %	4 %	2 %
Correlation velocity, m/s	0.735	0.155	0.298
Temperature, °C	27.4	27.4	27.4
Density, kg/m ³	996.41	996.41	996.41

The readings obtained indicate the presence of an error of less than 5 % for higher Re numbers, while with decreasing Re, an increase of the error is observed. This is explained by the significant (in comparison with the size of the energy-carrying vortices) distance between the WMS. The intensity

of turbulence in the mixing zone decreases with the decrease of Re number, which causes the decrease of correlation strength between the readings of the sensors. In this case, for $Re = 900$, there is no correlation between the readings of the sensors due to the homogeneity of the flow in the laminar mode.

Conclusion

The approbation of the method of correlation determination of the coolant flow carried out in this work on the basis of a conductometric measuring system for turbulent flow in a square channel made it possible to apply this method to measure channel flow rates in scale models of elements and equipment of the core of a nuclear power plant.

The discharge results obtained for various Reynolds flows indicate a strong dependence of the flow rate measurement accuracy on the turbulence intensity. Furthermore, measurement results for $Re = 900$ allow making a general conclusion about the presence of a lower limit of the measured flow rate which will depend on temperature, flow rate and distance between sensors. Hence this limit will be different for each specific event.

Acknowledgments

The work was funded by the grant of Russian Science Foundation (project No. 18-19-00473).

References

1. Barinov A.A., Varentsov A.V., Glavny V.G., Dmitriev S.M. Implementation of the method of spatial conductometry for experimental research of the processes of mixing intra-reactor flows in modern nuclear units.

Transactions of NNSTU n.a. R.E. Alekseev, 2017, no. 2, pp. 35–41.

2. Kapulla R., Dyck C., Witte M., Fokken J., Leder F. Optical flow and cross correlation techniques for velocity field calculation. Fachtagung "Lasermethoden in der Strömungsmesstechnik", 8–10 September 2009, Erlangen.

3. Mattson H., Owrang F., Nordlund A. Utilisation of N16 in Nuclear Power Plants. Department of Reactor Physics. Chalmers University of Technology, Gbteborg Sweden, 2003.

4. Aristov I.N. RF patent RU2225046C2, 27.03.2004. Method for measuring the flow rate of the primary loop of a nuclear reactor // Patent of Russia №2225046.

5. Borisov V.F., Strukov M.A. RF patent RU2457558C1, 27.07.2012. Method for measuring the flow rate of the primary loop of a nuclear reactor // Patent of Russia №2457558.

6. Kuzmin V.V.. Correlation measurements of the primary coolant flowrate by nitrogen-16 activity at Kalinin NPP. Transactions of the 9-th International scientific and technical conference "Safety assurance of NPP with WWER" Podolsk, OKB "GIDROPRESS", 2015, 410 p.

7. Fokken J., Kapulla R., Kuhn S. Stably stratified isokinetic turbulent mixing layers: comparison of PIV-measurements and numerical calculations. Fachtagung "Lasermethoden in der Strömungsmesstechnik", 2009, pp. 8–10.

8. Prasser H.M., Bottger A., Zschau J. A new electrode-mesh tomograph for gas-liquid flows. *Flow Meas. Instrum.*, 1998, no. 9, pp. 111–119.

Determination of Flow Characteristics in Technological Processes with Controlled Pressure

T. Reader, V.A. Tenenev, A.A. Chernova

Kalashnikov Izhevsk State Technical University,
Studencheskaya str., 7, Izhevsk 426069, Russia

Received 22.04.2020

Accepted for publication 02.09.2020

Abstract

Assessment of the environmental and economic performance of a safety valve requires information about the flow of the substance through the valve when it is actuated. The goal of this paper was to determine the flow rate of the discharged substance and the mass flow rate of the substance entering the safety valve when it is actuated.

Proposed a mathematical model to describe the processes occurring in the valve. The model includes a system of differential equations describing the physical laws of conservation in the internal volume of the valve and differential equations, which link the value of gas flow through the valve with the pressure and the amount of movement of the shut-off disk. Used a modified method by S.K. Godunov to solve gas-dynamic equations.

Established that the determination of the flow and power characteristics of the valve requires the preliminary construction of a mathematical model of the safety valve operation. Based on this, proposed a method for determining the flow rate of the discharged substance and the mass rate of the substance entering the safety valve when it is actuated.

Obtained the flow characteristics of the valves under review and the dynamics of movement of the shut-off disc of the valve, as well as the dependence of the pressure change on the opening time of the valve. Comparison of the calculated values with available experimental data gives good agreement of results (no more than 5.6 % for a gas flow rate, under 10 % for the movement of the valve and change the arrival of gas in time using the standard deviation function of the flow characteristics of 0.6 %), confirms the correctness of the defined mathematical model, used numerical schemes and algorithms, as well as the proposed method and recoverability of the arrival of gas in a pressure–time curve.

Keywords: safety valve, flow measurement, pressure monitoring, numerical simulation.

DOI: 10.21122/2220-9506-2020-11-3-204-211

Адрес для переписки:

А.А. Чернова
Ижевский государственный технический университет,
ул. Студенческая, 7, г. Ижевск 426063, Россия
e-mail: alicaaa@gmail.com

Address for correspondence:

A.A. Chernova
Kalashnikov Izhevsk State Technical University,
Studencheskaya str., 7, Izhevsk 426069, Russia
e-mail: alicaaa@gmail.com

Для цитирования:

T. Reader, V.A. Tenenev, A.A. Chernova.
Determination of Flow Characteristics in Technological Processes
with Controlled Pressure.
Приборы и методы измерений.
2020. – Т. 11, № 3. – С. 204–211.
DOI: 10.21122/2220-9506-2020-11-3-204-211

For citation:

T. Reader, V.A. Tenenev, A.A. Chernova.
Determination of Flow Characteristics in Technological Processes
with Controlled Pressure.
Devices and Methods of Measurements.
2020, vol. 11, no. 3, pp. 204–211.
DOI: 10.21122/2220-9506-2020-11-3-204-211

Определение расходных характеристик в технологических процессах с контролируемым давлением

Т. Редер, В.А. Тенев, А.А. Чернова

Ижевский государственный технический университет имени М.Т. Калашникова,
ул. Студенческая, 7, г. Ижевск 426063, Россия

Поступила 22.04.2020

Принята к печати 02.09.2020

Оценка экологичности и экономичности работы предохранительного клапана требует информации о расходе вещества через клапан при его срабатывании. Целью данной работы являлось определение величины расхода сбрасываемого вещества и массовой скорости поступления вещества в предохранительный клапан при его срабатывании.

Для описания процессов, протекающих в клапане, предложена математическая модель, включающая систему дифференциальных уравнений, описывающих физические законы сохранения во внутреннем объеме клапана и дифференциальные уравнения, связывающие величину расхода газа через клапан с давлением и величиной перемещения запорного диска. Для решения газодинамических уравнений применялся модифицированный метод С.К. Годунова.

Установлено, что определение расходной и силовой характеристик клапана требует предварительного построения математической модели функционирования предохранительного клапана. На основании чего предложена методика определения величины расхода сбрасываемого вещества и массовой скорости поступления вещества в предохранительный клапан при его срабатывании.

Получены расходные характеристики рассматриваемых клапанов и динамика перемещения запорного диска клапана, а также зависимость изменения давления от времени открытия клапана. Сопоставление расчётных значений с имеющимися экспериментальными данными даёт хорошее совпадение (не более 5,6 % для расхода газа, менее 10 % для перемещения клапана и изменения прихода газа во времени при среднеквадратичных отклонениях функции расходных характеристик 0,6 %) результатов, подтверждает корректность сформулированной математической модели, используемых численных схем и алгоритмов, предложенной методики и возможность восстановления прихода газа по кривой давление–время.

Ключевые слова: предохранительный клапан, измерение расходных характеристик, контроль давления, численное моделирование.

DOI: 10.21122/2220-9506-2020-11-3-204-211

Адрес для переписки:

А.А. Чернова
Ижевский государственный технический университет,
ул. Студенческая, 7, г. Ижевск 426063, Россия
e-mail: alicaaa@gmail.com

Address for correspondence:

A.A. Chernova
Kalashnikov Izhevsk State Technical University,
Studencheskaya str., 7, Izhevsk 426069, Russia
e-mail: alicaaa@gmail.com

Для цитирования:

T. Reader, V.A. Tenenev, A.A. Chernova.
Determination of Flow Characteristics in Technological Processes
with Controlled Pressure.
Приборы и методы измерений.
2020. – Т. 11, № 3. – С. 204–211.
DOI: 10.21122/2220-9506-2020-11-3-204-211

For citation:

T. Reader, V.A. Tenenev, A.A. Chernova.
Determination of Flow Characteristics in Technological Processes
with Controlled Pressure.
Devices and Methods of Measurements.
2020, vol. 11, no. 3, pp. 204–211.
DOI: 10.21122/2220-9506-2020-11-3-204-211

Introduction

Chemical and technological processes, oil and gas pipeline systems, and high-pressure devices require the use of pressure level monitoring. The safety valve refers to the class of pipeline fittings designed to protect against mechanical destruction of equipment and pipelines, which is caused by overpressure, using automatically relief of excess working medium from systems and pressure vessels in excess of the set pressure. The valve should also ensure that the discharge of the medium is stopped when the operating pressure is restored [1–3]. Dangerous overpressure may occur in the system due to foreign factors (improper operation of equipment, heat transfer from exterior sources, incorrectly assembled thermal and mechanical circuit), as well as due to internal physical processes caused by an event beyond the normal operation.

In this case, the safety valve refers to quick-operation devices [4] that require the use of specialized quick-operation measuring instruments [5], the range of operation of which is quite limited [6]. However, we need to find the values of the discharge flow rate to assess the economic and environmental impacts. The determination of the mass rate of the substance input due to the process deviation from the normal technological mode is required to eliminate the causes of abnormal operation.

If there is a record of measurement of the current pressure in the tank, the value of gas arrival, G_p , and gas flow through the valve, G_v , can be determined based on the mathematical model of the safety valve operation. Therefore, the goal of this paper was to determine the flow rate of the discharged substance and the mass flow rate of the substance entering the safety valve when it is actuated.

Mathematical model of gas arrival calculation

To obtain the dependence between the flow characteristics and the pressure in the tank, let us consider the mass balance equation:

$$W \frac{dp}{dt} = G_p - G_v,$$

where: ρ is the gas density; W is the operation capacity of the tank; t is the time.

In the adiabatic approximation, we obtain an equation that links the pressure change, p , to the flow characteristics, G_p , G_v :

$$\frac{dp}{dt} = \frac{kRT(0)}{W} (G_p - G_v) \left(\frac{p}{p(0)} \right)^{\frac{k-1}{k}}, \quad (1)$$

where k , R is the adiabatic exponent and the gas constant of the working medium; $T(0)$, $p(0)$ are the initial values of temperature and pressure in the tank.

The gas flow through the valve is a function dependant on the pressure and the value of the movement, X , of the shut-off disc: $G_v = G_v(p, X)$. We can obtain this dependence either experimentally or by calculation. We propose to find this dependence from the numerical solution of the equations of the mathematical model of valve operation [7, 8] with the verification using the results of experimental measurements for a specific type of valve. Equation (1) gives us the expression for the gas arrival:

$$G_p = G_v(X, p) + \frac{dp}{dt} \frac{W}{kRT(0)} \left(\frac{p(0)}{p} \right)^{\frac{k-1}{k}}. \quad (2)$$

Expression (2) includes the value of the movement of the valve disc, $X(t)$. We find this dependence from the solution of the disk movement equation [7]:

$$m_s \frac{d\eta}{dt} = F_f - F_s, \quad \frac{dX}{dt} = \eta. \quad (3)$$

The movement of the disk in the axial direction is determined by the action of the force from the gas, F_f , and the elastic force of the spring, $F_s = K_s(X + X_0)$. Here: K_s is the spring stiffness coefficient; X_0 is the initial spring compression (preload); η is the speed of the disk movement. Initial conditions: $X(0) = 0$, $\eta(0) = 0$. The height of the disk lift is limited by the value X_k .

For the numerical solution of the disk movement equations, we introduce a difference grid $\{t_0 < t_1 < \dots < t_n < \dots < t_q = t_k, h_n = t_{n+1} - t_n\}$ and a two-step difference scheme [8]:

To calculate the movement of the disk, we should define the dependence of the force acting on the disk from the gas on the movement and pressure, $F_f(X, p)$. To calculate dependencies, $G_v = G_v(p, X)$, $F_f(X, p)$, we use the following mathematical model.

$$X^{n+1} = \frac{(F_f(X^n, p(t_n)) - K_s X_0) h_n + K_d X^n + m_s \left(\frac{X^n - X^{n-1}}{h_n} + \frac{X^n}{h_n} \right)}{K_s h_n + \frac{m_s}{h_n}}.$$

Mathematical model of safety valve operation

Processes occurring in the valve are described by a mathematical model in the form of a system of

differential equations describing the physical laws of conservation in the internal volume of the valve. For a gas safety valve, we consider the processes of internal gas dynamics within the framework of the viscous compressible gas model. The change in the thermodynamic parameters of the gas in the tank is subject to the equation of state: $p = \rho RT$.

The continuity equation is written down in general form:

$$\frac{d\rho}{dt} + \rho \nabla \mathbf{U} = 0, \quad (4)$$

where \mathbf{U} is the gas flow rate vector. The momentum conservation equations and the energy conservation equation have the following form:

$$\rho \frac{d\mathbf{U}}{dt} = -\nabla p + \text{Div} P; \quad (5)$$

$$\rho \frac{d}{dt} \left(C_v T + \frac{\mathbf{U}^2}{2} \right) = \nabla (P\mathbf{U}) + \nabla \mathbf{q}, \quad (6)$$

where P is the tensor of viscous stresses; C_v is the specific heat capacity of the gas at a constant volume; \mathbf{q} is the heat flow vector.

The system of equations (4)–(6) is supplemented by equations for the transfer of the kinetic energy of turbulence and the rate of turbulence dissipation [9]. The axial component of the force acting on the disk from the gas is determined by the integral on the disk surface, S_d :

$$F_f = \int_{S_d} p ds. \quad (7)$$

The calculation area (Figure 1a) is divided into two parts.

The first part is axially-symmetric and it uses a cylindrical coordinate system (x, r, φ) . The second part uses a rectangular coordinate system (x, y, z) . We use the control volume method for the numerical solution of a system of gas-dynamic equations. We determine gas parameters at the boundaries of control volumes using the S.K. Godunov method [10]. To increase the order of approximation of the Godunov difference method, we use the *MUSCL (Monotone Upwind Schemes for Conservation Laws)* scheme. In accordance with this scheme, we define the values of gas-dynamic parameters for solving the problem of discontinuity decay using extrapolation with a limiter [11, 12]. For equations written down

in a cylindrical coordinate system, we construct a difference grid (Figure 1b) in the $\varphi = \text{const}$ plane using the complex method of boundary elements [13]. For equations written down in a Cartesian coordinate system, the difference grid is unstructured. The gradients of variables included in the tensor components P are calculated in the middle of each face through the values of variables in the surrounding control volumes, as described in [14]. For time integration, we use a two-step Runge–Kutta scheme with second-order accuracy.

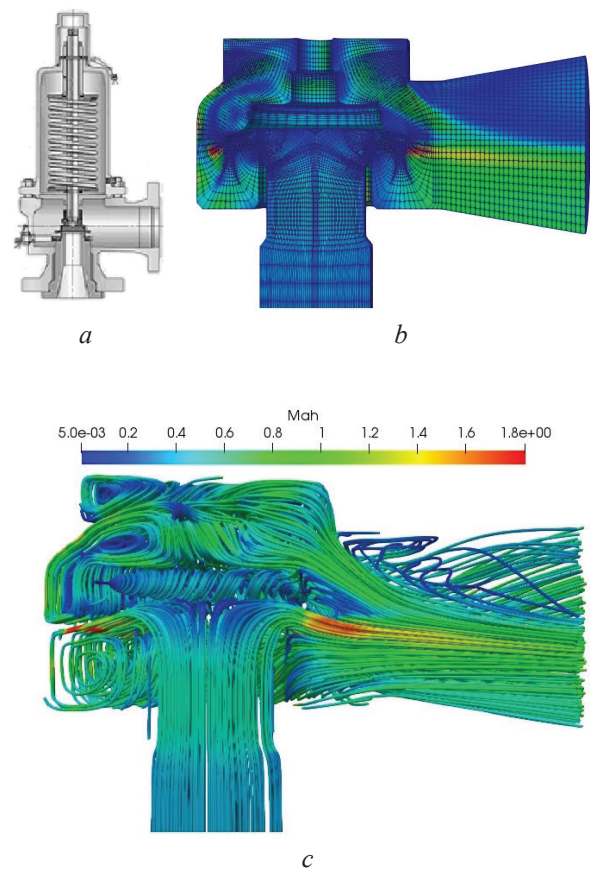


Figure 1 – Valve diagram (a), difference grid (b), and flow structure (c)

The gas-dynamic equations (4)–(7) are solved numerically together with the disk movement equations (3). The difference grid is adapted to the disk movement.

We consider two designs of the *LESER* safety valve, 2J3 and 441. The gas-dynamic force and flow through the valve are written down as: $F_f(X, p) = p\psi(X)$, $G_v(p, X) = p\gamma(X)$, where $\psi(X)$, $\gamma(X)$ functions are characteristics of the valve type. The calculated and experimental dependencies are shown in Figure 2.

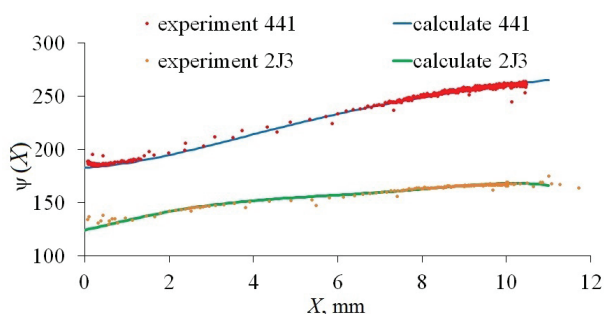


Figure 2 – Valve characteristics

The calculated dependencies, $\psi(X)$, are approximated by 5th-degree polynomials, $\psi(X) = \sum_{k=0}^5 \beta_k X^k$, with coefficients, β_k , in Table 1.

Table 1

Polynomial coefficients for $\psi(X)$

Valve	β_k					
441	182.5704	2.2713	2.4635	-0.3243	0.0155	-0.0002
2J3	123.8281	9.6135	0.1595	-0.3951	0.0570	-0.0024

The flow characteristics of valves obtained by calculation are approximated by 2nd-degree polynomials with coefficients from Table 2.

Table 2

Polynomial coefficients for $\gamma(X)$

Valve	β_k		
441	0	0.0345	-0.00071
2J3	0	0.0292	-0.001

The results of tests processing

The scheme for testing safety valves in accordance with the ASME PTC 25-2014 standard is shown in Figure 3.

The characteristics of the tested LESER 441 and 2J3 valves are shown in Table 3.

Table 3

Characteristics of valves

Valve	X_0 , mm	K_s , N/m	L , m	D_t , m
441	0.017	54700	1.2	0.05
2J3	0.025	26000	1.2	0.05

The tests were carried out in the air. The *vessel0* tank has a large volume under high pressure and

serves as a gas source for the *vessel* tank with pressure control. The intensity of the gas arrival is regulated by the operator during the test (regulator, R_1). One of the goals of the tests was to check the stability of the valves with a long pipe between the tank and the valve. A pipe with a length of L and a diameter of D_t connects the tank to the valve. Pressure and temperature are measured at the inlet and at the end of the pipe. The movement of the rod, X , is measured on the valve. The pressure is measured using a P900 series load cell with an error of 0.2 %. The force is measured using a U2B sensor with an accuracy class of 0.2. The movement of the disk is controlled by a WA standard displacement inductive transducer with an error of 1 %. Sensor readings are recorded in 0.000417 seconds.

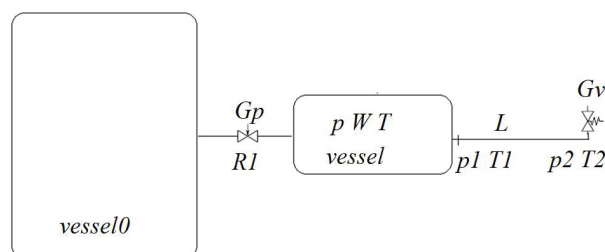


Figure 3 – Safety valve testing scheme: *vessel0* – a tank with a large volume under high pressure, which is the source of gas for the *vessel* tank; *vessel* – a pressure-controlled tank with operating parameters P, T, W ; R_1 – gas flow regulator; G_p – gas arrival; P_1, T_1 – gas pressure and temperature at the outlet of the tank with pressure control; L – length of a pipe with a diameter, D_t , connecting the tank to the valve; P_2, T_2 – gas pressure and temperature at the inlet to the valve; G_v – gas flow through the safety valve

The use of formula (2) for calculating the gas arrival value based on the results of experimental measurements of pressure, $p(t)$, and disk movement, $X(t)$, requires calculating the derivative $\frac{dp}{dt}$.

Differentiation of functions based on the results of experimental measurements is an incorrect operation. Figure 4 shows the measured dependence, $p(t)$ (red line).

The presence of acoustic oscillations and measurement errors leads to the occurrence of high-frequency oscillations. Therefore, the results of measuring all parameters were smoothed using smoothing cubic splines. The value of the derivative was determined by the value of the relevant spline coefficient. The smoothed dependency, $p(t)$, is shown in Figure 4 with a black line.

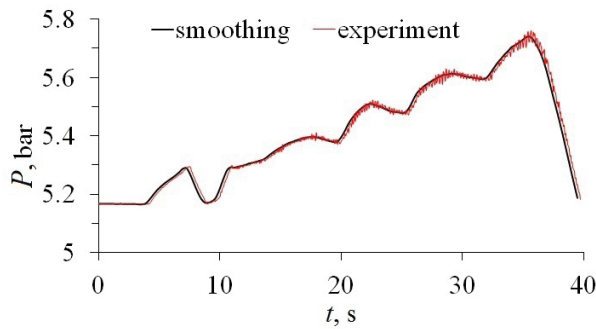


Figure 4 – Pressure versus time (valve 441)

The time change of the value of air arrival in the vessel tank, which is calculated using the formula (2), equations (3), and pre-calculated functions, $\psi(X)$, $\gamma(X)$, is shown in Figure 5.

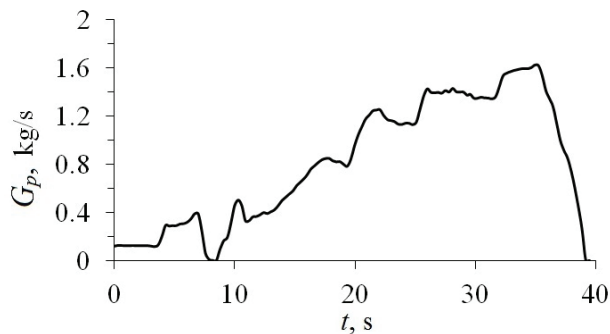


Figure 5 – Dependence of gas intake on time

The scheme of the valve tests under review provided for measuring the movement of the valve disc, as well as the pressure and temperature in two sections of the pipe (Figure 1). Based on this information, we can determine the value of gas flow through the valve during testing and compare it with the calculated dependence, $G_v(p, X) = p\gamma(X)$. If p_2 , T_2 are the pressure and temperature at the end of the pipe before the valve, we determine the mass flow of gas through the pipe using the following expression:

$$G_{\text{exp}} = \varphi_2 \pi \frac{D_t^2}{4} \sqrt{2(p - p_2) \frac{p_2}{RT_2}},$$

where φ_2 is the flow coefficient related to a sharp narrowing at the inlet to the pipe from the tank (Figure 6) and friction in the pipe. We determine the flow coefficient when solving the gas-dynamic problem in an axially-symmetric setting in the calculated area (Figure 6).

The value of the flow coefficient, $\varphi_2 = 0.814$. The measured movement of the valve disc is shown in Figure 7.

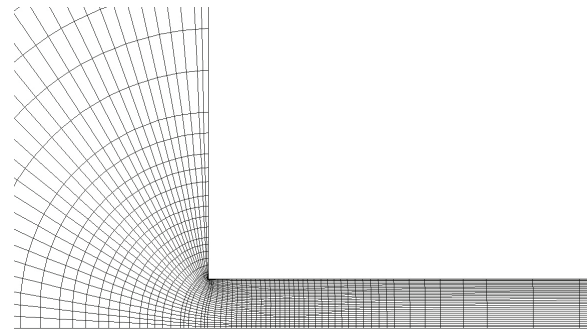


Figure 6 – Fragment of the vessel – pipe design area

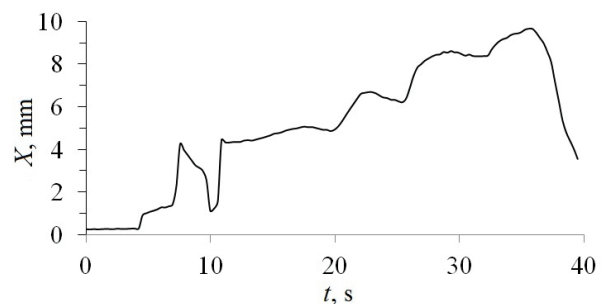


Figure 7 – Moving the valve disc

The calculated and experimental flow values corresponding to these values, X , are shown in Figure 8.

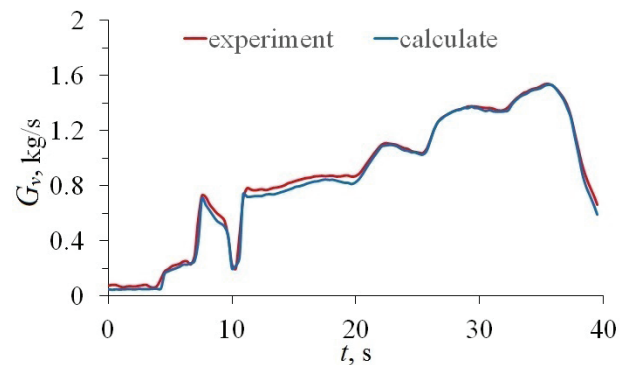


Figure 8 – Calculated and experimental dependencies for gas flow

The experimental and calculated, $\gamma(X) = 0.0345X - 0.00071X^2$, flow characteristics of the 441 valve are shown in Figure 9.

The average square deviation is 0.006. We may conclude from the presented comparison of the results of calculations and experiments that the design characteristics of the valve provide the determination of gas arrival in the controlled tank only through the pressure–time dependence.

Let us review the test results of the 2J3 valve. The time change in pressure is shown in Figure 10.

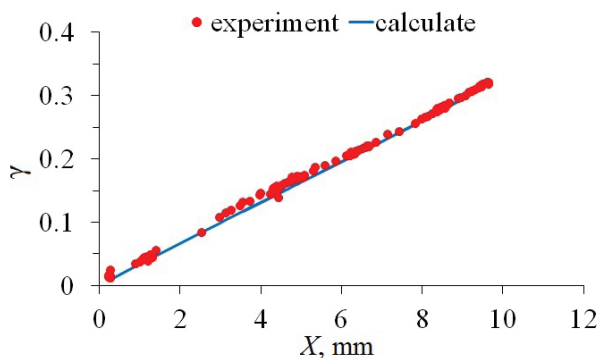


Figure 9 – Calculated and experimental flow characteristics

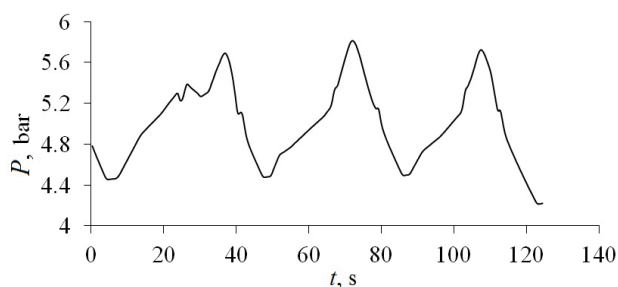


Figure 10 – Time dependence of pressure (2J3 valve)

During this time, the three-time actuation of the valve occurs, as shown in Figure 11.

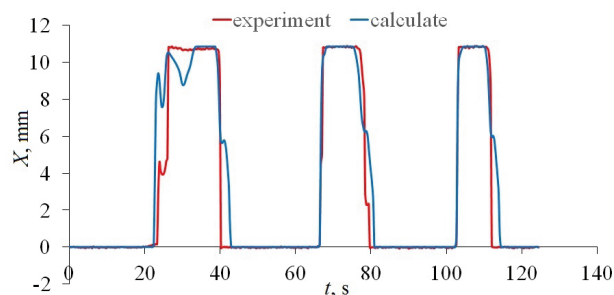


Figure 11 – Measured and calculated movement of the 2J3 valve disc

The time interval under review corresponds to the dependence of the gas arrival on time, which is obtained by the calculation and confirmed in experiments (Figure 12).

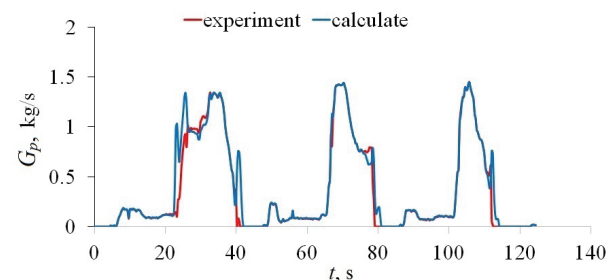


Figure 12 – Change of gas arrival in time (valve 2J3)

The comparison of the change in the value of the disk movement obtained in the experiment and by the calculated method (solution of equations (3) using the power characteristic of the valve 2J3, $\psi(X) = 123.8281 + 9.6135X + 0.159X^2 - 0.3951X^3 + 0.0570X^4 - 0.0024X^5$), which is shown in Figure 11, demonstrates that the power characteristic of the valve was obtained correctly.

Conclusion

We have shown that in order to find the arrival of a gas mass in a controlled technological tank, which leads to increase in pressure, it is required to have the following information: the pressure-time dependence recorded in the technological process; calculated flow and power characteristics of the valve. We confirmed during our work that the determination of the flow and power characteristics of the valve requires the preliminary construction of a mathematical model of the safety valve operation. Based on this, we proposed a method for determining the flow rate of the discharged substance and the mass rate of the substance entering the safety valve when it is actuated.

Following the numerical simulation, we obtained the flow characteristics of the valves under review and the dynamics of movement of the shut-off disc of the valve, as well as the dependence of the pressure change on the opening time of the valve. Comparison of the calculated values with available experimental data gives good agreement of results (no more than 5.6 % for a gas flow rate, under 10 % for the movement of the valve and change the arrival of gas in time using the standard deviation function of the flow characteristics of 0.6 %), confirms the correctness of the defined mathematical model, used numerical schemes and algorithms, as well as the proposed method in general and recoverability of the arrival of gas in a pressure-time curve in particular.

Acknowledgments

We have performed the paper within the framework of the Research Activity of the Udmurt Federal Research Center of the Ural Branch of the Russian Academy of Science "Artificial Intelligence in the Development, Training, and Support of Expert Systems for the Representation and Use of Knowledge in Natural-Scientific, Technical, and Socio-Humanitarian Fields" AAAA19-119092690104-4

References

1. Faizov A.R., Churakova S.K., Pruchay V.S. Simulation mode of emission from the distillation column. *Bashkir chemistry journal*, 2013, no. 2, pp. 52–54.
2. Beune A., Kuerten J.G.M., Schmidt J. Numerical calculation and experimental validation of safety valve flows at pressures up to 600 bar. *AIChE Journal*, 2011, vol. 57, pp. 3285–3298.
3. Bernad S.I., Susan-Resiga R. Numerical model for cavitation flow in hydraulic poppet valves. *Modelling and Simulation in Engineering*, 2012, vol. 2012, pp. 1–10. **DOI:** <https://doi.org/10.1155/2012/742162>
4. Tusyuk S.K., Belyanskaya E.S. Diagnostic internet – testing first – year students in the tula state university. *Izvestiya TulGU* [News of the Tula state university. Technical sciences], 2012, no. 12–2, pp. 262–267 (in Russian).
5. Boronenko M.P. Overview of application of high-velocity television measuring systems in a physical experiment. *Yugra state university*, 2014, no. 2(33), pp. 43–55.
6. Fyodorov S.A. Embedded software of high speed IP camera for optical diagnostic of the fleeting processes. *Proceedings of TUSUR*, no. 1, 2 part [25], pp. 225–229.
7. Song X., Cui L., Cao M., Cao W., Park Yo., Dempster W.M. A CFD analysis of the dynamics of a direct-operated safety relief valve mounted on a pressure vessel. *Energy Conversion and Management*, 2014, vol. 81, pp. 407–419. **DOI:** [10.1016/j.enconman.2014.02.021](https://doi.org/10.1016/j.enconman.2014.02.021)
8. Reader T., Tenenev V.A., Paklina N.V. Numerical 3D Simulation of Safety Valve Gas Dynamics. *Vestnik Izhevsk state technical University named after M.T. Kalashnikov* [Bulletin of Kalashnikov ISTU], 2018, vol. 21, no. 4, pp. 174–181 (in Russian). **DOI:** [10.22213/2410-9304-2018-2-28-40](https://doi.org/10.22213/2410-9304-2018-2-28-40)
9. Volkov K.N., Emelyanov V.N. Large-eddy simulation in the calculation of turbulent flows. Moscow. 2008, 368 p.
10. Godunov S.K., Kulikov I.M. Computation of discontinuous solutions of fluid dynamics equations with entropy nondecrease guarantee. *Computational Mathematics and Mathematical Physics*, 2013, vol. 53, no. 8, pp. 1179–1182. **DOI:** [10.1134/S0965542514060086](https://doi.org/10.1134/S0965542514060086)
11. Smirnova N.S. Comparison of flux splitting schemes for numerical solution of the compressible Euler equations. *Proceedings of MIPT*, 2018, vol. 10, no. 1, pp. 122–141.
12. Wesseling Pieter Dr. Principles of computational fluid dynamics. Springer series in computational mathematics, ISSN 0179-3632; 29. Mathematics Subject Classification, 1991: 76M,65M, XII, 644 p. **DOI:** [10.1007/978-3-642-05146-3](https://doi.org/10.1007/978-3-642-05146-3)
13. Tenenev V.A., Gorokhov M.M., Rusyak I.G. Numerical study of particle Gorenje in a two-phase flow. *Mathematical modeling*, 1997, vol. 9, no. 5, pp. 87–96.
14. Wesseling P., Segal A., Kassel C.G.M. Computing Flows on General Three-Dimensional Nonsmooth Staggered Grids. *Journal of Computational Physics*, 1999, vol. 149, pp. 333–362. **DOI:** [10.1007/978-94-017-1564-5_2](https://doi.org/10.1007/978-94-017-1564-5_2)

Features of Measuring the Hardness of a Metal Surface Modified with Ultrafine Particles of Minerals

A.V. Skazochkin¹, G.G. Bondarenko², P. Żukowski³

¹Kaluga branch of the Russian Presidential Academy of National Economy and Public Administration,
Okruzhnaya str., 4, building 3, Kaluga 248030, Russia

²National Research University Higher School of Economics,
Myasnitskaya str., 20, Moscow 101000, Russia

³Lublin University of Technology,
Nadbystrzycka str., 38a, Lublin 20-618, Poland

Received 07.07.2020

Accepted for publication 03.09.2020

Abstract

One of the important characteristics of the surface properties of metal parts subjected to friction is hardness. Hardness measurements are important for determining the operational characteristics of parts and monitoring the technological regimes of surface modification. However, hardness measurements of thin modified layers made by different methods can lead to differences in measurement results. The aim of the article was to study the hardness of a metal surface modified with ultrafine particles of minerals by two different methods (instrumental indentation and Vickers hardness measurement) and a comparative analysis of the measurement results obtained by these methods.

Standard Vickers hardness measurements at loads of 0.025, 0.1 and 0.5 kgf showed a qualitative difference between the hardness values of the two samples modified with different mixtures of ultrafine particles of minerals and a large heterogeneity of the hardness values over the area. By the method of instrumental hardness, standard measurements were performed without preliminary selection of the indentation site (at a load of 1.05 N) and measurements during indentation into even sections (at low loads of 10 mN).

It is noted that the high precision of measurements implemented by instrumental indentation, due to the large roughness of the samples, leads to large values of the error in calculating the measurement results. An additional difference in the results of measurements performed by two methods at shallow indentation depths may be due to the fact that the object under study has a complex structure consisting of a metal matrix and particles distributed over the depth of the sample. A possible way out of the situation lies in the transition from the use of hardness measures when calibrating instruments to standard samples of properties for which the constancy of mechanical properties in the measured range of indentation depths will be ensured, but which are not yet available in research practice. Therefore, at present, when carrying out work related to the search for optimal conditions for obtaining thin wear-resistant layers on the surface of metals modified with ultrafine particles of minerals, comparative measurements performed by one measurement method are recommended.

Keywords: hardness, metal surface, Vickers measurements, industrial indentation, mineral coatings.

DOI: 10.21122/2220-9506-2020-11-3-212-221

Адрес для переписки:

A.V. Сказочкин.
Калужский филиал Российской академии народного хозяйства
и государственной службы,
ул. Окружная 4, стр. 3, Калуга 248030, Россия
e-mail: avskaz@rambler.ru

Address for correspondence:

A.V. Skazochkin.
Kaluga branch of the Russian Presidential Academy of National
Economy and Public Administration,
Okruzhnaya St., 4, building 3, Kaluga 248030, Russia
e-mail: avskaz@rambler.ru

Для цитирования:

A.V. Skazochkin, G.G. Bondarenko, P. Żukowski.
Features of Measuring the Hardness of a Metal Surface
Modified with Ultrafine Particles of Minerals.
Приборы и методы измерений.
2020. – Т. 11, № 3. – С. 212–221.
DOI: 10.21122/2220-9506-2020-11-3-212-221

For citation:

A.V. Skazochkin, G.G. Bondarenko, P. Żukowski.
Features of Measuring the Hardness of a Metal Surface
Modified with Ultrafine Particles of Minerals.
Devices and Methods of Measurements.
2020, vol. 11, no. 3, pp. 212–221.
DOI: 10.21122/2220-9506-2020-11-3-212-221

Особенности измерения твёрдости металлической поверхности, модифицированной ультрадисперсными частицами минералов

А.В. Сказочкин¹, Г.Г. Бондаренко², П. Жуковский³

¹Калужский филиал Российской академии народного хозяйства и государственной службы,
ул. Окружная, 4, стр. 3, Калуга 248030, Россия

²Национальный исследовательский университет «Высшая школа экономики»,
ул. Мясницкая, 20, Москва 101000, Россия

³Люблинский технологический университет
ул. Надбыстрицкая, 38А, Люблин 20-618, Польша

Поступила 07.07.2020

Принята к печати 03.09.2020

Одной из важных характеристик свойств поверхности металлических деталей, подвергающихся трению, является твёрдость. Измерения твёрдости важны для определения эксплуатационных характеристик деталей и контроле технологических режимов модификации поверхности. Однако измерения твёрдости тонких модифицированных слоёв, выполненные разными методами, могут приводить к различию результатов измерений. Целью данной работы являлось исследование твёрдости поверхности металла, модифицированной ультрадисперсными частицами минералов, двумя различными методами (инструментального индентирования и измерения твёрдости по Виккерсу) и сравнительный анализ результатов измерений, полученных этими методами.

Стандартные измерения твёрдости по Виккерсу при нагрузках 0,025, 0,1 и 0,5 кгс показали качественное отличие значений твёрдости двух образцов, модифицированных разными смесями ультрадисперсных частиц минералов и большую неоднородность значений твёрдости по площади. Методом инструментальной твёрдости выполнены стандартные измерения без предварительного выбора места индентирования (при нагрузке 1,05 Н) и измерения при индентировании в ровные участки (при малых нагрузках 10 мН).

Отмечено, что высокая прецизионность измерений, реализуемая методом инструментального индентирования, из-за большой шероховатости образцов приводит к большим значениям погрешности при расчёте результатов измерений. Дополнительную разницу результатов измерений, выполненных двумя методами на малых глубинах индентирования, может вносить то, что исследуемый объект имеет сложную структуру, состоящую из матрицы металла и частиц, распределённых по глубине образца. Возможный выход из ситуации заключается в переходе от использования мер твёрдости при калибровке приборов к стандартным образцам свойств, для которых будет обеспечено постоянство механических свойств в измеряемом диапазоне глубин индентирования, но которые пока отсутствуют в исследовательской практике. Поэтому в настоящее время при проведении работ, связанных с поиском оптимальных условий получения тонких износостойких слоёв на поверхности металлов, модифицированных ультрадисперсными частицами минералов, рекомендуются сравнительные измерения, выполненные одним методом измерения.

Ключевые слова: твёрдость, металлическая поверхность, измерения по Виккерсу, промышленное индентирование, минеральные покрытия.

DOI: 10.21122/2220-9506-2020-11-3-212-221

Адрес для переписки:

А.В. Сказочкин.
Калужский филиал Российской академии народного хозяйства
и государственной службы,
ул. Окружная 4, стр. 3, Калуга 248030, Россия
e-mail: avskaz@rambler.ru

Address for correspondence:

A.V. Skazochkin.
Kaluga branch of the Russian Presidential Academy of National
Economy and Public Administration,
Okruzhnaya St., 4, building 3, Kaluga 248030, Russia
e-mail: avskaz@rambler.ru

Для цитирования:

A.V. Skazochkin, G.G. Bondarenko, P. Żukowski.
Features of Measuring the Hardness of a Metal Surface
Modified with Ultrafine Particles of Minerals.
Приборы и методы измерений.
2020. – Т. 11, № 3. – С. 212–221.
DOI: 10.21122/2220-9506-2020-11-3-212-221

For citation:

A.V. Skazochkin, G.G. Bondarenko, P. Żukowski.
Features of Measuring the Hardness of a Metal Surface
Modified with Ultrafine Particles of Minerals.
Devices and Methods of Measurements.
2020, vol. 11, no. 3, pp. 212–221.
DOI: 10.21122/2220-9506-2020-11-3-212-221

Introduction

The properties of the surface layers of the metal, modified with ultrafine particles of minerals, depend on the technological conditions of production, the composition of mineral mixtures and can vary widely. For example, changing only some technological regimes using the technology of mineral coatings [1], which ensure that microparticles of minerals enter the metal, it is possible to obtain modified layers of various roughness Ra (average roughness) on structural steel samples, differing by almost an order of magnitude [2]. The interest in modified layers enriched with microparticles of minerals is due to their prospects as wear-resistant and/or antifriction coatings on the surfaces of friction pairs of various metals – steels [1], titanium [3], aluminum [4] operating in an aggressive environment – abrasive, marine water, in the presence of gases, acid solutions, under thermocyclic loads [5, 6]. Studies show that the thickness of the modified layer, the coefficient of friction, the hardness of the layers depend both on the composition of the mineral mixtures and on the modes of particles entering the metal and the properties of the modified metal surface. In this case, a huge role is played by the quantitative determination of some tribological parameters of the created modified layers, in particular, the determination of such a parameter as hardness for comparison with the macroscopic properties of the part itself and the evaluation of the practical benefits of creating layers [7].

The most common method for determining the hardness of thin modified layers is instrumental indentation, which is the basis of the ISO 14577 standard. The essence of the measurement method consists in the process of indenting a trihedral diamond pyramid (Berkovich pyramidal indenter) with recording the indentation diagram and then calculating the hardness of the dependence of the applied force on the implementation in accordance with standard ISO 14577 [8, 9].

Also, to measure the hardness of thin microlayers, the Vickers method of measuring microhardness (ISO 6507 standard) is used, which is methodologically close to the instrumental indentation method [10]. Its essence is in measuring the diagonal of the resulting fingerprint when an indenter is introduced into the metal in the form of a tetrahedral pyramid (Vickers pyramidal indenter) [11]. However, due to the arising effect of elastic indentation of the indentation when the indentation size is less than

10 μm and the resolution of the optical microscope is limited when measuring the diagonal of an imprint of this size, this method is used to measure the hardness of films with a thickness of at least 10 μm [12].

There are common problems for all methods in determining the hardness of thin layers and coatings, such as the effect of the substrate, surface roughness, and the presence of residual stresses, which can make a significant correction in the measurement results [4]. For example, the influence of the base metal substrate in measuring hardness consists in the fact that the recorded response of the material during measurement depends on the modified layer and on the properties of the metal volume [13].

Such features of thin layers modified with ultrafine particles of minerals, such as the absence of a clear interface between the layer and the substrate [1], as well as the requirement to control not only the properties of the surface layer, but also the depth distribution, increase the requirements for hardness determination methods.

It should be noted that, despite the similarity of the industrial indentation method and the Vickers method, namely, that the indenters have the same projection area with the same penetration depths and the imprint geometry is independent of the penetration depth, their difference is also quite significant [14]. The difference between the methods is that in the Vickers method, hardness is defined as the ratio of the applied load to the surface area of the restored fingerprint, and in the industrial indentation method, the hardness is equal to the ratio of the maximum applied load to the projected area of the unrepaired fingerprint [14, 15]. In general, hardness, as a dimensionless quantity, characterizes the behavior of the material under strictly specified test conditions [12], is not a function of primary physical quantities and depends on the measurement technique [8, 11]. Therefore, situations are possible in which differences in the hardness determination procedures by these two methods can lead to differences in the results of hardness measurements of thin modified metal layers with a thickness of several tens of microns, which is typical when microparticles are modified with minerals. On the one hand, the instrumental indentation method provides the largest locality and precision of measurements [8, 9, 13, 14], the largest of all existing methods for measuring the hardness of thin layers, on the other hand, the hardness tester that implements the instrumental indentation method is a complex laboratory complex, and the price of the instrument, implementing this

method, often differs by an order of magnitude from the price of a Vickers microhardness tester, which makes it difficult to use when scaling the technology. It should also be noted that the implementation of both methods in modern instruments provides automatic hardness measurement, touch control, and automatic focusing.

The purpose of this article is to study the hardness of a metal surface (steel 20X13 – Russian analogue of steel X20Cr13 (EU)), modified with ultrafine particles of minerals, by two different methods (instrumental indentation and Vickers microhardness measurement) and a comparative analysis of the measurement results obtained by these methods.

The development of procedures for measuring such a parameter of thin layers as the hardness of a metal surface modified by mineral particles is aimed at developing solutions to such problems of technological control of layer parameters as adapting methods to specific technological processes, developing automation of measurements and possible remote control of measurements.

Materials and methods

Two samples of steel 20X13, with a diameter of 5 (sample No. 1) and 8 cm (sample No. 2), about 1 cm thick, were made by turning with subsequent standard grinding. On the surface of the samples layers were created, modified with ultrafine particles of mixtures of minerals according to the basic technology of SPC "Geoenergetika" [1]. The layers were created using different types of mineral mixtures under the same technological conditions, which implies the difference in their hardness from each other. The thickness of each modified layer, based on the technological parameters during its creation and earlier experiments, was not less than 20 μm [1, 2]. Comparative measurements of surface roughness, hardness, and elastic modulus (Young) were performed on the samples.

The surface roughness was measured on a Model 130 profilometer (PROTONMIET manufacturer), the measurement method was profilometry. Measurement procedure parameters: profile length – 12.5 mm, profile measurement speed – 0.5 mm/s.

Hardness measurement was carried out by two methods and, accordingly, by two devices:

1. Microhardness meter DuraScan (EMCO-TEST, Austria). Parameters of the measurement procedure: indenter – tetrahedral pyramid of the Vickers type, load range: 0.025 kgf – 0.5 kgf.

2. Nanohardness tester "NanoScan-3D" (manufacturer FGBNU TISNUM). Parameters of the measurement procedure: indenter – a trihedral pyramid of the Berkovich type, loading time – 10 s, unloading time – 10 s, time to maintain maximum load – 3 s, load range: 10mN–1.05 N.

Research results and discussion

The roughness measurement was carried out by measuring the surface profile of the samples, the roughness parameters are shown in Table 1.

Table 1

Comparison of sample roughness parameters

Sample	Ra, μm	Rz, μm	Sm, μm
№ 1	2.03 ± 0.02	10.7 ± 0.3	236 ± 13
№ 2	2.62 ± 0.02	14.3 ± 0.1	206 ± 6

From the Table 1 it follows that the samples have a similar roughness Ra, which is quite predictable, given the constancy of technological conditions. To exclude the influence of such roughness, it is necessary to perform indentation at a depth of $\approx 100 \mu\text{m}$, which significantly exceeds the estimated thickness of the modified layer (about 20 μm). At the same time, a large roughness step ($Sm \approx 200 \mu\text{m}$) allows one to find sufficiently even sections for the location of the indent, which was done during indentation by the Vickers method.

Before presenting the results of hardness measurements by two methods, it should be noted that the surface after modification is rather heterogeneous due to the fact that the process operations of the technology of mineral coatings lead to the formation of a flat surface (about 90 %) and randomly located microcavities (about 10 %) throughout the entire working sample surfaces [1, Figure 1] (or Figure 6 and 7 of this article, see below). The resulting and existing surface defects of a flat surface, as well as microcavities, are filled with particles of minerals and undergo further technological operations. Particle filling of surface defects of a flat surface, as well as microcracks and microcavities, and changes that occur with defects in a surface hardened layer during further technological operations, increase the wear resistance of the material [2]. But then, when conducting micromerements, the question arises about the place of measurements and the

correctness of the obtained parameters for the characteristics of the surface. Given the state of the surface, it is obvious that when carrying out measurements it is necessary to adhere to two measurement strategies:

- taking measurements of consciously selected areas of the modified surface;
- performing measurements on a large number of measurement sites selected at random and statistical processing of the results.

Considering that it is precisely the even sections of the modified surface that play the dominant role in the friction processes, and it is the parameters of the even sections of the surface that are the characteristics of the surface during friction and wear [1], indentation by both methods must be carried out precisely in the even sections of the modified surface. On the other hand, with further automation of the hardness measurement process, indentation locations will be randomly selected, which means that it is necessary to take into account the presence of microcracks and microcavities that will introduce distortions into the final result.

Vickers microhardness measurement

As indicated above, the samples have a significant roughness, and to measure hardness, a flat section was preliminarily selected and then indentation was performed. An example of the image obtained after indentation with a load of 0.5 kgf is shown in Figure 1.

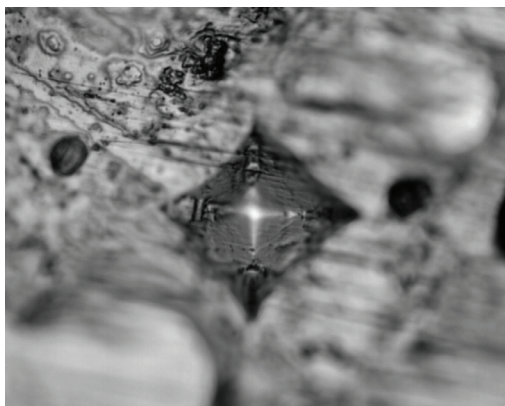


Figure 1 – Optical image of the fingerprint obtained after indentation with a load of 0.5 kgf (magnification $\times 60$)

For measuring the samples, we selected the loads of 0.025 kgf, 0.1 kgf and 0.5 kgf. The measurement results are shown in Table 2.

A graphical representation of the results is presented in Figure 2. Measurement at each load

was carried out 5 times, the standard deviation is presented as an error.

Table 2

Vickers (HV) measurement results with different loads

Sample	0.025 kgf	0.1 kgf	0.5 kgf
№ 1	1215 ± 180 (HV)	1080 ± 225 (HV)	382 ± 58 (HV)
№ 2	600 ± 120 (HV)	530 ± 140 (HV)	320 ± 40 (HV)

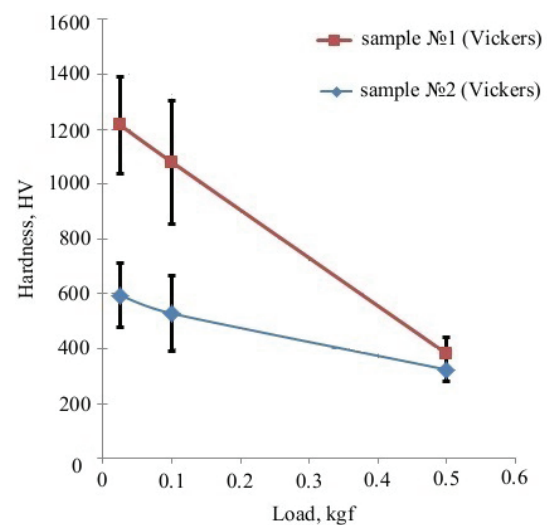


Figure 2 – Dependence of the measured Vickers hardness (HV) on the indentation load

The results of Tables 2 and 3 show a qualitative difference in hardness measured on samples 1 and 2, and a large heterogeneity of hardness (greater than 100 %), measured over the area of the samples.

Table 3

Hardness (HV), measured according to Vickers in different places of the samples

Sample	Hardness in the center of the sample (HV)	Hardness in the middle of the sample, between center and edge (HV)	Hardness at the edge of the sample (HV)
№ 1	933 ± 90	500 ± 145	1133 ± 275
№ 2	563 ± 210	519 ± 50	732 ± 175

When measuring hardness by instrumental indentation (nanoindentation), an attempt was made to measure with the two measurement

strategies indicated above. It should be noted that the instrumental indentation method can determine the values of hardness and elastic modulus of a material under loads of micronewtons or more. However, it is precisely at these load values that the quality requirements of the modified surface increase.

Measurement of tool hardness (hardness determined by instrumental indentation method) and elastic modulus (nanoindentation): processing of a large number of indentations.

Measurements in the nanoindentation mode were carried out as follows: an array of injections was applied to each of the obtained samples with a load of 1.05 N. The measurements were performed without first selecting the indentation site and, thus, were significantly affected by roughness and the presence of microcavities. The array contained 10×10 points with a distance of $300 \mu\text{m}$ between the points (total size of the indented surface: $3 \times 3 \text{ mm}$). The measurements were carried out with a tip in the form of a Berkovich pyramid, (for estimates: the transverse size of the indent is ≈ 6 times the contact depth, which in this case of small elastic recovery is close to the maximum depth). The results of measuring hardness H and elastic modulus E are shown in the Figure 3 below.

It can be seen that the dependence of hardness on depth is easily described by a curve of the form $\sim 1/h^2$, which is due to the effect of roughness. The value of hardness and elastic modulus of the material can be determined by the peaks of the distribution density of the measured values N (the maximum value on the histogram) in Figures 4 and 5.

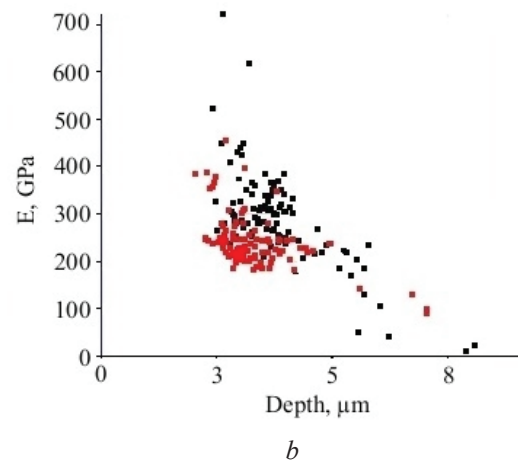
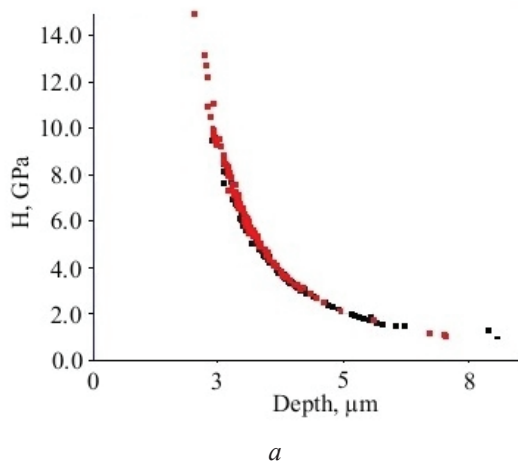


Figure 3 – Measurement of hardness (a) and elastic modulus (b) depending on the maximum indentation depth. Red dots – sample № 1; black dots – sample № 2

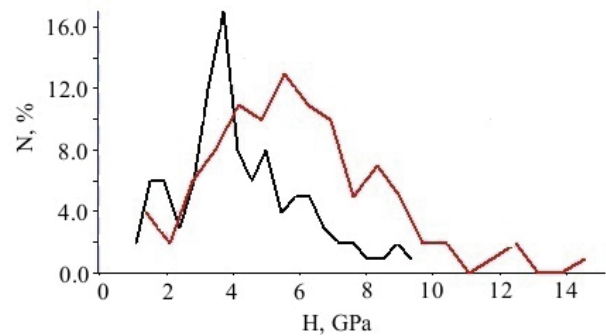


Figure 4 – Distribution of measured hardness. Red dots – sample № 1; black dots – sample № 2

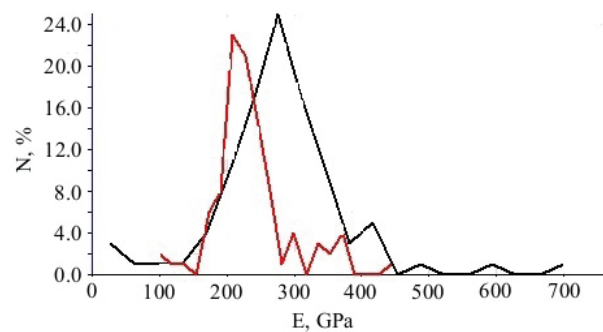


Figure 5 – Distribution of the measured elastic modulus. Red dots – sample № 1, black dots – sample № 2

The positions of the maxima in Figures 4 and 5 correspond to the following values of the hardness H_{hyst} and the elastic modulus E_{hyst} , shown in the Table 4. It also presents the average values of hardness and modulus (index "media"), as well as extreme values.

Table 4

Hardness and elastic modulus of the samples, determined by the distribution maxima of the corresponding quantities

Sample	H_{hyst} , GPa	H_{mean} , GPa	H_{min} , GPa	H_{max} , GPa	E_{hyst} , GPa	E_{mean} , GPa	E_{min} , GPa	E_{max} , GPa
№ 1	5.6	6.2	1.07	14.9	215	243	92	363
№ 2	3.7	4.4	0.89	9.6	275	292	10.4	720

Measurement of tool hardness and elastic modulus (nanoindentation): indentation in flat areas

In both samples, indentation was performed in preselected surface areas. The indentation load was 10 mN, an example of the location of indentation sites for sample No. 1 is shown in Figure 6. A similar image for sample No. 2 is shown in Figure 7. In these photographs, even areas that were selected for nanoindentation, as well as microcavities, which indicated in [1]. Identification with such a small load into preselected flat surface areas is logical, since measurement with such a load in arbitrary places, due to the presence of cavities, caverns and other defects, can lead to measurement results very different from the main population. On the other hand, it is the results of measurements with such a small load that are closest to the values of surface hardness.

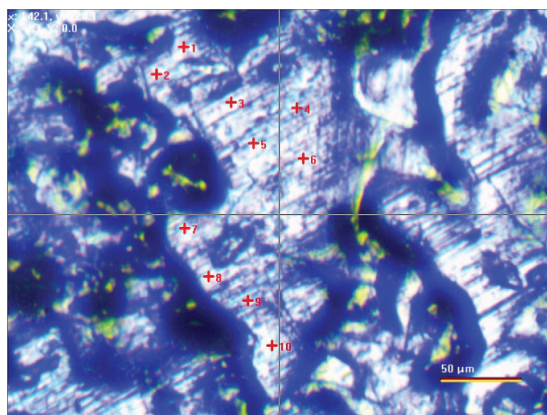


Figure 6 – Optical micrograph of the distribution of indentation sites in sample № 1 (magnification $\times 60$, aperture 0.85)

As a result of processing the obtained data, the dependences of hardness and elastic modulus were obtained, presented in Figure 8 and in Table 5. Measurements significantly different from the main population were deleted.

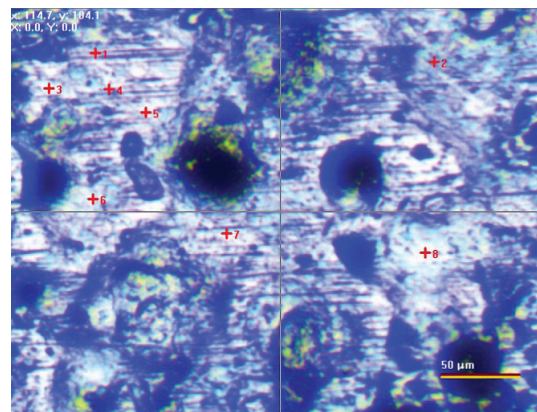


Figure 7 – Optical micrograph of the distribution of indentation sites in sample № 2 (magnification $\times 60$, aperture 0.85)

Table 5

Hardness and modulus of elasticity of the samples, determined when indented in flat areas with a load of 10 mN

Sample	H, GPa	E, GPa
№ 1	14.2 ± 2.1	268 ± 47
№ 2	9.5 ± 2.2	260 ± 33

A comparison of the measured hardness values by the two methods is shown in the Figure 9.

In Figure 9, the values of "nanoindentation" of samples No. 1 and No. 2, determined at a load of $1 H \approx 0.1 \text{ kgf}$, refer to the indices located arbitrarily.

The values of "nanoindentation 10 mN" on samples No. 1 and No. 2 refer to the indices located on a flat surface area (load $10 \text{ mN} \approx 0.001 \text{ kgf}$).

There are a number of methodological sources of uncertainty in the results of measurements of hardness by the above methods: 1) hardware related to the calibration of the measuring installation [8]; 2) methodological associated with assumptions in the calculation methodology [8, 15]; 3) sources associated with the physicomechanical properties

of the studied material [16, 17]. Without considering the hardware and methodological components of the uncertainty of the measurement results by the Vickers and industrial indentation methods, we note the sources of uncertainty associated with the physical properties of the mineral coatings of the metal surface. In particular, the high precision of measurements implemented by the instrumental indentation method leads to the fact that the minimum deviation of the interfering

parameters, in particular, the roughness, leads to large error values when calculating the measurement results [13, 14], which is clearly recorded graphically in Figure 9 when comparing results measured by two methods. The role of roughness as an uncertainty factor and the associated error is affected by the actual contact area with the indenter [14, 18], which is especially noticeable when measuring at shallow indentation depths (at a load of less than 0.1 kgf in Figure 9).

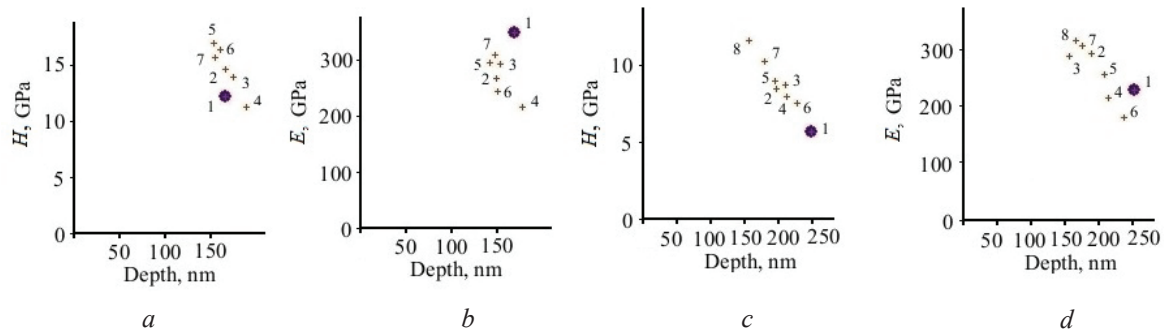


Figure 8 – The dependence of hardness H and elastic modulus E on the maximum indentation depth for sample No. 1 (a, b) and sample No. 2 (c, d)

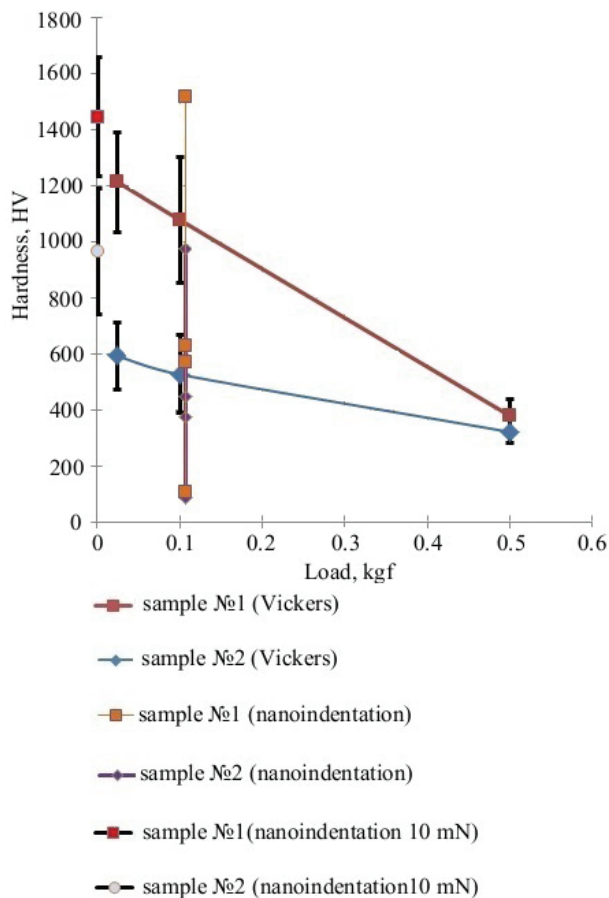


Figure 9 – The dependence of hardness on the indentation load, measured by two methods

An additional difference in the results of measurements performed by two methods at shallow indentation depths, which is clearly fixed in Figure 9, can be made by the fact that the object under study is a complex structured material [1], consisting of a metal matrix and fine particles distributed over the depth of the sample. Given that when calculating the values of hardness and elastic modulus from the load–injection diagram according to the standard method [8, 9], all the calculation formulas are deduced from the assumptions about the interaction of the indenter with a homogeneous isotropic half-space [15, 17], the complex structure of the distribution of particles and how consequence, properties, can lead to distortion of the results. A similar overestimation of hardness values at a small indentation depth, measured on thin modified layers of various metals and alloys, has been observed in many works (see, for example, [18]).

All of the above leads to problems in determining the actual properties of thin layers modified by ultrafine particles of minerals. A possible way out of the situation was identified in several works and consists in the transition from the use of hardness measures in calibrating instruments that implement the instrumental indentation method to standard property samples for which the mechanical properties will be constant in the indentation depth

range in which measurements are carried out (see, for example [19, 20]). However, at the moment, such reference samples are absent both in the markets of materials and research instruments, and in wide research practice. Therefore, the comparison of the results of measurements of the hardness of the layers of the metal surface modified with ultrafine particles of minerals, performed by two methods, the Vickers method and the industrial indentation method, can be carried out with a considerable degree of conventionality, especially at loads less than 0.1 kgf. When carrying out experimental design work related to changes in technological conditions and the search for optimal conditions for obtaining thin wear-resistant layers on the surface of metals modified with ultrafine particles of minerals, comparative measurements performed by one of the measurement methods are preferable.

Conclusion

A comparative study of the hardness of a metal surface (steel 20X13) modified with ultrafine particles of minerals was performed using two different methods (instrumental indentation and Vickers hardness measurement), taking into account the features of measuring the hardness of thin layers modified with ultrafine particles of minerals. Given the state of the surface after modification, indentation by both methods was carried out in flat sections of the modified surface. Additionally, taking into account the perspective automation of the measurement process, the hardness was measured by instrumental indentation at randomly selected locations. Standard Vickers hardness measurements at loads of 0.025, 0.1 and 0.5 kg showed a qualitative difference between the hardness values of the two samples modified with different mixtures of ultrafine mineral particles (1215 ± 180 HV and 600 ± 120 HV for samples No. 1 and 2, respectively) and a large heterogeneity of values hardness by area. By the method of instrumental hardness, standard measurements were performed without preliminary selection of the indentation site (at a load of 1.05 N) and measurements during indentation into even sections (at low loads of 10 mN). In addition, measurements of roughness and elastic modulus were performed.

In discussing the differences in the measurement results performed by different methods, emphasis is placed on the sources of uncertainty in the results associated with the physicomechanical properties

of the material under study. In particular, the high precision of measurements implemented by the instrumental indentation method leads to the fact that the minimum deviation of the interfering parameters, in particular, roughness, leads to large values of the error in calculating the measurement results. An additional difference in the results of measurements performed by two methods at shallow indentation depths can be made by the fact that the object under study is a material with a complex structure. All of the above leads to problems in determining the actual properties of thin layers modified by ultrafine particles of minerals.

A possible way out of the situation lies in the transition from the use of hardness measures in the calibration of instruments that implement the instrumental indentation method to standard samples of properties for which the constancy of mechanical properties will be ensured in the range of indentation depths in which measurements are carried out. Given the absence of such samples, it is preferable, when conducting experimental design work, related to changes in technological conditions and the search for optimal conditions for obtaining thin wear-resistant layers on the surface of metals modified with ultrafine particles of minerals, are comparative measurements performed by one of the measurement methods.

References

1. Kislov S.V., Kislov V.G., Skazochkin A.V., Bondarenko G.G., Tikhonov A.N. Effective mineral coatings for hardening the surface of metallic materials. *Russian Metallurgy (Metally)*, 2015, no. 7, pp. 558–564.
DOI: 10.1134/S0036029515070095
2. Skazochkin A., Bondarenko G., Kislov S. Research of Tribological Features of Steel Surface by Creating Mineral Coatings. *Journal of Engineering Science and Technology Review*, 2018, no. 11(6), pp. 138–143.
DOI: 10.25103/jestr.116.17
3. Skazochkin A.V., Useinov A.S., Kislov S.V. Surface hardening of titanium alloy by minerals. *Letters on Materials*, 2018, no. 8(1), pp. 81–87.
DOI: 10.22226/2410-3535-2018-1-81-87
4. Skazochkin A.V., Bondarenko G.G., Zukowski P. Research of Surface Wear Resistance of Aluminum Alloy Modified with Minerals using Sclerometry Method. *Devices and Methods of Measurements*, 2019, vol. 10, no. 3, pp. 263–270.
DOI: 10.21122/2220-9506-2019-10-3-263-270
5. Khodabakhshi F., Simchi A., Kokabi A.H. Surface modifications of an aluminum-magnesium alloy through reactive stir friction processing with titanium

oxide nanoparticles for enhanced sliding wear resistance. *Surface and Coatings Technology*, 2017, vol. 309, pp. 114–123. **DOI:** 10.1016/j.surfcoat.2016.11.060

6. Adebisi A.A., Maleque M.A., Rahman Md.M. Metal matrix composite brake rotor: historical development and product life cycle analysis. *International Journal of Automotive and Mechanical Engineering*, 2011, vol. 4, pp. 471–480. **DOI:** 10.15282/ijame.4.2011.8.0038

7. Oliver W.C., Pharr G.M. Measurement of hardness and elastic by instrumented indentation: Advances in understanding and refinements to methodology. *J. Mater. Res.*, 2004, vol. 19, no. 1, pp. 3–20.

8. Potapov A.I., Gogolinskiy K.V., Syasko V.A., Umanskiy A.S., Kondratiev A.V. Methodological and metrological aspects of materials mechanical properties measurements by instrumented indentation. *Testing. Diagnostics*, 2016, no. 8, pp. 16–21.

DOI: 10.14489/td.2016.08.pp.016-021

9. Useinov S., Solov'ev V., Gogolinskiy K., Useinov A., L'vova N. [Measurement of the mechanical properties of materials with nanometer resolution]. *Nanoindustriya* [Nanoindustry], 2010, no. 2, pp. 30–35 (in Russian).

10. Morozov E.M., Zernin M.V. *Kontaktnye zadachi mekhaniki razrusheniya* [Contact problems of fracture mechanics]. M: Mashinostroenie, 1999, 543 p.

11. Oliver W.C., Pharr G.M. An improved technique for determining hardness and elastic modulus using load and displacement sensing indentation experiments. *J. Mater. Res.*, 1992, vol. 7, no. 6, pp. 1564–1583.

12. Bhushan B. *Modern Tribology Handbook*, Two Volume Set, USA, CRC Press Inc, 2000, p. 1760.

13. Useinov A., Gogolinskiy K., Reshetov V. Mutual consistency of hardness testing at micro- and nanometer scales. *Int. J. Mater. Res.*, 2009, vol. 100, pp. 968–972.

DOI: 10.3139/146.110138

14. Potapov A.I., Gogolinskiy K.V., Kondratiev A.V., Umanskiy A.S. Indirect assessment of indenter area function for measuring mechanical properties by instrumented indentation. *Testing. Diagnostics*, 2017, no. 2, pp. 28–32. **DOI:** 10.14489/td.2017.02.pp.028-032

15. Maslenikova I., Reshetov V.N., Useinov A.S. Mapping the Elastic Modulus of a Surface with a NanoScan 3D Scanning Microscope. *Instruments and Experimental Techniques*, 2015, vol. 58, no. 5, pp. 711–717. **DOI:** 10.1134/S0020441215040223

16. Bhushan B., Li X. Micromechanical and tribological characterization of doped single-crystal silicon and polysilicon films for microelectromechanical systems devices. *Journal of Materials Research*, 1997, vol. 12, no. 1, pp. 54–63.

17. Zhang P., Li S.X., Zhang Z.F. General relationship between strength and hardness. *Materials Science and Engineering A.*, 2011, vol. 529, pp. 62–73.

DOI: 10.1016/j.msea.2011.08.061

18. Grishin A.M., Khartsev S.I., Bohlmark J., Ahlgren M. Ultra-hard AlMgB₁₄ coatings fabricated by RF magnetron sputtering from stoichiometric target. *Journal of Experimental and Theoretical Physics Letters*, 2015, vol. 100, pp. 680–687.

DOI: 10.1134/S0021364014220056

19. Gogolinskiy K.V., Reshetov V.N., Useinov A.S. [On the unification of the determination of hardness and the possibility of transition when measuring it to dimensional values]. *Izmeritel'naya tekhnika* [Measuring technique], 2011, no. 7, pp. 28–34 (in Russian).

20. Aslanyan A.E., Aslanyan E.G., Gavrilkin S.M., Doinikov A.S., Temnitskiy I.N., Shipunov A.N. [State primary standard of rigidity according to Martens scales and indentation scales GET 211-2014]. *Izmeritel'naya tekhnika* [Measuring technique], 2016, no. 6, pp. 3–6 (in Russian).

Determination of Parameters of Electrode Metal Transported Drops by Simulation and Visualization

D.P. Ilyaschenko^{1,2}, A.V. Kryukov¹, E.V. Lavrova³, M.A. Kuznetsov¹, E.V. Verkhoturova^{4,5}

¹*Yurga Institute of Technology National Research Tomsk Polytechnic University,
Leningradskaya str., 26, Yurga 652055, Russia*

²*Institute of Strength Physics and Materials Science of Siberian Branch Russian Academy of Sciences,
Academic Ave., 2/4, Tomsk 634055, Russia*

³*Priazovskiy State Technical University,
Universitetska str., 7, Mariupol 87500, Ukraine*

⁴*Irkutsk National Research Technical University,
Lermontova str., 83, Irkutsk 664074, Russia*

⁵*Kaliningrad State Technical University,
Sovetsky Ave., 1, Kaliningrad 236022, Russia*

Received 20.06.2020

Accepted for publication 03.09.2020

Abstract

The nature of the molten electrode metal melting and transfer is the main process parameter of manual metal arc welding (MMA) with coated electrodes. It significantly affects the efficiency of the welding process. For this reason the relevant task is to identify the parameters of the transferred molten electrode metal drops and their further transfer into the weld pool with maximum accuracy. The aim of the given paper is to develop a method and visual representation of the form and the geometrics (volume, area, mass) of a molten electrode metal drop.

We have developed the method of simulation modeling and visualization for molten electrode metal drops transfer and their parameters. It allows obtaining highly reliable input data to be used for developing and verification of mathematical models for the thermal fields distribution along the welded item surface. The algorithm is realized as the calculation programs for specifying the molten metal drop parameters and means of its geometrics and space form visualization.

We used this method to specify a number of molten electrode metal drop parameters: volume, mass, center-of-gravity position, surface area.

We have established that it is possible to conduct the measurements with maximum

The suggested method significantly decreases the labor intensity of experimental studies aimed at specifying the size of electrode metal drops in comparison to the standard methods. When we know the size of the drops under certain welding conditions we can control the drop transfer process, i. e. reduce the heat input into the welded item and produce weld joints with the tailored performance characteristics.

Keywords: MMA, a drop of molten electrode metal, parameters, simulation method, visualization.

DOI: 10.21122/2220-9506-2020-11-3-222-227

Адрес для переписки:

Д.П. Ильященко
Юргинский технологический институт (филиал) Национального
исследовательского Томского политехнического университета,
ул. Ленинградская, 26, г. Юрга 652055, Россия
e-mail: mita8@rambler.ru

Address for correspondence:

D.P. Ilyaschenko
Yurga Institute of Technology National Research Tomsk Polytechnic
University, Leningradskaya st., 26, 652055, Yurga, Russian Federation
e-mail: mita8@rambler.ru

Для цитирования:

D.P. Ilyaschenko, A.V. Kryukov, E.V. Lavrova, M.A. Kuznetsov,
E.V. Verkhoturova.

Determination of Parameters of Electrode Metal Transported
Drops by Simulation and Visualization.

Приборы и методы измерений.

2020. – Т. 11, № 3. – С. 222–227.

DOI: 10.21122/2220-9506-2020-11-3-222-227

For citation:

D.P. Ilyaschenko, A.V. Kryukov, E.V. Lavrova, M.A. Kuznetsov,
E.V. Verkhoturova.

Determination of Parameters of Electrode Metal Transported
Drops by Simulation and Visualization.

Devices and Methods of Measurements.

2020, vol. 11, no. 3, pp. 222–227.

DOI: 10.21122/2220-9506-2020-11-3-222-227

УДК 621.791.75

Определение параметров переносимых капель электродного металла методом имитационного моделирования и визуализации

Д.П. Ильященко^{1,2}, А.В. Крюков¹, Лаврова Е.В.³, М.А. Кузнецов¹, Е.В. Верхотурова^{4,5}

¹Юргинский технологический институт (филиал) Национального исследовательского Томского политехнического университета,
ул. Ленинградская, 26, г. Юрга 652055, Россия

²Институт физики прочности и материаловедения Сибирского отделения Российской академии наук,
пр-т Академический, 2/4, г. Томск 634055, Россия

³Приазовский государственный технический университет,
ул. Университетская, 7, г. Мариуполь 87500, Украина

⁴Иркутский национальный исследовательский технический университет,
ул. Лермонтова, 83, г. Иркутск 664074, Россия

⁵Калининградский государственный технический университет,
Советский пр-т, 1, г. Калининград 236022, Россия

Поступила 20.06.2020

Принята к печати 03.09.2020

Основным технологическим параметром процесса ручной дуговой сварки, покрытым электродами, существенно влияющим на эффективность его протекания, является характер плавления и переноса расплавленного электродного металла. Поэтому актуальным является вопрос максимально точного определения параметров переносимых капель расплавленного электродного металла и их последующего перехода в сварочную ванну. Целью данной работы являлась разработка методики и визуального представления формы и геометрических параметров (объём, площадь, масса) капли расплавленного электродного металла.

Разработан метод имитационного моделирования и визуализации переноса капель расплавленного электродного металла и их параметров, что позволит получить входные данные с высокой степенью достоверности для разработки математических моделей распределения температурных полей по поверхности свариваемого изделия и её верификации. Алгоритм реализован в виде расчётных программ для определения параметров капли расплавленного металла и средств визуального представления её геометрии и пространственной формы.

С помощью данного метода определён ряд параметров капель расплавленного электродного металла: объём, масса, положение центра масс, площадь поверхности.

Установлено, что возможно с максимальной достоверностью производить измерения, увеличить число измеряемых параметров, а также наглядно представить происходящие процессы.

Предложенный метод значительно упрощает трудоёмкость проведения экспериментальных исследований по определению размера капель электродного металла в сравнении со стандартными методами. Зная размер капель при определённых режимах сварки, можно управлять процессом каплепереноса, т. е. уменьшать тепло-вложение в свариваемое изделие и получать сварные соединения с заданными эксплуатационными свойствами.

Ключевые слова: ручная дуговая сварка, капля расплавленного электродного металла, метод имитационного моделирования, визуализация.

DOI: 10.21122/2220-9506-2020-11-3-222-227

Адрес для переписки:

Д.П. Ильященко
Юргинский технологический институт (филиал) Национального исследовательского Томского политехнического университета,
ул. Ленинградская, 26, г. Юрга 652055, Россия
e-mail: mita8@rambler.ru

Address for correspondence:

D.P. Ilyaschenko
Yurga Institute of Technology National Research Tomsk Polytechnic University, Leningradskaya st., 26, 652055, Yurga, Russian Federation
e-mail: mita8@rambler.ru

Для цитирования:

D.P. Ilyaschenko, A.V. Kryukov, E.V. Lavrova, M.A. Kuznetsov, E.V. Verkhoturva.
Determination of Parameters of Electrode Metal Transported Drops by Simulation and Visualization.
Приборы и методы измерений.
2020. – Т. 11, № 3. – С. 222–227.
DOI: 10.21122/2220-9506-2020-11-3-222-227

For citation:

D.P. Ilyaschenko, A.V. Kryukov, E.V. Lavrova, M.A. Kuznetsov, E.V. Verkhoturva.
Determination of Parameters of Electrode Metal Transported Drops by Simulation and Visualization.
Devices and Methods of Measurements.
2020, vol. 11, no. 3, pp. 222–227.
DOI: 10.21122/2220-9506-2020-11-3-222-227

Introduction

The main technological parameter of the process of manual arc welding (MMA) with coated electrodes, which significantly affects the efficiency of its flow, is the nature of melting and transfer of molten electrode metal from the end of the electrode to the weld pool. The geometric parameters of the transferred droplets of molten electrode metal have a significant effect on the mechanical and operational properties of the welded joint. Determination of the regularities of the droplet transfer process, such as the formation and size of a drop at the edge of the electrode, makes it possible to create methods for controlling the volume of drops, choose the optimal options for implementing the technological process and serves as the basis for solving a wide range of practical problems.

Now, methods are used to study the transfer of electrode metal [1]: direct (separation and weighing of drops and X-ray and video filming) and indirect (oscillography of current and voltage), which are significantly laborious.

There are various methods for determining the size of drops of electrode metal based on the construction of mathematical models [2–4]. These methods used with various simplifications (assumptions), for example, the arc column is stationary and coaxial with the electrode, and a drop of molten metal has the shape of a segment or a glob, etc., which significantly reduce the reliability of the results obtained. The use of modern computational and graphic programs [5–7] makes it possible to perform calculations with a high degree of reliability and reduces the processing time of experimental data.

The aim of this work is to develop a method for determining the parameters (volume, surface area and mass) of the transferred drops of electrode metal through the arc gap of the MMA process using a software package.

Visualization of the manual metal arc welding with coated electrodes

We applied a numerical algorithm, visualization of molten electrode metal droplets transfer and specification of their dimensional parameters (volume, area, mass) to develop a simulation model of a molten electrode metal. The method of simulation and visualization will allow predicting heat input into the welded metal, as well as predicting the mechanical and operational properties of welded joints.

The construction of a spatial model of a liquid droplet of molten electrode metal was carried out on the basis of frames of high-speed video filming carried out earlier [8] using the Kompas 3D software package from ASCON.

An experimental setup for high-speed shooting and process oscillography shown in Figure 1.

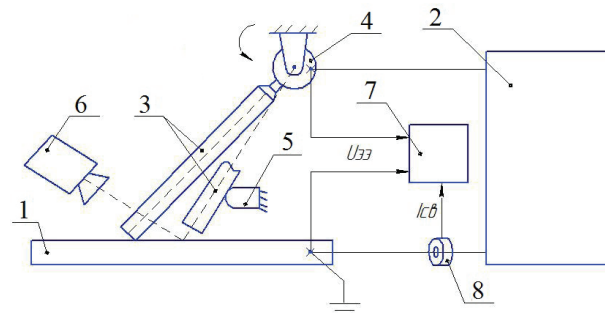


Figure 1 – The experimental setup for high-speed shooting and oscillography of the welding process: 1 – metal plate; 2 – power source; 3 – coated electrode, 4 – rotating electrode holder, 5 – electrode movement limiter, 6 – digital high-speed video camera, 7 – electronic oscilloscope, 8 – current sensor

A visual representation of the welding process and the transition of molten electrode metal droplets from the end of the electrode into the liquid weld pool presented in the form of filming and oscillograms shown in Figures 2 and 3, respectively.

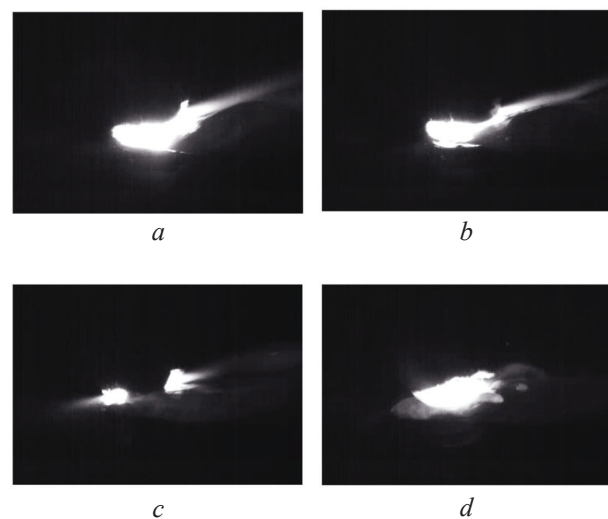


Figure 2 – Filming of the process of transferring drops of electrode metal during MMA: *a* – the beginning of the formation of a drop on the surface of the coated electrode; *b* – the growth of a drop of liquid metal on the surface of the electrode; *c* – drop transition from the electrode surface to the weld pool with the closure of the arc gap; *d* – the process of the onset of nucleation of the subsequent drop

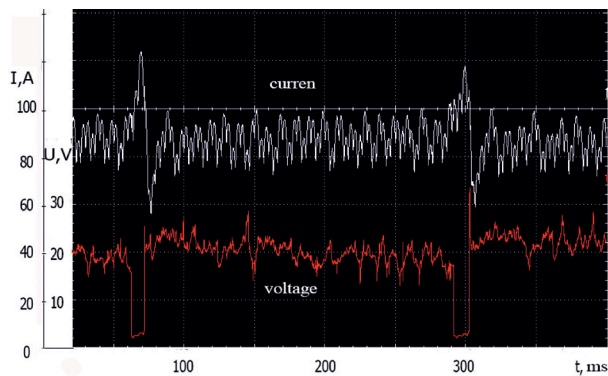


Figure 3 – Oscillograms of current and voltage (electrodes of the TsL-11 brand with a diameter of 3 mm, power supply VD-306)

Simulation modeling

In order to simplify the simulation, it was assumed, that in any section of the drop, by a plane perpendicular to the axis of the electrode, a simple geometric figure is obtained – a circle. In this case, the sequence of constructing the calculated visual model was as follows:

1. The image obtained during high-speed video filming (Figure 2) was opened in the program window, "Kompas 3D", where using the "spline" command, the contour of the liquid drop was visualized (Figure 4). At this stage, the scale of the construction is determined based on the actual size of the electrode (an electrode diameter of 3 mm was used).

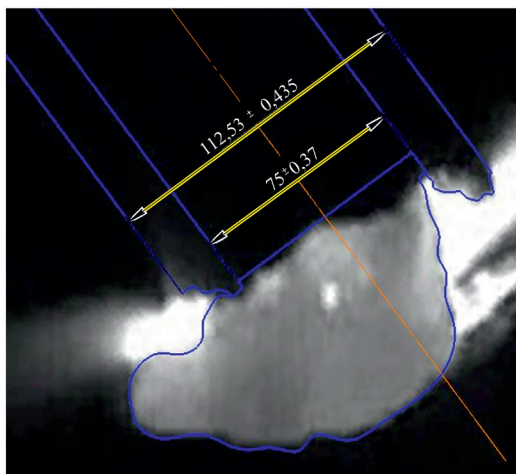


Figure 4 – Liquid drop contour

2. On the rendered contour of the drop, lines were drawn corresponding to the position of the future secant planes. At the same time, the lines were initially drawn in places where the direction

of the contour changed, then with the same interval between them.

3. The obtained image (Figure 5) was used to determine the diameters of the section circles and the position of the circle center relative to the axis coinciding with the electrode axis.

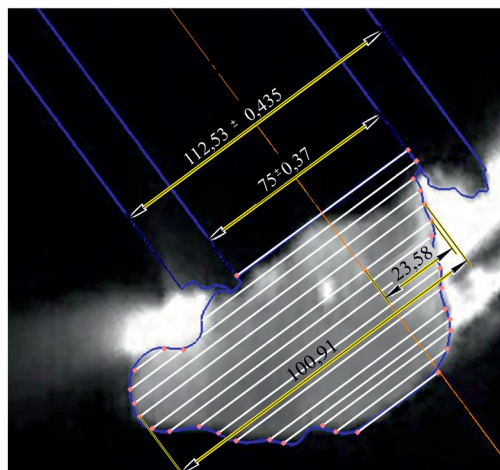


Figure 5 – Placement of secant planes

4. Simulation of the droplet volume was carried out in three-dimensional modeling mode in the "Kompas 3D" application. For this, a number of parallel planes were built (their position was determined in point 2) in which the droplet sections were constructed (according to the sizes determined in point 3). Then, using the "Lines" function, a volumetric body corresponding to the shape of a liquid drop was built (Figure 6).

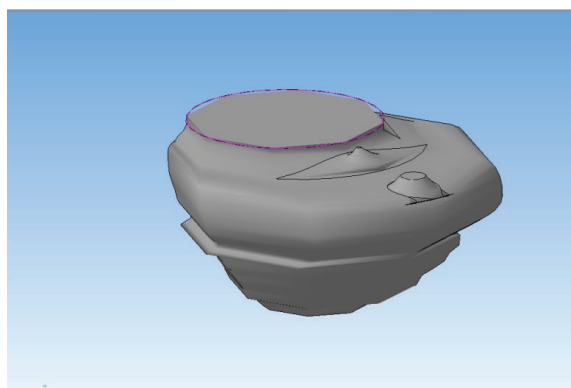


Figure 6 – Solid modeling of the spatial shape of a drop

5. Measurements were made of various parameters of the spatial model of the drop (volume, mass, position of the center of mass, surface area, etc., Figure 7) using the "MCM model" function presented in the "Kompas 3D" program.

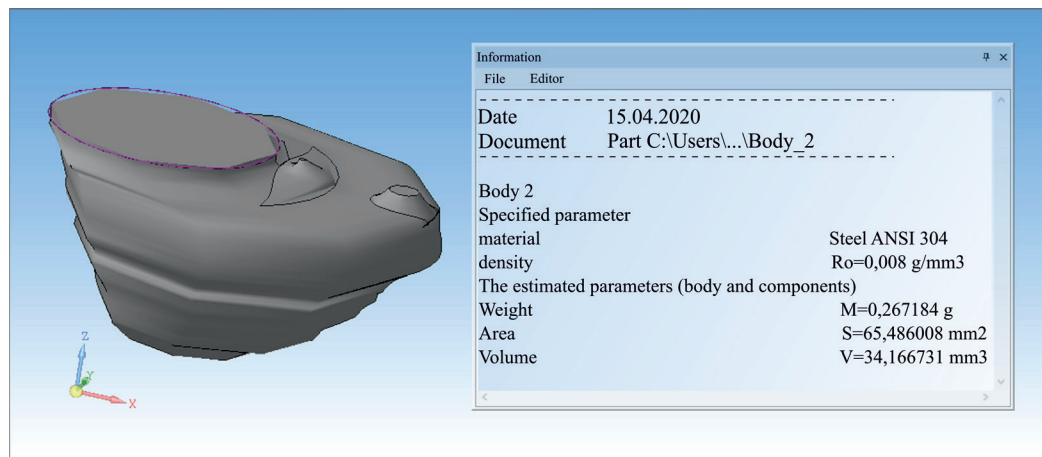


Figure 7 – Determination of the parameters of the spatial droplet model

Analysis of the method adequacy

The method of simulation modeling and visualization of a molten electrode metal droplet geometrics was tested by comparing the results obtained with the transferred drops parameters obtained by the indirect method [2] after oscillograms

processing (Figure 3) according to the following method [8].

The convergence of the results of theoretical studies and the amount of deposition recommended by the manufacturer of the electrode (table), according to: the proposed method – 5 %, the indirect method [8] – 23 %.

Table

Comparison of theoretical and experimental data of certain parameters of transferred drops

Data retrieval method	Electrode type, power supply	$t_{s.c} \cdot 10^{-3}$, sec	Drop weight m , g	Drop volume V , mm^3	Deposition coefficient a , g/A·h
Calculated, according to the methodology [8]	CL-11, diode rectifier	12 ± 3.8	0.37 ± 0.04	45.48 ± 4.9	13.6 ± 0.4
Visualization, according to the proposed method			0.264 ± 0.05	34.167 ± 2.5	10.5 ± 0.3
Manufacturer data*					11

*SpetsElectrode Company, <https://www.spetselectrode.ru/electrod/cl11.htm>

The proposed method will allow taking into account the peculiarities of the configuration of the transferred droplets when developing models: thermal processes during welding [9–11] and predicting the chemical composition and operational properties of the deposited weld metal [12], which increases its adequacy.

Conclusion

To determine the shape and size of a drop of molten electrode metal, a method of simulation and

visualization was developed, including a mathematical model, a spatial model of a drop of molten electrode metal using a computer program package. Using this method, a number of parameters of molten electrode metal droplets were determined: volume, mass, position of the center of mass, surface area. It was found, that the proposed method significantly simplifies the complexity of experimental studies to determine the size of drops of electrode metal in comparison with standard methods. Definition the droplet size for different welding modes allow to control the droplet transfer process, i. e. to reduce heat

input into the welded product and to obtain welded joints with specified operational properties.

Acknowledgments

The Russian Science Foundation, grant no. 18-79-10035, supported this work.

References

1. Saraev Y.N., Chinakhov D.A., Ilyashchenko D.I., Kiselev A.S., Gordynets A.S. Investigation of the stability of melting and electrode metal transfer in consumable electrode arc welding using power sources with different dynamic characteristics. *Welding International*, 2017, no. 31(10), pp. 784–790.

DOI: 10.1080/09507116.2017.1343977

2. Milyutin V.S. *Ispytaniya svarochnykh svoystv oborudovaniya dlya dugovoy svarki* [Testing the welding properties of equipment for arc welding]. Ekaterinburg, 2019, 466 p.

3. Lebedev V. Determination of the volume of the different drop of electrode metal in the conditions of vibrations of the bath and electrode with arc mechanized welding. *Нові матеріали і технології в металургії та машинобудуванні*, 2017, no. 2, pp. 95–99 (in Ukrainian).

4. Makarenko V.D., Paly R.V., Mukhin M.Yu. *Tekhnologicheskie svoystva montazhnoj svarki truboprovodov* [Technological properties of assembly welding of pipelines]. ed. V.D. Makarenko. Moscow: Nedra-Business Center LLC Publ., 2001, 118 p.

5. Krampit A.G., Krampit N.Yu. Method for determining the geometric dimensions and area of the weld. *Welding production*, 2012, no. 10, pp. 40–42.

6. Votnova E.B., Shalimov M.P. Application of the complete material balance method to estimate the transition of elements in flux cored arc welding. *Solid State Phenomena*, 2020, vol. 299 SSP, pp. 559–564.

7. Makarenko V.D., Shatilo S.P. Calculation of the kinetic characteristics of electrode droplets during their passage through the arc gap during welding with coated electrodes. *Welding production*, 1999, no. 12, pp. 6–10.

8. Il'yaschenko D.P., Chinakhov D.A., Kirichenko K.Y., Sydorets V.N. Mathematical formula to determine geometrical dimensions of electrode metal droplets transferred with short circuits. *Materials Science Forum*, 2018, vol. 938, pp. 1–6.

DOI: 10.4028/www.scientific.net/MSF.938.1

9. Ilyashchenko D.P., Berg V.I., Kryukov A.B., Saranchin A.A. Numerical simulation of thermal processes in welding with pulsed electrode wire feeding. *Materials Science Forum*, 2018, vol. 927 MSF, pp. 55–63.

DOI: 10.4028/www.scientific.net/MSF.927.55

10. Chiocca A., Frenzo F., Bertini L. Evaluation of heat sources for the simulation of the temperature distribution in gas metal arc welded joints. *Metals*, 2019, vol. 9(11), p. 1142.

DOI: 10.3390/met9111142

11. Yonggang Z., Yanhong Z. High accuracy Numerical simulation on 3D weld-pool shape of large parts. *Journal of Physics: Conference Series*, 2019, vol. 1187(3), pp. 032–055.

DOI: 10.1088/1742-6596/1187/3/032055

12. Votnova E.B., Shalimov M.P. Application of the complete material balance method to estimate the composition of weld metal in manual arc welding. *Solid State Phenomena*, 2017, vol. 265 SSP, pp. 762–766.

DOI: 10.4028/www.scientific.net/SSP.265.762

Application of Two-Channel Principle in Measuring Devices to Compensate for Disturbing Influences of Unknown Physical Nature

V.N. Nesterov^{1,2,3}, A.R. Li¹

¹JCS Samara Electromechanical Plant,
Stepan Razin str., 16, Samara 443099, Russia

²Samara National Research University,
Moskovskoe highway, 34A, Samara 443086, Russia

³Povolzhskiy State University of Telecommunications and Informatics,
L. Tolstoy str., 23, Samara 443010, Russia

Received 28.01.2020

Accepted for publication 05.06.2020

Abstract

The article notes the advantages of the method of constructing absolutely invariant measuring transducers for working in conditions with disturbing influences. However, this method is not universal. Its limitations are due to the impossibility of "symmetric" transmission of all disturbing influences into parallel measuring channels. A broader interpretation of the two-channel principle is proposed to overcome these limitations. The aim of the study was to substantiate and implement a method for constructing quasi-invariant measuring transducers and systems that retain their metrological characteristics under external disturbances of unknown physical nature.

The theory that develops the two-channel principle to a full-fledged technological method is presented in the article. The theory includes the necessary and sufficient conditions for physical feasibility this method. Two fundamental tasks have been solved in the work. The first task is to identify signs that reflect the essence of the technological method in to specific cases and the second is to implement a methodology that allows these signs to be effectively applied in practice.

In the examples, a complex of technologies is defined for groups of elements of quasi-invariant transducers that provide compensation of the influencing factors acting on them with acceptable accuracy.

There are significant advantages in discussed method. It gives hope for acceptable measurement results under conditions when character and even physical principle of influencing a priori are unknown.

Keywords: technological method, quasi-invariance, disturbing influences, measuring transducer.

DOI: 10.21122/2220-9506-2020-11-3-228-235

Адрес для переписки:

В.Н. Нестеров
Самарский национальный исследовательский университет
имени академика С.П. Королёва
Московское шоссе, 34А, Самара 443086, Россия
e-mail: nesterov.ntc@yandex.ru

Address for correspondence:

V.N. Nesterov
Samara National Research University,
Moskovskoe highway, 34A, Samara 443086, Russia
e-mail: nesterov.ntc@yandex.ru

Для цитирования:

V.N. Nesterov, A.R. Li.
Application of Two-Channel Principle in Measuring Devices
to Compensate for Disturbing Influences of Unknown Physical Nature.
Приборы и методы измерений.
2020. – Т. 11, № 3. – С. 228–235.
DOI: 10.21122/2220-9506-2020-11-3-228-235

For citation:

V.N. Nesterov, A.R. Li.
Application of Two-Channel Principle in Measuring Devices
to Compensate for Disturbing Influences of Unknown Physical Nature.
Devices and Methods of Measurements.
2020, vol. 11, no. 3, pp. 228–235.
DOI: 10.21122/2220-9506-2020-11-3-228-235

УДК 681.2.088

Применение принципа двухканальности в измерительных устройствах для компенсации возмущающих воздействий неизвестной физической природы

В.Н. Нестеров^{1, 2, 3}, А.Р. Ли¹

¹Самарский электромеханический завод,
ул. Степана Разина, 16, Самара 443099, Россия

²Самарский национальный исследовательский университет имени академика С.П. Королёва,
Московское шоссе, 34А, Самара 443086, Россия

³Поволжский государственный университет телекоммуникаций и информатики,
ул. Л. Толстого, 23, Самара 443010, Россия

Поступила 28.01.2020

Принята к печати 05.06.2020

В статье отмечены преимущества метода построения абсолютно инвариантных измерительных преобразователей для работы в условиях с возмущающими воздействиями. Однако этот метод не является универсальным. Его ограничения обусловлены невозможностью «симметричной» передачи всех возмущающих воздействий в параллельные измерительные каналы. Для преодоления названных ограничений предложена более широкая трактовка принципа двухканальности. Целью исследования являлись обоснование и реализация метода построения квазиинвариантных измерительных преобразователей и систем, которые сохраняют свои метрологические характеристики в условиях внешних возмущений неизвестной физической природы.

Представлена теория, развивающая принцип двухканальности до полноценного технологического метода, включающего необходимые и достаточные условия его физической реализуемости. В работе решены две принципиальные задачи. Первая из них заключается в выявлении признаков, отражающих сущность технологического метода применительно к конкретным случаям, вторая – в реализации методики, позволяющей эти признаки эффективно применить на практике.

В примерах определён комплекс технологических мероприятий для групп элементов квазиинвариантных преобразователей, которые обеспечивают компенсацию действующих на них влияющих факторов с приемлемой точностью.

Рассмотренный метод имеет существенные преимущества. Он даёт надежду на приемлемые результаты измерений в условиях, когда характер и даже физический принцип влияющих факторов априори неизвестны.

Ключевые слова: технологический метод, квазиинвариантность, возмущающие воздействия, измерительный преобразователь.

DOI: 10.21122/2220-9506-2020-11-3-228-235

Адрес для переписки:

В.Н. Нестеров
Самарский национальный исследовательский университет
имени академика С.П. Королёва
Московское шоссе, 34А, Самара 443086, Россия
e-mail: nesterov.ntc@yandex.ru

Address for correspondence:

V.N. Nesterov
Samara National Research University,
Moskovskoe highway, 34A, Samara 443086, Russia
e-mail: nesterov.ntc@yandex.ru

Для цитирования:

V.N. Nesterov, A.R. Li.
Application of Two-Channel Principle in Measuring Devices
to Compensate for Disturbing Influences of Unknown Physical Nature.
Приборы и методы измерений.
2020. – Т. 11, № 3. – С. 228–235.
DOI: 10.21122/2220-9506-2020-11-3-228-235

For citation:

V.N. Nesterov, A.R. Li.
Application of Two-Channel Principle in Measuring Devices
to Compensate for Disturbing Influences of Unknown Physical Nature.
Devices and Methods of Measurements.
2020, vol. 11, no. 3, pp. 228–235.
DOI: 10.21122/2220-9506-2020-11-3-228-235

Introduction

The problems of accuracy have been and will be relevant in measurement theory always regardless of the place, time and type of measurement. This explains the huge number of articles and their number has been increasing steadily growing as humanity expands its area of interests. The exploration of the nearest outer space and in the future deep space, oceans, technologies accompanied by various unfavorable factors, for example, in nuclear energy or chemical industry, poses new challenges to the science of measurements. New applications and operating conditions of the measuring instruments in harsh conditions accompanied by various external and internal disturbances require serious correction of the results. In order to solve these problems method of auxiliary measurements, method of reference signals, method that using tests and others have been developed [1–5]. Their correct application can significantly reduce the errors of measuring instruments in abnormal operating conditions.

To solve these problems, methods of auxiliary measurements, of reference measures, of test measures and others have been developed. Their correct application can significantly reduce the errors of measuring instruments in abnormal operating conditions. However, each method requires certain conditions to be met. If these conditions are not met, then the effectiveness of the method may be reduced. Moreover, incorrect use of the method can result in the opposite result.

For example, the method of auxiliary measurements requires knowledge of the functions of the influence of interfering quantities, the auxiliary measurements of which allow you to enter the appropriate correction. But each auxiliary channel contributes its share to the total error of the measuring device. The test method requires additional channels, which receive a measurable value, functionally associated with exemplary tests. The methods of invariance theory, which are designed to compensate for the effect on the system of external perturbations, stand out in the theory of measurements. Initially, these methods were used in the theory of automatic control. But very soon there appeared papers in which ideas were expressed on the connection between the theory of invariance and the theory of stability of measuring systems [6, 7]. Academician B.N. Petrov formulated the two-channel principle [7], which was essentially a necessary condition for compensating external

disturbing influences on measuring devices. The combination of necessary and sufficient conditions, which is based on the mentioned principle, makes it possible to formulate and implement in the corresponding structures methodical features, which form the basis of a particular method and are implemented in the corresponding class of invariant measuring devices [8–11]. The fundamental difference between the methods of the theory of invariance and the methods of automatic correction of errors is such an organization of the structure of the system that provides compensation for disturbances inside it with the general instability of the component elements.

A series of works that consistently develops the two-channel principle to the structural method, allowed covering the classes of nonequilibrium measuring bridges and voltage dividers [12]. The absolute invariance of the transformation functions of the parametric transducers with respect to the instability of the power supply was achieved for all representatives of the class. Accordingly, the expression of the error from the instability of the EMF of the power source is identically equal to zero for all representatives of the class of two-channel parametric measuring transducers:

$$\Delta F = \frac{\partial F}{\partial U_1} \frac{\partial U_1}{\partial E} \Delta E + \frac{\partial F}{\partial U_2} \frac{\partial U_2}{\partial E} \Delta E \equiv 0,$$

where F is two-channel transducer conversion function; U_1 и U_2 are conversion functions of the first and second measuring channels; E is EMF of power supply; ΔE is deviation of power supply EMF from nominal value.

However, the physical feasibility of the methodological features [12], which provide absolute invariance of the transducers with respect to the effect of influencing factors on all elements of the devices, is limited by structural or economic reasons. Sources of errors of measuring devices are instability and technological variation of parameters of all elements included in them. But it is not always possible to provide "symmetry" of the influence of these elements on measuring channels.

Further analysis of the problem led to an understanding and a wider interpretation of the two-channel principle. This made it possible to formulate methodological features the implementation of which leads to compensation of disturbing actions on a wider set of elements of the measuring device. A preliminary analysis of the essence of these

methodological features allows us to propose the name of the method.

Technological method for constructing quasi-invariant measuring transducers

As already noted, the two-channel principle is a necessary but not sufficient condition for compensation of external disturbing influences on measuring devices. Therefore, a formal apparatus that develops the two-channel principle to the level of necessary and sufficient conditions the fulfillment of which due to specific technical or technological solutions will compensate for the instability of the device as a whole is the basis of the method, the name of which was set in the heading of the section.

Formal features that develop the two-channel principle to a full-fledged technological method, which includes the necessary and sufficient conditions for its physical feasibility, can be stated in the form of the following three points.

1. There should be q elements $q \geq 2$ in the system structure that are affected by disturbing factors ζ_j .

2. It should be possible to implement special technological measures leading to the "differential-symmetric" effect of disturbing factors on the parameters of the elements included in the system:

$$\left\{ \frac{\Delta k_{ir}(\zeta_j)}{k_{ir0}} - \frac{\Delta k_{il}(\zeta_j)}{k_{il0}} \right\} \rightarrow 0, \quad r \neq l; \quad r, l \in q, \quad (1)$$

where $\Delta k_{ir}(\zeta_j), \Delta k_{il}(\zeta_j)$ are deviations of the k -th parameter, respectively, of the r -th and l -th elements of the i -th conversion channel from the nominal values under the influence of disturbing factors ζ_j .

3. The following criterion must be met:

$$\Delta F = \sum_{i=1}^n \sum_{j=1}^q \frac{\partial F}{\partial Y_i} \frac{\partial Y_i}{\partial k_{ij}} \Delta k_{ij}(\zeta_j) \rightarrow 0, \quad (2)$$

where: F is resulting system conversion function; Y_i is conversion function of i -th channel; n is number of channels.

In the limit case if the expressions (1) turn into an identity then the criterion (2) reaches a zero extremum. Then we can talk about achieving absolute invariance of the system relative to disturbing factors. However, such a case is ideal. Therefore, the fundamental task is the methodological task of searching for paired elements and the corresponding technological measures that lead to the closest

possible fulfillment of criterion (2) in each specific case. In essence, we are talking about identifying the technological "know-how" for each pair (group) of elements that make up the measuring circuit.

Based on the above the problem to be solved is divided into two. The first task is to identify signs that reflect the principle essence of the technological method in a specific case. The second task is to implement a technique that allows these signs to be effectively applied in practice.

The technique for identifying technological "know-how" is based on the use of criterion (2). Since the left part of the criterion is an expression of error the source of which is the effect of perturbing factors on the elements, then equating it to zero and carrying out the necessary transformations it is possible to find in analytical form the conditions for minimizing the this error:

$$\frac{\Delta k_{ir}(\zeta_j)}{k_{ir0}} = \frac{\Delta k_{il}(\zeta_j)}{k_{il0}}, \quad r \neq l; \quad r, l \in q. \quad (3)$$

The latter will determine technological conditions, the physical essence and feasibility of which in each particular case depends on the physics of influencing factors and the structural and technological design of the device and its elements.

It should be emphasized that the fundamental issue for the implementation of the method is the possibility of identifying one or more groups of technologically similar (identical) elements in the device, where the number of elements in the group meets the requirement $q \geq 2$.

We emphasize that the fundamental issue for the implementation of the method is the possibility of identifying one or more groups of technologically similar (identical) elements in the device, where the number of elements in the group meets the requirement $q \geq 2$.

The implementation of the technological method

Let's consider the operation of the method using the example of a half-bridge two-channel transducer [13], which is shown in Figure 1. This transducer contains two differentially included primary converters 1 and 2 of the resistive type, the third converter 3, made in the form of a resistor, a power supply 4, differential amplifiers 5, 6 and 7 and a division unit 8.

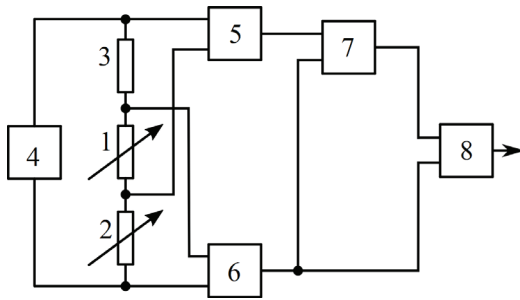


Figure 1 – Half-bridge invariant measuring transducer: 1, 2 – sensors; 3 – resistor; 4 – source of power; 5, 6, 7 – differential amplifiers; 8 – division block

The signals at the outputs of differential amplifiers 5 and 6 are determined by the expressions:

$$U_1 = \frac{k_1 E [(z_1 + \Delta z) + z_3]}{[(z_1 + \Delta z) + (z_2 - \Delta z) + z_3]}; \quad (4)$$

$$U_2 = \frac{k_2 E [(z_1 + \Delta z) + (z_2 - \Delta z)]}{[(z_1 + \Delta z) + (z_2 - \Delta z) + z_3]}, \quad (5)$$

where k_1 и k_2 are transmission coefficients for voltage of differential amplifiers 5 and 6, respectively; $(z_1 + \Delta z)$ and $(z_1 - \Delta z)$ are parameter values of transducers 1 and 2; (z_1 and z_2 are initial parameter values, and Δz is informative increment of parameters); z_3 is converter parameter value 3; E is EMF of power supply 4.

Signals (4) and (5) are supplied to direct and inverting inputs of differential amplifier 7,

respectively. And we get a difference signal at its output, when the condition $k_1 = k_2 = k$ is met:

$$U_1 - U_2 = \frac{k E [z_3 - (z_2 - \Delta z)]}{[(z_1 + \Delta z) + (z_2 - \Delta z) + z_3]}. \quad (6)$$

Next, the signals (5) and (6) are processed by the division unit 8. When the condition $z_1 = z_2 = z_3 = z$ is met we obtain at its output:

$$F_1 = \frac{U_1 - U_2}{U_2} = \frac{\Delta z}{2z}. \quad (7)$$

Using (4), (5) and (7), we obtain:

$$\Delta F_1 = \frac{\partial F_1}{\partial U_1} \frac{\partial U_1}{\partial E} \Delta E + \frac{\partial F_1}{\partial U_2} \frac{\partial U_2}{\partial E} \Delta E \equiv 0.$$

Thus, this transducer provides absolute invariance with respect to the power supply EMF instability. However, the instability of the parameters of the remaining elements is the source of additional errors.

Based on the proposed procedure we can identify groups of technologically similar elements in the measuring transducer. These groups comprise converters 1–3 and differential amplifiers 5 and 6.

We will be writing an appropriately structured expression of the error from the action of influencing factors on these groups of elements in accordance with criterion (2):

$$\begin{aligned} \Delta F_1 = & \frac{[(z_1 + \Delta z)_0 + z_{30}]}{[(z_1 + \Delta z)_0 + (z_2 - \Delta z)_0]} \left\{ \left(\frac{\Delta k_1}{k_0} - \frac{\Delta k_2}{k_0} \right) + \right. \\ & + \frac{(z_1 + \Delta z)_0 (z_2 - \Delta z)_0}{[(z_1 + \Delta z)_0 + (z_2 - \Delta z)_0 + z_{30}] [(z_1 + \Delta z)_0 + z_{30}]} \left[\frac{\Delta(z_1 + \Delta z)}{(z_1 + \Delta z)_0} - \frac{\Delta(z_2 - \Delta z)}{(z_2 - \Delta z)_0} \right] + \\ & + \frac{(z_2 - \Delta z)_0 z_{30} [2(z_1 + \Delta z)_0 + (z_2 - \Delta z)_0 + z_{30}]}{[(z_1 + \Delta z)_0 + (z_2 - \Delta z)_0 + z_{30}] [(z_1 + \Delta z)_0 + z_{30}] [(z_1 + \Delta z)_0 + (z_2 - \Delta z)_0]} \times \\ & \times \left[\frac{\Delta z_3}{z_{30}} - \frac{\Delta(z_2 - \Delta z)}{(z_2 - \Delta z)_0} \right] + \frac{(z_1 + \Delta z)_0 z_{30}}{[(z_1 + \Delta z)_0 + (z_2 - \Delta z)_0 + z_{30}] [(z_1 + \Delta z)_0 + (z_2 - \Delta z)_0]} \times \\ & \times \left. \left[\frac{\Delta z_3}{z_{30}} - \frac{\Delta(z_1 + \Delta z)}{(z_1 + \Delta z)_0} \right] \right\} \rightarrow 0, \end{aligned} \quad (8)$$

where $\frac{\Delta(z_1 + \Delta z)}{(z_1 + \Delta z)_0}$, $\frac{\Delta(z_2 - \Delta z)}{(z_2 - \Delta z)_0}$, $\frac{\Delta z_3}{z_{30}}$, $\frac{\Delta k_1}{k_0}$, $\frac{\Delta k_2}{k_0}$ are relative

changes, respectively, of the parameters of elements 1, 2, 3 and the transmission coefficients of differential amplifiers 5 and 6 under the action of influencing factors.

The error expression (8) will tend to zero with the "differential-symmetric" effect of destabilizing factors on the parameters of the corresponding groups of elements:

$$\left\{ \frac{\Delta k_1}{k_0} - \frac{\Delta k_2}{k_0} \right\} \rightarrow 0; \left\{ \frac{\Delta(z_1 + \Delta z)}{(z_1 + \Delta z)_0} - \frac{\Delta(z_2 - \Delta z)}{(z_2 - \Delta z)_0} \right\} \rightarrow 0; \quad (9)$$

$$\left\{ \frac{\Delta z_3}{z_{30}} - \frac{\Delta(z_2 - \Delta z)}{(z_2 - \Delta z)_0} \right\} \rightarrow 0; \left\{ \frac{\Delta z_3}{z_{30}} - \frac{\Delta(z_1 + \Delta z)}{(z_1 + \Delta z)_0} \right\} \rightarrow 0.$$

From expression (9) we obtain the conditions for compensating the influence of destabilizing factors on the corresponding groups of transducer elements:

$$\frac{\Delta k_1}{k_0} = \frac{\Delta k_2}{k_0}; \quad \frac{\Delta(z_1 + \Delta z)}{(z_1 + \Delta z)_0} = \frac{\Delta(z_2 - \Delta z)}{(z_2 - \Delta z)_0} = \frac{\Delta z_3}{z_{30}}. \quad (10)$$

The analysis of conditions (10) allows us to determine the complex of technological measures relating to the corresponding groups of elements of the considered converter, which will provide compensation for disturbing factors acting on them with an accuracy of:

The analysis of the conditions (10) allows us to determine a set of technological measures relating to the corresponding groups of elements of the transducer considered, which will provide compensation for the disturbing factors acting on them with an accuracy up to ε :

1. The elements in the group must be technologically identical. For example, they must be made of the same material, made of identical components, taken from the same batch, etc.

2. Elements of the group must be in identical conditions with respect to any disturbing influences.

3. The active elements in the group should be of the same brand, preferably from the same batch and, if possible, have a common power source.

If the listed requirements are fully fulfilled it is possible to approach the fulfillment of the conditions (10). And, accordingly, additional error of the transducer, the model of which is represented by the expression (8), will be reduced.

Expression (8) does not take into account the contribution of differential amplifier 7. Taking into account the transmission coefficient of the differential amplifier 7 after similar transformations we can (10) supplement with the condition:

$$\frac{\Delta k_1}{k_0} = \frac{\Delta k_2}{k_0} = \frac{\Delta k_3}{k_0}.$$

Operational amplifiers have very high input impedance that tends to infinity. Therefore, the transmission coefficients of differential amplifiers based on them are determined by the parameters of the mounted resistors. Accordingly, their instability depends on the instability of the parameters of the mounted resistors.

By revealing the technical content of the differential amplifier 7, which is shown in Figure 2, we detect a group of similar resistors 9–12, which determine its conversion function.

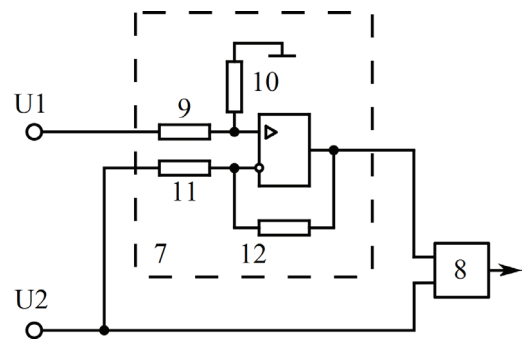


Figure 2 – Differential amplifier as part of the measuring transducer (see Figure 1): 9–12 – resistors of one type

The output voltage of differential amplifier 7 is determined by the expression:

$$U_3 = U_1 \frac{R_{10}}{R_9 + R_{10}} \left(1 + \frac{R_{12}}{R_{11}} \right) - U_2 \frac{R_{12}}{R_{11}}, \quad (11)$$

where $R_9, R_{10}, R_{11}, R_{12}$ are resistance of the resistors 9–12, accordingly.

Obviously, when the condition $R_9 = R_{10} = R_{11} = R_{12}$ is met, the expression (11) takes the form:

$$U_3 = U_1 - U_2,$$

which is required in accordance with the algorithm of the circuit.

It can be seen from (11) that the instability of this differential amplifier is determined by the instability of the resistances: $R_9, R_{10}, R_{11}, R_{12}$. The expression of the error resulting from the instability of these resistances is as follows:

$$\Delta U_3 = \frac{\partial U_3}{\partial R_9} \Delta R_9 + \frac{\partial U_3}{\partial R_{10}} \Delta R_{10} + \frac{\partial U_3}{\partial R_{11}} \Delta R_{11} + \frac{\partial U_3}{\partial R_9} \Delta R_9 + \frac{\partial U_3}{\partial R_{12}} \Delta R_{12} = U_1 \frac{R_9 R_{10}}{(R_9 + R_{10})^2} \left(1 + \frac{R_{12}}{R_{11}} \right) \left[\frac{\Delta R_{10}}{R_{10}} - \frac{\Delta R_9}{R_9} \right] + \frac{R_{12}}{R_{11}} \left(U_1 \frac{R_{10}}{R_9 + R_{10}} - U_2 \right) \left[\frac{\Delta R_{12}}{R_{12}} - \frac{\Delta R_{11}}{R_{11}} \right]. \quad (12)$$

In accordance with criterion (2) from expression (12), the need for a "differential-symmetric" effect of destabilizing factors on the parameters of the corresponding groups of resistors is revealed R_9 , R_{10} and R_{11} , R_{12} :

$$\left\{ \frac{\Delta R_{10}}{R_{10}} - \frac{\Delta R_9}{R_9} \right\} \rightarrow 0; \quad \left\{ \frac{\Delta R_{12}}{R_{12}} - \frac{\Delta R_{11}}{R_{11}} \right\} \rightarrow 0. \quad (13)$$

Then from (13) we obtain the conditions for compensating the influence of destabilizing factors on the differential amplifier:

$$\frac{\Delta R_{10}}{R_{10}} = \frac{\Delta R_9}{R_9}; \quad \frac{\Delta R_{12}}{R_{12}} = \frac{\Delta R_{11}}{R_{11}}. \quad (14)$$

Conditions (14) are implemented due to technological measures:

– resistors R_9 , R_{10} and R_{11} , R_{12} constituting paired groups must be technologically identical, made of the same material and on the basis of identical components, and taken from the same batch, etc.;

– resistors R_9 , R_{10} and R_{11} , R_{12} constituting paired groups must be in identical conditions with respect to any disturbing influences.

Obviously, the same requirements are true for differential amplifiers 5 and 6.

Conclusion

The presented method allows one to create circuits from unstable components that have minimal sensitivity to disturbances in harsh operating conditions. This is especially important for conditions in which the nature of these disturbances is unknown in advance.

The specific technology for bringing the devices to the most stringent fulfillment of the conditions of invariance is ensured both at the level of design of the device and at the level of technology for its manufacture. This essentially constitutes "know-how" on a case-by-case basis.

The method discussed has a significant advantage. This method not only improves the accuracy of measuring devices in abnormal

operating conditions, but gives hope for acceptable measurement results in conditions where the nature and even physical principles of influencing factors are unknown. We are talking about applications in deep space and the depths of the oceans. The method is also relevant for use in nuclear power plants, where in case of emergency situations, change sudden s in operating conditions are possible.

In conclusion, we note that the use of certain methods of increasing accuracy should be accompanied by a correct metrological analysis confirming the correctness and effectiveness of the measures applied. Otherwise, the result of applying the method may not meet expectations and even lead to the opposite result.

References

1. Bondarenko L.N., Nefediev D.I. [Analysis of test methods to improve measurement accuracy]. *Izmerenie. Monitoring. Upravlenie. Kontrol'*. [Measurement. Monitoring. Management. Control], 2014, no. 1(7), pp. 15–20 (in Russian).
2. Blockin-Mechtaln Yu.K. [Methods and instruments to improve the accuracy of measuring transducers and systems for experimental aerodynamics]. *Datchiki i sistemy* [Sensors and systems], 2011, no. 7, pp. 8–18 (in Russian).
3. Cooper V.Ya., Rubtsov M.G. [Algorithmic methods for increasing measurement accuracy based on inverse interpolation models]. *Vestnik Samarского gosudarstvennogo tekhnicheskogo universiteta. Seriya "Tekhnicheskie nauki"* [Bulletin of Samara State Technical University. Technical Sciences Series], 2010, no. 3(28), pp. 67–72 (in Russian).
4. Ashanin V.N., Larkin S.E., Regeda O.N. [Error correction of measuring circuits of parametric sensors]. *Izmerenie. Monitoring. Upravlenie. Kontrol'*. [Measurement. Monitoring. Management. Control], 2016, no. 2(16), pp. 103–109 (in Russian).
5. Chekushkin V.V., Bulkin V.V. [Improving the accuracy of measuring systems with unstable parameters]. *Izmeritel'naya tekhnika* [Measurement Techniques], 2006, no. 1, pp. 7–11 (in Russian).
6. Ivakhnenko A.G. [The connection between the theory of invariance and the theory of stability of

measuring systems]. *Avtomatika* [Automation], 1960, no. 5, pp. 35–40 (in Russian).

7. Petrov B.N., Viktorov V.A., Lunkin B.V., Sovlukov A.S. *Princip invariantnosti v izmeritel'noj tekhnike* [The principle of invariance in measurement technology]. Moscow, Nauka Publ., 1976, 244 p.

8. Nesterov V.N., Lee A.R. [The theory and practice of designing of invariant measurement transducers and systems based on the two-channel principle]. *Izvestiya Samarskogo nauchnogo centra Rossijskoj akademii nauk* [Bulletin of the Samara Scientific Center of the Russian Academy of Sciences], 2016, vol. 18, no. 4(7), pp. 1414–1422 (in Russian).

9. Svistunov B.L. [Measuring transducers for parametric sensors using analytical redundancy]. *Izmerenie. Monitoring. Upravlenie. Kontrol'*. [Measurement. Monitoring. Management. Control], 2017, no. 2(20), pp. 94–100 (in Russian).

10. Chernetsov M.V., Churakov P.P. [Invariant transformation in measuring systems with parametric sensors]. *Izmerenie. Monitoring. Upravlenie. Kontrol'*.

[Measurement. Monitoring. Management. Control], 2018, no. 1(23), pp. 11–17 (in Russian).

11. Keil Stefan. Technology and practical use of strain gages: with particular consideration of stress analysis using strain. *Dual-channel principle*, Berlin, Wiley. Ernst, Wilhelm & Sohn (Verlag), 2017, pp. 197–200.

12. Nesterov V.N. [New class of invariant transducers: construction methods and implementation for special purpose instruments and systems]. *Informacionnye, izmeritel'nye i upravlyayushchie sistemy. Nauchno-tekhnicheskij sbornik Samarskogo otdeleniya Povolzhskogo centra Metrologicheskoy akademii Rossii* [Information, measuring and control systems. Scientific and technical collection of the Samara branch of the Volga center of the Metrological Academy of Russia], ed. V.N. Nesterov, Samara, Samara Scientific Center of the Russian Academy of Sciences Publ., 2007, no. 3, pp. 18–37 (in Russian).

13. Nesterov V.N., Mukhin V.M. *Izmeritel'nyj preobrazovatel'* [Measuring transducer]. Patent RF, no. 2297638. 2005.

Analysis of Requirements and the Feasible Limit for Error Reduction in Two-Parameter Magnetic Determination of Steels' Hardness

S.G. Sandomirski

Joint Institute of Mechanical Engineering of the National Academy of Sciences of Belarus,
Akademicheskaya str., 12, Minsk 220072, Belarus

Received 20.03.2020

Accepted for publication 28.07.2020

Abstract

All measurements of mechanical properties of materials in the magnetic structural analysis are indirect and relationships between the measured parameters are correlated. An important physical parameter of steel is hardness. An increase in the correlation coefficient R and a reduction in the standard deviation (SD) are achieved when controlling the hardness of steels with two-parameter magnetic methods compared to methods that use a single measured parameter. However, the specific conditions and requirements for application of the two-parameter methods remain unclear. The purpose of this article was to analyze conditions and the achievable error reduction limit for two-parameter indirect determination of steels hardness and to compare those with one-parameter methods.

In particular, we considered the mean Square Deviation (SD), σ_F , of indirect calculation of the physical quantity F using two measured parameters x_1 and x_2 that are correlated with F . It was found that reduction of σ_F is most pronounced when x_1 and x_2 are inversely correlated with the maximum modulus $|R|$ of the correlation coefficient R between them. The most significant reduction in σ_F occurs at similar values of the SDs σ_1 and σ_2 between the true value of F and the values calculated based on the results of indirect measurements of F using each of the parameters x_1 and x_2 . The Results of the analysis are confirmed by an example of reduction in SD when determining the hardness of carbon steels by measuring their remanent magnetization and coercive force compared to use any one of these parameters.

This result can be applied to measurements in non-destructive testing and in related fields of physics and technology. The Results of the analysis allow us to compare different parameters for indirect two-parameter determination of a physical quantity, to select the optimal parameters, and to evaluate the minimum achievable measurement error of a physical quantity by a two-parameter method before performing the measurements.

Keywords: indirect physical measurements, correlation coefficient, hardness, remanent magnetization, coercive force.

DOI: 10.21122/2220-9506-2020-11-3-236-244

Адрес для переписки:

S.G. Сандомирский
Объединенный институт машиностроения Национальной
академии наук Беларуси,
ул. Академическая, 12, г. Минск 220072, Беларусь
e-mail: sand_work@mail.ru

Address for correspondence:

S.G. Sandomirski
Joint Institute of Mechanical Engineering of the National Academy
of Sciences of Belarus,
Akademicheskaya str., 12, Minsk 220072, Belarus
e-mail: sand_work@mail.ru

Для цитирования:

S.G. Sandomirski.
Analysis of Requirements and the Feasible Limit for Error Reduction
in Two-Parameter Magnetic Determination of Steels' Hardness.
Приборы и методы измерений.
2020. – Т. 11, № 3. – С. 236–244.
DOI: 10.21122/2220-9506-2020-11-3-236-244

For citation:

S.G. Sandomirski.
Analysis of Requirements and the Feasible Limit for Error Reduction
in Two-Parameter Magnetic Determination of Steels' Hardness.
Devices and Methods of Measurements.
2020, vol. 11, no. 3, pp. 236–244.
DOI: 10.21122/2220-9506-2020-11-3-236-244

53.088 : 620.179.14

Анализ условий и достижимого предела снижения погрешности двухпараметрового магнитного определения твёрдости сталей

С.Г. Сандомирский

Объединённый институт машиностроения Национальной академии наук Беларуси,
ул. Академическая, 12, г. Минск 220072, Беларусь

Поступила 20.03.2020

Принята к печати 28.07.2020

Все измерения физико-механических свойств материалов в магнитном структурном анализе являются косвенными, а связи между параметрами имеют корреляционный характер. Важным физическим параметром стали является твёрдость. Исследователи добились повышения коэффициента R корреляции и снижения среднего квадратичного отклонения при контроле твёрдости сталей двухпараметровым магнитным методом по сравнению с однопараметровым. Но оптимальные условия применения двухпараметрового метода остаются не установленными. Целью статьи являлся анализ условий и достижимого предела снижения погрешности двухпараметрового косвенного определения твёрдости сталей по сравнению с однопараметровым.

Исследовано среднее квадратичное отклонение σ_F косвенного определения физической величины F с использованием двух параметров x_1 и x_2 , корреляционно связанных с F . Получено, что эффект снижения σ_F сильнее всего проявляется при обратной корреляционной связи между x_1 и x_2 с максимальным модулем $|R|$ коэффициента R корреляции между ними. Наиболее существенное снижение σ_F имеет место при близких величинах средних квадратичных отклонений σ_1 и σ_2 между истинными значениями F и значениями, рассчитанными по результатам косвенных измерений F с использованием каждого из параметров x_1 и x_2 . Результаты анализа подтверждены примером снижения среднего квадратичного отклонения определения твёрдости углеродистых сталей по результатам измерения их остаточной намагниченности и коэрцитивной силы по сравнению с использованием любого из этих параметров.

Область применения результата – измерения в неразрушающем контроле и смежных областях физики и техники. Результаты анализа позволят выбрать оптимальные параметры для косвенного двухпараметрового определения твёрдости сталей, оценить достижимую погрешность определения твёрдости.

Ключевые слова: косвенные физические измерения, коэффициент корреляции, твёрдость, остаточная намагниченность, коэрцитивная сила.

DOI: 10.21122/2220-9506-2020-11-3-236-244

Адрес для переписки:

С.Г. Сандомирский
Объединённый институт машиностроения Национальной академии наук Беларуси,
ул. Академическая, 12, г. Минск 220072, Беларусь
e-mail: sand_work@mail.ru

Address for correspondence:

S.G. Sandomirski
Joint Institute of Mechanical Engineering of the National Academy of Sciences of Belarus,
Akademicheskaya str., 12, Minsk 220072, Belarus
e-mail: sand_work@mail.ru

Для цитирования:

S.G. Sandomirski.
Analysis of Requirements and the Feasible Limit for Error Reduction in Two-Parameter Magnetic Determination of Steels' Hardness.
Приборы и методы измерений.
2020. – Т. 11, № 3. – С. 236–244.
DOI: 10.21122/2220-9506-2020-11-3-236-244

For citation:

S.G. Sandomirski.
Analysis of Requirements and the Feasible Limit for Error Reduction in Two-Parameter Magnetic Determination of Steels' Hardness.
Devices and Methods of Measurements.
2020, vol. 11, no. 3, pp. 236–244.
DOI: 10.21122/2220-9506-2020-11-3-236-244

Introduction

An important physical parameter of steel is hardness – property of a material to resist plastic deformation upon contact in the surface layer. HRC hardness according to Rockwell is most often used to characterize the hardness of heat-treated steel [1]. The importance of this parameter is also determined by the fact that the hardness of the metal is closely related to its mechanical properties: the conditional yield strength $\sigma_{0,2}$; the tensile strength σ_B ; and the relative restriction ψ [1]. The results of HRC hardness measurements can be used to determine (or at least to provide a very accurate estimate) for the $\sigma_{0,2}$, σ_B , and ψ of steels [2]. This means that a non-destructive method for determining the hardness of steels allows one to control an entire set of its mechanical properties.

Magnetic structural analysis consists in the non-destructive determination of the mechanical properties of materials by measuring their magnetic parameters [3]. Measurements of the mechanical properties of materials in magnetic structural analysis are indirect. The physical basis for the presence of correlations between the mechanical and magnetic properties of steels is that these properties (each in its own way) are determined by the structure of the metal (stresses, distribution of dispersed particles in the alloy matrix, defects in the crystal lattice, grain size) formed during heat treatment [3, 4]. These dependencies are influenced by random factors. Therefore, the relationships between the mechanical and magnetic parameters of steels are not functional, but correlative. The coefficient R of correlation between the results of direct and indirect measurements of the mechanical properties of steels is also influenced by the inevitable errors in the measurement of mechanical [1] and magnetic parameters [5].

To increase the reliability of magnetic structural analysis, a combined use of several magnetic parameters was proposed. Analysis of the theoretical foundations of such methods, experiments, and modeling showed a strong influence of errors in measuring the parameters used in multiparameter regression equations on the reliability of control [6–10]. Nevertheless, multi-parameter models are used to calculate the hardness of HRC steels [11, 12]. The results of measuring the coercive force H_c of steels, their relaxation magnetization M_{Hr} , relaxation magnetic susceptibility χ_r , quadratic terms H_c^2 , χ_r^2 and the product $\chi_r M_{Hr}$ are summed with different

weight coefficients. This made it possible to obtain ultra-high correlation coefficients (up to $R \approx 0.9999$ [11, Table 1]) and small mean square deviations (SD) between the results of measuring hardness and its determination using the developed indirect calculations. Similar results were obtained in studies [13–15] and other works. However, it was established in [5] that the numerical values of H_c , M_{Hr} and χ_r given in [4] are substituted into the multiparameter equations for calculating the HRC of steels in [11, 12]. Ultra-high correlation coefficients R between the results of calculation and measurement of HRC of steels and small SD between them in [11, 12] were obtained by choosing the weight coefficients of the terms. The inevitable errors in measuring magnetic parameters and calculating algebraic combinations were not taken into account. A set of statistical control data under the influence of interfering factors and correlation analysis were not carried out.

In [16], an analysis of the technique [11, 12] was performed. In the analysis, "for the sake of simplification", it was assumed that in the methodology [11, 12] "the initial independent variables had an error of 1 %, and those obtained by calculation from the initial ones had a 2 % error". It was found that the error in calculating the HRC of steels according to the method [11, 12] "can be tens of percent or more". However, it was shown in [17] that the measurement error for each of the relaxation magnetic parameters used in [11, 12] is not 1 %, but itself can be tens of percent. And algebraic operations inevitably increase the resulting calculation error [18]. Therefore, the practical application of multiparameter control of the structure of steels according to the method [11, 12] and similar ones has not been reported so far.

Meanwhile, the authors of [19] have achieved an increase in the correlation coefficient and a decrease in the root-mean-square error of control of the hardness of steel pipes in industrial conditions by the two-parameter method (from H_c and remanent induction B_r) in comparison with the one-parameter (from H_c) method. The optimal conditions for the application of the two-parameter method have not been established, however. The formula for the indirect measurement error for the case of a function of two variables is given in [20]. This formula does not take into account the correlations observed in practice between the measured variables. This hinders the effective use of multiparametric magnetic structural analysis methods in practice.

The purpose of the article was to analyze the conditions and the achievable limit for reducing the error of two-parameter indirect measurement of steel hardness in comparison with one-parameter methods.

Table 1

The results of measuring the magnetic parameters and HRC hardness of carbon steels in [4] and the results of calculating their HRC using different formulas

Steel	T _t , °C	Measurement results in [4]			HRC calculation results using the formulas:			
		H _c , kA/m	M _r , MA/m	HRC	(11)	(12)	(3), (11) and (12)	(13), (11) and (12)
30	20	2.3	0.865	46	52	49.8	50.9	50.9
	150	2.25	0.870	45	51.5	49.7	50.6	50.6
	200	2.1	0.876	44.5	49.9	49.7	49.8	49.8
	250	1.43	0.970	43.5	41.1	47.7	44.4	44.3
	300	1.22	1.007	44	37.4	46.3	41.85	41.6
	350	1.13	1.070	41	35.7	43.3	39.5	39.3
	400	0.995	1.145	38	32.8	38.5	35.65	35.5
	450	0.873	1.248	34	29.8	29.9	29.85	29.8
	500	0.876	1.265	32	29.8	28.2	29	29
	550	0.866	1.277	26	29.6	27	28.3	28.3
	600	0.834	1.280	23	28.7	26.7	27.7	27.7
	650	0.730	1.235	19	25.6	31.1	28.35	28.2
45	20	3.0	0.910	60	58.1	49.2	53.65	53.5
	150	2.7	0.919	55	55.7	49	52.35	52.2
	200	2.46	0.932	53	53.5	48.7	51.1	51
	250	1.55	1.027	50	42.9	45.5	44.2	44.2
	300	1.34	1.018	45	39.6	45.9	42.75	42.6
	350	1.26	1.021	45	38.2	45.8	42	41.8
	400	1.12	1.136	42	35.5	39.2	37.35	37.3
	450	1.02	1.271	37	33.3	27.6	30.45	30.3
	500	1.03	1.276	34	33.6	27.1	30.35	30.2
	550	1.05	1.280	29	34	26.7	30.35	30.1
	600	1.04	1.248	26	33.8	29.9	31.85	31.8
	650	0.880	1.250	20	29.9	29.7	29.8	29.8
Correlation coefficient R of the results of calculation and measurement of HRC					0.868	0.860	0.901	0.899
SD between calculation and measurement of HRC, HRC units					4.81	4.58	4.17	4.22

Physical model for analysis

Let us establish that the physical quantity *F* (in the particular case, the HRC hardness of a steel) can be determined by measuring the correlated parameters *x*₁ and *x*₂ related to it based on the dependencies:

$$F(x_1) = \phi_1(x_1) \tag{1}$$

and

$$F(x_2) = \phi_2(x_2). \tag{2}$$

Moreover, we denote the root-mean-square deviations (SD) of the results of determining the quantity F according to equations (1) and (2) from its true values as σ_1 and σ_2 , respectively, and assume that the parameters x_1 and x_2 are correlated with each other with the correlation coefficient R ($-1 \leq R \leq 1$). We use the results of measurements of both parameters x_1 and x_2 to determine the physical quantity F . The value of F is calculated as the arithmetic mean of its definition by formulas (1) and (2):

$$F(x_1, x_2) = 0.5[\phi_1(x_1) + \phi_2(x_2)]. \quad (3)$$

Analysis and its results

Let us analyze how the SD values, σ_1 and σ_2 and the value of the correlation coefficient R between the parameters x_1 and x_2 affect the SD σ_F of the indirect determination of the physical quantity F by equation (3). It is known from the theory of probability that the variance $D(x_1 + x_2)$ of the sum of two random variables x_1 and x_2 in the general case is equal to [21]:

$$D(x_1 + x_2) = D(x_1) + D(x_2) + 2K_{x_1x_2}, \quad (4)$$

where $D(x_1)$ is the variance of x_1 ; $D(x_2)$ – variance x_2 ; σ_1 and σ_2 – SD values x_1 and x_2 ; R is the correlation coefficient between them; $K_{x_1x_2} = R\sigma_1\sigma_2$ – their correlation moment.

From (4), the SD σ_Σ of the sum of the quantities x_1 and x_2 is [21]:

$$\sigma_\Sigma = \sqrt{\sigma_1^2 + 2R\sigma_1\sigma_2 + \sigma_2^2}. \quad (5)$$

Taking into account (5) and (3), we obtain the SD σ_F of the indirect determination of the physical quantity F according to equation (3) an analytical expression:

$$\sigma_F = 0.5\sqrt{\sigma_1^2 + 2R\sigma_1\sigma_2 + \sigma_2^2}. \quad (6)$$

To generalize the analysis, we introduce the relative values:

$$\bar{\sigma}_2 = \sigma_2/\sigma_1 \quad \text{and} \quad \bar{\sigma}_F = \sigma_F/\sigma_1. \quad (7)$$

The value $\bar{\sigma}_F$ shows how the use of the second parameter x_2 to determine the value of F decreases (if $\bar{\sigma}_F < 1$) or increases (if $\bar{\sigma}_F > 1$) the SD of the indirect measurement according to equation (3) compared to using only the parameter x_1 . In the notation (7), from (6) we obtain:

$$\bar{\sigma}_F = 0.5\sqrt{1 + 2R\bar{\sigma}_2 + \bar{\sigma}_2^2}. \quad (8)$$

Figure 1 shows the results of calculating the dependences $\bar{\sigma}_F = \bar{\sigma}_F(\bar{\sigma}_2)$ by formula (8) in the range $0 \leq \bar{\sigma}_2 \leq 3$ for different coefficients R of the correlation between the parameters x_1 and x_2 in the possible range $-1 \leq R \leq 1$ of its change. Figure 2 shows the results of calculating the dependences by $\bar{\sigma}_F = \bar{\sigma}_F(R)$ formula (8) at different values in the range of $-1 \leq R \leq 1$. Taking into account the symmetric influence of the parameters x_1 and x_2 on the result of calculating the value of $F(x_1, x_2)$ by formula (3), for analysis in the case of $0 \leq \bar{\sigma}_2 \leq 1$, the parameters x_1 and x_2 can be swapped and the case $\bar{\sigma}_2 \geq 1$ can be considered.

The analysis of the dependences shown in Figures 1 and 2 shows that values $\bar{\sigma}_F < 1$ cannot be achieved at any values of R if $\bar{\sigma}_2 \geq 3$. In these cases, the use of the two-parameter method cannot provide a decrease in SD for indirect measurement of F in comparison with the one-parameter method. At $1 \leq \bar{\sigma}_2 < 3$, the value decreases as R decreases and approaches the value -1 . From (8) it follows that the condition $\bar{\sigma}_F \leq y$ is satisfied for values of R satisfying the equation:

$$R \leq (4y - 1 - \bar{\sigma}_2^2) / (2\bar{\sigma}_2). \quad (9)$$

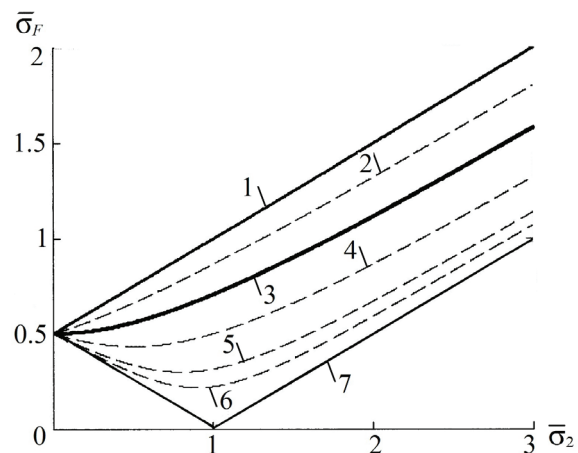


Figure 1 – Dependence of the relative standard deviation $\bar{\sigma}_F$ of the results of determining the physical quantity F according to the formula (3) on the relative standard deviation $\bar{\sigma}_2$ of the second parameter: 1 – 7 – respectively at $R = 1; 0.5; 0; -0.5; -0.8; -0.9; -1$. Calculation according to the formula (8)

Figure 3 shows the isolines of the function $\bar{\sigma}_F = y$ at different y in coordinates $(\bar{\sigma}_2, R)$. The analysis of the dependences shown in Figure 3 shows that a necessary condition for a two-fold ($y \approx 0.5$) decrease in the SD of the measurement of the parameter F by the two-parameter method compared with the one-parameter method is the simultaneous fulfillment of

the conditions $R < -0.5$ and $1 \leq \bar{\sigma}_2 < 2$. In practice, one can note that an approximately four-fold ($y \approx 0.25$) reduction of the SD can be achieved for a two-parameter measurement of a physical quantity F in comparison with a one-parameter measurement: this requires the simultaneous fulfillment of the conditions $R < -0.9$ and $1 \leq \bar{\sigma}_2 < 1.5$ (area below curve 4 in Figure 3).

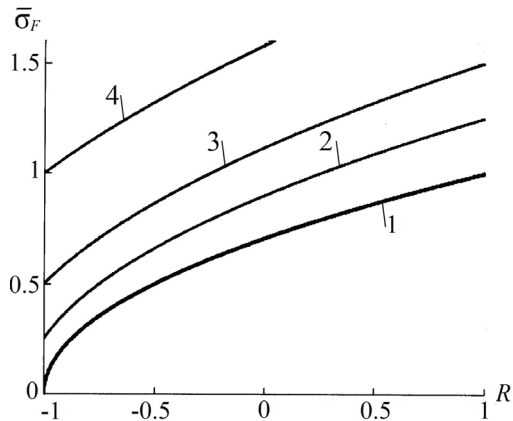


Figure 2 – Dependence of the relative root-mean-square deviation $\bar{\sigma}_F$ of the results of determining the physical quantity F according to the formula (3) on the coefficient R of the correlation between the parameters x_1 and x_2 : 1 – 4 – with the relative standard deviation $\bar{\sigma}_2$ of the second parameter, respectively, equal to 1; 1.5; 2; 3. The calculation according to the formula (8)

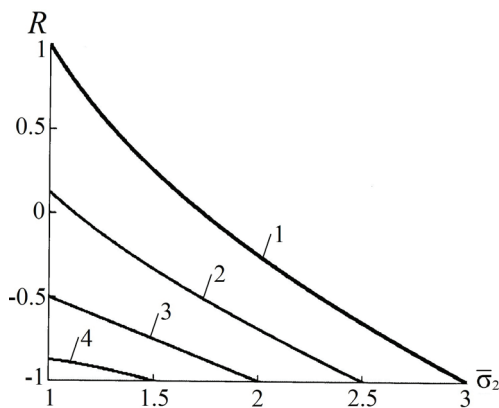


Figure 3 – Isolines of the function $\bar{\sigma}_F = y$ in coordinates $(\bar{\sigma}_2, R)$: 1 – 4 – when y is equal to: respectively, 1; 0.75; 0.5; 0.25. Calculation by the formula (9)

Solving inequality (9) with respect to the parameter $\bar{\sigma}_2$, we obtain:

$$\bar{\sigma}_2 \leq -R + \sqrt{R^2 + 4y^2} - 1. \quad (10)$$

Knowing the correlation coefficient R between the parameters x_1 and x_2 , it is possible to calculate the ratio $\bar{\sigma}_2 = \sigma_2 / \sigma_1$ ($1 \leq \bar{\sigma}_2 < 3$) using equation (10), which, when determining the value of F by the

parameters x_1 and x_2 , will provide the required decrease ($0 < y \leq 1$) in the SD $\bar{\sigma}_F$ for the indirect measurement of F by the two-parameter method compared to the one-parameter method.

As an example, the results of the analysis are confirmed by a decrease in the error in determining the hardness HRC of carbon steels after tempering at a temperature T_t , by measuring their coercive force H_c and remanent magnetization M_r , compared to using any one of these parameters (Table 1, Figures 4, 5). For analysis, we used the measurement results in [4, Tables 1.1 and 1.3] of H_c , M_r , and HRC of steels 30 and 45. The parameters H_c and M_r given in [4] were measured by standard methods GOST 8.377–80 "Magnetically soft materials. Measurement technique for determining static magnetic characteristics". The relative error of their measurement does not exceed $\pm 2\%$ and $\pm 3\%$, respectively. The correlation coefficient R between H_c and M_r according to Table 1 was -0.853 .

Statistical processing of correlation dependencies between H_c and HRC (Figure 4a), M_r and HRC (Figure 4b) and plotting the trend lines of these dependencies were performed in the Microsoft Excel program. The following equations were obtained for determining the hardness HRC of the investigated steels from the results of measuring their H_c and M_r (where $\tau_1 = 1$ m/kA and $\tau_2 = 1$ m/MA are dimensional factors):

$$\text{HRC} = \phi_1(H_c) = 22.965 \cdot \ln(\tau_1 H_c) + 32.874 \cdot \tau_1 H_c; \quad (11)$$

$$\text{HRC} = \phi_2(M_r) = -115.76 \cdot (\tau_2 M_r)^2 + 192.61 \cdot \tau_2 M_r - 30.228. \quad (12)$$

The data given in Table 1 show that the value of the SD between the results of calculating the hardness HRC of the investigated steels according to formula (3), using formulas (11) and (12), and the results of its measurement (Figure 5) amounted to 86% and 91%, respectively, of the SD values between the results of calculating the HRC hardness of these steels according to formulas (11) and (12) and its measurement.

The analysis results can be extended to other functional processing of the indirect measurements $F(x_1)$ and $F(x_2)$, that provide the same additional relative error of calculation as the algorithm (3) [18]. For example, the analysis can be applied to the geometric mean of the results of determining the physical quantity F according to formulas (1) and (2):

$$F(x_1, x_2) = \sqrt{\phi_1(x_1) \cdot \phi_2(x_2)}. \quad (13)$$

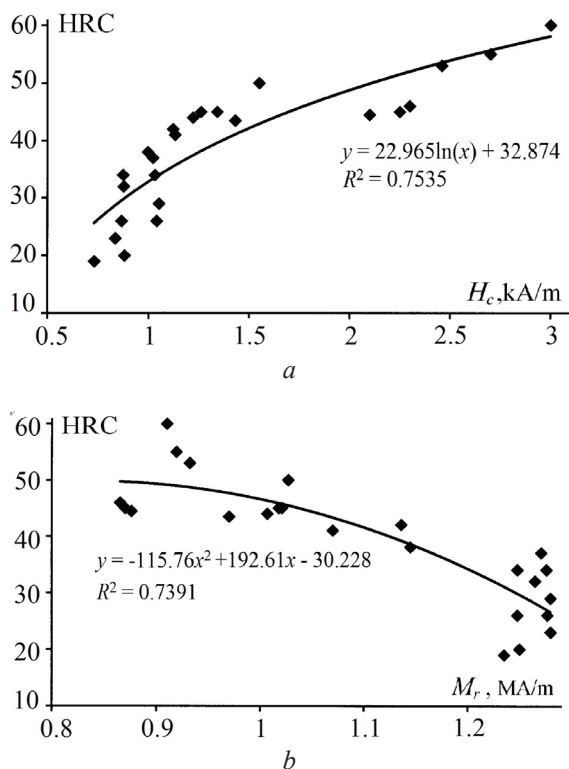


Figure 4 – Correlation fields of dependences between H_c and HRC (a), M_r and HRC (b) of steels 30 and 45, the results of measuring the parameters of which in [4] are given in Table 1, and the trend lines of these dependences

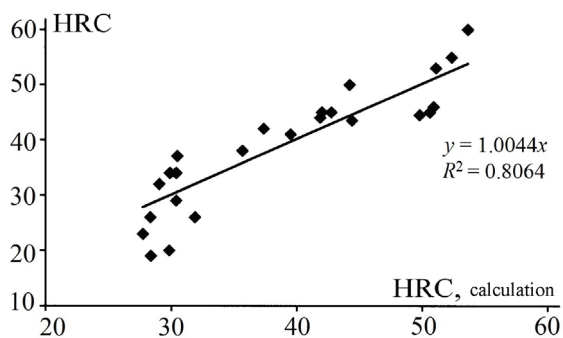


Figure 5 – Correlation field of the relationship between the results of calculating the HRC hardness of the studied steels according to formula (3) and the results (Table 1) of its measurement in [4] and the trend line of this dependence

Indeed, let the value of F be determined using the results of measuring the parameter x_1 by formula (1) with a relative error δ_1 , and using the results of measuring the parameter x_2 using formula (2) – with a relative error δ_2 . In this case, $F(x_1) \approx F(x_2)$. We use (Table 2) formulas [22] to calculate the relative measurement errors introduced by algebraic operations.

Table 2

Absolute and relative errors arising from the application of certain algebraic functions

Function type	Absolute error	Relative error
$A = a + b$	$\Delta A = \Delta a + \Delta b$	$\frac{\Delta A}{A} = \frac{\Delta a + \Delta b}{a + b}$
$A = ab$	$\Delta A = a\Delta b + b\Delta a$	$\frac{\Delta A}{A} = \frac{\Delta a}{a} + \frac{\Delta b}{b}$
$A = a^n$	$\Delta A = na^{n-1}\Delta a$	$\frac{\Delta A}{A} = n \frac{\Delta a}{a}$

We obtain for the relative errors δ_3 and δ_{13} the determination of the physical quantity F , respectively, by formulas (3) and (13):

$$\delta_3 \approx 0.5(\delta_1 + \delta_2), \tag{14}$$

(taking into account the fact that $F(x_1) \approx F(x_2)$),

$$\delta_{13} = 0.5(\delta_1 + \delta_2). \tag{15}$$

Close relative errors δ_3 and δ_{13} of determining the physical quantity F by formulas (3) and (13), in addition to formulas (14) and (15), are shown (Table 1) by close results of applying algorithms (3) and (13) to determine hardness HRC of carbon steels according to the results of their M_r and H_c measurements, given in Table 1.

The analysis of the influence of different factors on the mean square deviation σ_F of the indirect determination of the physical quantity F using two parameters x_1 and x_2 correlated with F allows us to draw the following conclusions.

Conclusion

The effect of reducing the mean square deviation σ_F for determining the steel hardness (physical quantity F) when using the second parameter x_2 is most pronounced when the inverse correlation between the parameters x_1 and x_2 with the maximum modulus $|R|$ the correlation coefficient R between them. In this case, the most significant decrease in σ_F occurs at close values of the SD σ_1 and σ_2 between the true values of F and the values calculated from the results of indirect measurements of F using each of the parameters x_1 and x_2 .

The application of the two-parameter method will not provide a decrease in σ_F for determining

the hardness of steel (physical quantity F) compared with the one-parameter method if the SD σ_2 of measurements of F using the second parameter x_2 is more than 3 times greater than the SD σ_1 of calculating F using the first parameter x_1 .

Knowing the correlation coefficient R between the parameters x_1 and x_2 , it is possible to calculate the ratio σ_2/σ_1 that, when determining the hardness of steel (physical quantity F) by the parameters x_1 and x_2 , will provide a specified reduction in the error of its determination by the two-parameter method compared to the one-parameter method. Achievable in practice is an approximately four-fold decrease in σ_F when measuring the hardness of steels by the two-parameter method compared to the one-parameter method: this requires the simultaneous fulfillment of the conditions $R < -0.9$ and $\sigma_2/\sigma_1 < 1.5$.

The field of application of the result is measurements in non-destructive testing and related fields of physics and technology. The results of the analysis will make it possible to select the optimal parameters for the indirect two-parameter determination of the hardness of steels and to estimate the achievable error in determining the hardness with their use.

References

1. Agamirov L.V. *Mashinostroenie. Enciklopediya. Fiziko-mekhanicheskie svoystva. Ispytaniya metallicheskih materialov. Materialy v mashinostroenii*. [Engineering. Encyclopedia. Materials in mechanical engineering. Physical-mechanical properties. Tests of metallic materials]. Moscow: Mashinostroenie Publ., 2010, vol. 40, razd. 2, 851 p.
2. Sandomirski S.G. [Statistical analysis of the relationship between mechanical properties and hardness of steel 41Cr4 (DIN)]. *Aktual'nye voprosy mashinovedeniya. Sbornik nauchnykh trudov* [Current issues of machine science. Collection of proceedings. Minsk, OIM NAN Belarusi], 2018, vol. 7, pp. 339–341 (in Russian).
3. *Nerazrushajushhij kontrol'. Spravochnik* [Nondestructive Testing. Directory]: vol. 8, edited by V.V. Kljuev. Kljuev V.V., Muzhickij V.F., Gorkunov Je.S., Shherbinin V.E. *Magnitnye metody kontrolja* [Magnetic Methods of Testing]. Moscow: Mashinostroenie Publ., vol. 6: kn. 1, 2006, 848 p.
4. Bida G.V., Nichipuruk A.P. *Magnitnye svoystva termoobrabotannykh stalej* [Magnetic Properties of Heat-Treated Steels]. Ekaterinburg: Ural branch RAN, 2005, 218 p.
5. Sandomirski S.G. Effect of Measurement Accuracy and Range of Variation of a Physical Quantity on the Correlation Coefficient. *Measurement Techniques*, 2014, vol. 57, iss. 10, pp. 1113–1120. DOI: 10.1007/s11018-015-0588-3
6. Kostin K.V., Kostin V.N., Smorodinskii Ya.G., Tsar'kova T.P., Somova V.M., Sazhina E.Yu. Choice of the Parameters and Algorithm for the Magnetic Hardness Testing of Thermally Treated Carbon Steels by the Method of Regression Modeling. *Russian Journal of Nondestructive Testing*, 2011, vol. 47, iss. 2, pp. 89–95. DOI: 10.1134/S1061830911020094
7. Kostin V.N., Smorodinskii Y.G. Multipurpose Software-Hardware Systems for Active Electromagnetic Testing as a Trend. *Russian Journal of Nondestructive Testing*, 2017, vol. 53, iss. 7, pp. 493–504. DOI: 10.1134/S1061830917070075
8. Danilevich S.B., Kolesnikov S.S., Palchun Yu.A. Use of Simulation Monitoring for Checking Monitoring and Testing Procedures. *Measurement Techniques*, 2011, vol. 54, iss. 7, pp. 846–850. DOI: 10.1007/s11018-011-9814-9
9. Zhagora N.A. *Vlijanie tochnosti izmerenij na rezul'taty ocenki sootvetstvija* [The effect of measurement accuracy on conformity assessment results]. *Kontrol' kachestva produkcii* [Product quality control], 2016, no. 4, pp. 29–34 (in Russian).
10. Danilevich S.B., Tret'jak V.V. *Metrologicheskoe obespechenie dostovernosti rezul'tatov kontrolja* [Metrological assurance of the reliability of control results]. *Kontrol'. Diagnostika* [The control. Diagnostics], 2018, no. 7, pp. 56–60 (in Russian). DOI: 10.14489/td.2018.07.pp.056-060
11. Bida G.V., Stashkov A.N. Multipurpose Use of Magnetic Properties of Steels in Nondestructive Testing of the Quality of Heat-Treated Workpieces. *Russian Journal of Nondestructive Testing*, vol. 39, iss. 4, 2003, pp. 310 – 316. DOI: 10.1023/B:RUNT.0000009087.64604.82
12. Bida G.V., Nichipuruk A.P. Multiparameter Methods in Magnetic Structuroscopy and Nondestructive Testing of Mechanical Properties of Steels. *Russian Journal of Nondestructive Testing*, 2007, vol. 43, iss. 8, pp. 493 – 509. DOI: 10.1134/S1061830907080013
13. Mel'gui M.A. Multiparameter Methods in Magnetic Structuroscopy and Instruments for Their Realization (Review): II. The Pulsed Magnetic Multiparameter Method and IMA-M Instrument for Its Performance. *Russian Journal of Nondestructive Testing*, 2015, vol. 51, iss. 3, pp. 138–145. DOI: 10.1134/S1061830915030055
14. Matyuk V.F. *Pribory magnitnoj strukturoskopii na osnove lokal'nogo ciklicheskogo impul'snogo peregnetivaniya* [Instruments of magnetic structuroscopy based on the local cyclic pulse magnetization]. *Nerazrushajushhij kontrol' i diagnostika* [Non-Destructive

Testing and Diagnostics], 2013, no. 1, pp. 3–27 (in Russian).

15. Burak V.A., Korotkevich Z.M. *Informativnye parametry dlja magnitnogo kontrolja kachestva otpuska instrumental'noj uglerodistoj stali U8A* [Informative parameters for magnetic testing grade of tempering tool carbon steel U8A]. *Nerazrushajushhij kontrol' i diagnostika* [Non-Destructive Testing and Diagnostics], 2013, no. 4, pp. 29–39 (in Russian).

16. Osipov A.A., Burak B.A., Korotkevich M., Schastnyj A.S. *Ocenka regressionnyh mnogoparametrovyyh modelej v zadachah magnitnogo nerazrushajushhego kontrolja* [Evaluation of regression multi-parameter models in problems of magnetic non-destructive testing]. *Nerazrushajushhij kontrol' i diagnostika* [Non-Destructive Testing and Diagnostics], 2018, no. 4, pp. 32–44 (in Russian).

17. Sandomirski S.G. Analysis of the Systematic Error When Measuring the Magnetization of Steels in the Coercive Recovery Process. *Measurement Techniques*, 2013, vol. 56, iss. 2, pp. 195–200.

DOI: 10.1007/s11018-013-0179-0

18. Sandomirski S.G. Application of Magnetic Information Parameters for Nondestructive Testing of the Hardness of Medium-Carbon Alloy Steels. *Measurement Techniques*, 2019, vol. 62, iss. 8, pp. 722–728.

DOI: 10.1007/s11018-019-01685-z

19. Kostin V.N., Osintseva A.A., Sazhina E.Yu. Improving Reliability of Magnetic Testing Data on Strength Properties of not-Rolled Pipes from 37G2S Steel. *Russian Journal of Nondestructive Testing*, 2002, vol. 38, iss. 12, pp. 909–933.

DOI: 10.1023/A:1023813108082

20. Obuhov I.V. *Sluchajnye pogreshnosti izmerenij: Uchebnoe posobie* [Random Measurement Errors: Study Guide]. Moscow: Knizhnyj dom "LIBROKOM", 2017, 80 p.

21. Novickij P.V., Zograf I.A. *Ocenka pogreshnostej rezul'tatov izmerenij* [Estimation of errors of measurement results]. Leningrad: Jenergoatomizdat, 1985, 248 p.

22. Mastjaeva I.N., Semehina O.N. *Chislennye metody* [Numerical Methods]. Moscow: Moskovskij mezhdunarodnyj institut jekonometriki, informatiki, finansov i prava, 2004, 103 p.

УДК 614.841

Контраст изображения объекта, наблюдаемого в условиях задымления, при поляризационной фильтрации излучения, рассеянного частицами дыма

А.И. Кицак

*НИИ пожарной безопасности и проблем чрезвычайных ситуаций
Министерства по чрезвычайным ситуациям Республики Беларусь,
ул. Солтыса, 183а, г. Минск 220046, Беларусь*

Поступила 20.03.2020

Принята к печати 18.08.2020

Целью работы являлось исследование контраста изображения объекта, наблюдаемого в задымленной среде, с применением поляризационной фильтрации излучения, рассеянного частицами дыма в сторону наблюдателя, и сопоставление данного контраста с контрастом изображения, формируемого без фильтрации, для оценки возможности разработки комплекта оптических принадлежностей пожарного-спасателя, улучшающего видение объектов в условиях дымообразования при пожаре.

Достижение поставленной цели осуществлялось методом экспериментального моделирования процесса передачи изображений чёрно-белого объекта с резкой границей перехода чёрное/белое через различные типы аэрозолей дыма с применением поляризационной фильтрации излучения, рассеянного частицами дыма, и без фильтрации и оценке контрастов изображений.

Проведены исследования контрастов изображений для различных оптических плотностей дымов в двух схемах регистрации, когда приёмная оптическая система расположена вблизи источника подсветки объекта на расстоянии ≈ 150 мм от него, и когда она расположена на удалении от источника подсветки объекта на расстоянии ≈ 800 мм.

Установлено, что способ формирования изображения объекта с применением поляризационной фильтрации излучения помехи обратного рассеяния (ПОР) позволяет снизить скорость уменьшения контраста изображения с увеличением оптической плотности дыма в сравнении с регистрацией изображения без фильтрации ПОР. Существенная разница в контрастах изображений, регистрируемых с поляризационной отсечкой ПОР и в отсутствие фильтрации, наблюдается для «светлых» дымов (пиролиз древесины, тление хлопка) на средних удельных оптических плотностях дыма.

Полученные результаты могут быть использованы при разработке оптических принадлежностей пожарного-спасателя для улучшения условий наблюдения объектов в неблагоприятных условиях видения: задымлении, парообразовании, тумане.

Ключевые слова: дым, дальность наблюдения, помеха обратного рассеяния излучения, контраст изображения, поляризационная фильтрация.

DOI: 10.21122/2220-9506-2020-11-3-245-254

Адрес для переписки:

А.И. Кицак
НИИ пожарной безопасности и проблем чрезвычайных ситуаций
МЧС Республики Беларусь,
ул. Солтыса, 183а, г. Минск 220046, Беларусь
e-mail: kitsak48@yandex.ru

Address for correspondence:

A.I. Kitsak
Research Institute of Fire Safety and Emergencies of the Ministry
for Emergency Situations of the Republic of Belarus,
Soltys str., 183a, Minsk 220046, Belarus
e-mail: kitsak48@yandex.ru

Для цитирования:

А.И. Кицак.
Контраст изображения объекта, наблюдаемого в условиях задымления, при поляризационной фильтрации излучения, рассеянного частицами дыма.
Приборы и методы измерений.
2020. – Т. 11, № 3. – С. 245–254.
DOI: 10.21122/2220-9506-2020-11-3-245-254

For citation:

A.I. Kitsak.
[Contrast of Image of an Object Observed in Smoke Conditions using Polarizing Filtering of Radiation Scattered by Smoke Particles].
Devices and Methods of Measurements.
2020, vol. 11, no. 3, pp. 245–254 (in Russian).
DOI: 10.21122/2220-9506-2020-11-3-245-254

Contrast of Image of an Object Observed in Smoke Conditions using Polarizing Filtering of Radiation Scattered by Smoke Particles

A.I. Kitsak

Research Institute of Fire Safety and Emergencies of the Ministry for Emergency Situations of the Republic of Belarus,
Soltys str., 183a, Minsk 220046, Belarus

Received 20.03.2020

Accepted for publication 18.08.2020

Abstract

The aim of the work was to study the contrasts of the images of an object observed in a smoky environment, using polarizing filtering of radiation scattered by smoke particles towards the observer, and without filtering. Prospects for developing optical accessories for firefighters to improve the observation of objects in smoke were evaluated by comparing image contrasts.

The goal was achieved by experimentally simulating the process of transmitting images of a black- and-white object with a sharp black/white transition boundary through various types of smoke aerosols using polarizing filtering of radiation scattered by smoke particles, and without filtering and evaluating image contrasts.

Studies of image contrasts for different optical densities of smoke in two registration schemes were performed, when the receiving optical system is located near the illumination source of the object at a distance of ≈ 150 mm from it, and when it is located at a distance from the illumination source of the object at a distance of ≈ 800 mm.

It is established that the method of forming the image of the object using polarization filtering of radiation backscattering (RBS) reduces the rate of image contrast reduction with an increase in optical smoke density compared to image registration without filtering (RBS).

A significant difference in the contrasts of images recorded with filtration (RBS) and in the absence of it is observed for "light" fumes (smoldering of wood, cotton) at average optical densities of smoke.

The results obtained can be used in the development of optical accessories for firefighter-rescuer to improve the conditions of observation of objects in adverse conditions of vision: smoke, vaporization, fog.

Keywords: smoke, range of observations, the backscattering of laser light, the image contrast, polarization filtering.

DOI: 10.21122/2220-9506-2020-11-3-245-254

Адрес для переписки:

А.И. Кицак
НИИ пожарной безопасности и проблем чрезвычайных ситуаций
МЧС Республики Беларусь,
ул. Солтыса, 183а, г. Минск 220046, Беларусь
e-mail: kitsak48@yandex.ru

Address for correspondence:

A.I. Kitsak
Research Institute of Fire Safety and Emergencies of the Ministry
for Emergency Situations of the Republic of Belarus,
Soltys str., 183a, Minsk 220046, Belarus
e-mail: kitsak48@yandex.ru

Для цитирования:

А.И. Кицак.
Контраст изображения объекта, наблюдаемого в условиях задымления, при поляризационной фильтрации излучения, рассеянного частицами дыма.
Приборы и методы измерений.
2020. – Т. 11, № 3. – С. 245–254.
DOI: 10.21122/2220-9506-2020-11-3-245-254

For citation:

A.I. Kitsak.
[Contrast of Image of an Object Observed in Smoke Conditions using Polarizing Filtering of Radiation Scattered by Smoke Particles].
Devices and Methods of Measurements.
2020, vol. 11, no. 3, pp. 245–254 (in Russian).
DOI: 10.21122/2220-9506-2020-11-3-245-254

Введение

В настоящее время на рынке снаряжений пожарного-спасателя предлагается широкий выбор различных типов и конструкций фонарей. Использование в современных фонарях мощных светодиодных источников излучения позволяет добиться высоких значений светового потока и обеспечить приемлемую освещённость в отсутствие рассеивающей среды на расстояниях ≈ 170 – 300 метров. Особенностью применения таких мощных фонарей для наблюдения объектов в аэрозольных средах является появление интенсивного излучения, рассеянного частицами дыма в сторону наблюдателя, приводящего к его частичному ослеплению и фактически к уменьшению дальности видения.

Известно [1], что в разрабатываемых в настоящее время системах наблюдения в случайно неоднородных средах (вода, атмосферный аэрозоль) для подавления помехи обратного рассеяния излучения используется поляризационная фильтрация. Она заключается в расположении на входе приёмной оптической системы поляризатора, ось поляризации которого ориентируется под определённым углом для устранения фона рассеянного излучения. Эффективность отсеки излучения обратного рассеяния определяется степенью поляризации излучения подсветки объекта и оптическими свойствами неоднородной среды (размерами и формой рассеивающих частиц, а также оптической плотностью среды).

Применение поляризационного способа фильтрации рассеянного излучения для улучшения видения в аэрозолях дыма до настоящего времени на практике не рассматривалось.

Целью данной работы является исследование характеристик качества изображений (контраста изображения), формируемых в задымленных средах с применением поляризационной фильтрации рассеянного излучения, и сопоставление данных характеристик с характеристиками изображений, получаемых традиционным способом, для оценки возможности разработки комплекта оптических принадлежностей пожарного-спасателя, улучшающих видение объектов в условиях дымообразования при пожаре.

Основные характеристики качества изображения объекта, формируемого оптической системой через случайно-неоднородную среду, и способы их оценки

Основными характеристиками качества изображения объекта, наблюдаемого глазами или

формируемого оптической системой (объективом фотокамеры), являются пространственное разрешение (угловое либо линейное) по объекту, контрастность и отношение сигнал/шум.

Под пространственным разрешением понимают минимальное угловое либо линейное расстояние между двумя деталями изображения объекта, наблюдаемыми отдельно при идеальном зрении. Величина разрешения, например углового γ , определяется средней длиной волны излучения λ , в котором формируется изображение объекта, и размером приёмной апертуры оптической системы d , регистрирующей изображение (диаметром объектива фотокамеры). Математически связь γ с параметрами λ и d выражается соотношением вида:

$$\gamma = \frac{1,21\lambda}{d}. \quad (1)$$

Контраст изображения характеризует степень различимости светлых и тёмных участков изображения. Величина контраста K определяется выражением:

$$K = \frac{I_{\max} - I_{\min}}{I_{\max} + I_{\min}}, \quad (2)$$

где I_{\max} – максимальная яркость светлого участка изображения; I_{\min} – минимальная яркость тёмного участка изображения. Значение контраста зависит от условий наблюдения (регистрации изображения) объекта. Например, величины освещённости объекта, мощности собственных шумов регистрирующего приёмника, наличия фоновой засветки.

Параметр отношение сигнал/шум η учитывает влияние на качество изображения объекта собственных шумов регистрирующего материала приёмника излучения, фона посторонней засветки приёмника, флуктуаций мощности полезного сигнала и определяется соотношением:

$$\eta = \frac{I_{\text{пс}}}{I_{\text{пм}}}, \quad (3)$$

где $I_{\text{пс}}$ – интенсивность полезного сигнала; $I_{\text{пм}}$ – интенсивность помехи.

Учёт параметра η важен, когда интенсивность полезного сигнала сравнивается с интенсивностью помехи.

При наблюдении (регистрации изображений) объектов в случайно-неоднородных средах типа толщи воды, различного рода аэрозолей (тумана,

дыма) часть излучения, исходящего от объекта, рассеивается на оптических неоднородностях этих сред, теряет фазовую и амплитудную информацию об объекте, что приводит в итоге к размытию деталей изображения объекта, ухудшению его контрастности и уменьшению дальности наблюдения.

Величина разрешаемого элемента изображения в данном случае определяется угловым или линейным размером изображения пятна размытия точечного диффузного источника, расположенного в плоскости объекта и сформированного используемой оптической системой через толщину аэрозольной среды, расположенной между объектом и оптической системой.

Существенное ухудшение условий наблюдения объектов в аэрозольных средах происходит в активном режиме наблюдения, т. е. когда осуществляется направленная подсветка объектов с помощью специальных фонарей, прожекторов. Основной причиной снижения видимости объектов (уменьшения контрастности) является излучение, рассеянное частицами аэрозоли в направлении «назад», которое попадает в глаза наблюдателя либо накладывается на изображение, регистрируемое оптической системой.

В случае наблюдения крупных объектов в условиях пожара, когда разрешением мелких деталей можно пренебречь, основной характеристикой качества изображения может являться степень его контрастности, т. е. отличимость объекта наблюдения от окружающего фона. Данный фон может создаваться, например, освещением от источника пожара, а также излучением, рассеянным на частицах аэрозоли дыма, пара и других неоднородностях воздушной среды в зоне пожара. Предельное значение контраста K изображения объекта, при котором объект может быть отличим человеком от фона, удовлетворяет условию $K \geq 0,02$.

Для улучшения качества изображения объектов, наблюдаемых в аэрозольных средах, применяются различные способы и устройства обработки и формирования изображений, позволяющие снизить или исключить влияние рассеянного на частицах аэрозоля излучения на качество изображения [1, 2–6].

В настоящее время для наблюдения объектов в задымленной среде при пожаре применяются тепловизионные камеры. Несмотря на высокое качество формируемых ими изображений объек-

тов, излучающих тепло, широкое применение их ограничено высокой стоимостью, сравнительно большим весом и ухудшением работы при длительном нахождении в зоне теплового излучения пожара [4].

Наиболее простейшим способом повышения качества изображения объектов является поляризационная фильтрация фона рассеянного излучения (излучения, рассеянного, например, подстилающей поверхностью Земли, атмосферным аэрозолем, аэрозолем дыма), различного рода бликов. Этот способ часто используется в обычной фотографии в пассивном режиме получения изображений, т. е. когда регистрируется излучение самого объекта (тепловое) либо отражённое им излучение естественных источников.

Фотографирование объектов в данном случае осуществляется через поляризационный фильтр, установленный с определённой ориентацией плоскости поляризации перед объективом фотокамеры. При больших плотностях аэрозольных сред существенного улучшения качества изображения в пассивном режиме формирования изображений достичь невозможно вследствие малых различий степеней поляризации полезного сигнала, отражённого от объекта, и рассеянного аэрозолем излучения.

Большой интерес вызывает применение поляризационной фильтрации рассеянного излучения в активных схемах наблюдения с применением подсветки объекта непрерывным либо импульсным полностью поляризованным излучением. Примером источников такого излучения могут являться лазерные излучатели.

Как показал проведённый анализ литературных данных [7] по исследованию поляризационных характеристик излучения, распространяющегося в различных типах аэрозольных сред, таких, например, как атмосферная аэрозоль, аэрозоль дыма, наблюдается высокая степень поляризации излучения, рассеянного частицами аэрозолей в направлении «назад». Выявленный факт высокой поляризации излучения, рассеянного «назад», и то, что плоскость поляризации этого излучения ортогональна плоскости поляризации исходного излучения, позволяет надеяться на эффективную его блокировку на этапе формирования изображения объекта поляризационным фильтром, установленным перед приёмной оптической системой.

Схема экспериментальной установки для регистрации изображения объекта через различные типы аэрозолей дыма методом поляризационной фильтрации рассеянного излучения и обычным фотографированием

Для оценки эффективности поляризационного способа повышения качества изображения объектов, наблюдаемых в аэрозолях дымов, была собрана экспериментальная установка для регистрации изображений объекта через задымленную среду. Оптическая схема установки представлена на рисунке 1.

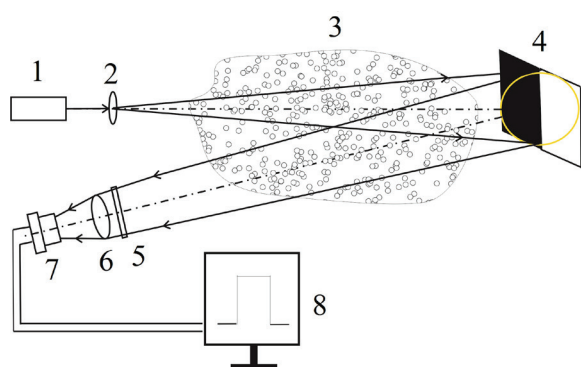


Рисунок 1 – Оптическая схема регистрации изображения объекта через аэрозоль дыма: 1 – лазер; 2 – микролинза; 3 – оптически неоднородная среда (дым); 4 – бинарный объект; 5 – поляризационный фильтр; 6 – приёмная оптическая система; 7 – ПЗС- датчик; 8 – компьютер

Figure 1 – Optical scheme of object image registration through a smoke aerosol: 1 – laser; 2 – microlens; 3 – optically inhomogeneous medium (smoke); 4 – binary object; 5 – polarizing filter; 6 – receiving optical system; 7 – CCD sensor; 8 – computer

Схема включает лазерный источник излучения 1 мощностью 20 мВт, генерирующий на длине волны $\lambda = 532$ нм, микролинзу 2 диаметром 5 мм с фокусным расстоянием 9 мм, чёрно-белый объект 4, поляризатор 5, приёмную оптическую систему 6 с апертурой 55 мм и фокусным расстоянием 80 мм, фотоприёмник 7, компьютер 8.

В качестве поляризатора использовалась поляризационная плёнка [8–9] с коэффициентом пропускания k излучения на длине волны $\lambda = 532$ нм, равном $k = 0,56$, и степенью поляризации $P = 0,3$. Плёнка крепилась во вращающемся в вертикальной плоскости барабане с нанесёнными на его ободке значениями градусов. Значения

градусов отсчитываются относительно риски, нанесённой на другом (неподвижном) барабане, связанном с узлом крепления поляризатора.

Фотоприёмником являлся многоэлементный датчик с пространственно-зарядовой связью марки *TohibaTCD1304AP* (ПЗС-датчик). Элементарные приёмники датчика расположены вдоль одной линии, поэтому его ещё называют ПЗС-линейкой. Светочувствительная площадка элементарного приёмника ПЗС-датчика имеет форму прямоугольника шириной 14 мкм и высотой 200 мкм. Число микроприёмников равно 3647.

Регистрация изображений на установке осуществлялась следующим образом. Линейно поляризованное излучение (степень поляризации $P = 0,3$) полупроводникового лазера непрерывного действия с длиной волны $\lambda = 532$ нм, диаметром пучка 5 мм и расходимостью ≈ 3 мрад направлялось на положительную линзу 2 с фокусным расстоянием 9 мм. Расширенное линзой излучение освещало объект 4. В качестве объекта использовался плоский непрозрачный экран с наклеенными на нём двумя широкими чёрной и белой полосами, образующими резкий переход от чёрного к белому. Изображение объекта представлено на рисунке 2.



Рисунок 2 – Исходное изображение объекта

Figure 2 – Initial image of the object

Ширина полос объекта равнялась 400 мм, высота – 800 мм. Отражённое от объекта 4 излучение (рисунок 1), пройдя через поляризатор 5, попадало в приёмную оптическую систему 6, которая формировала изображение объекта в плоскости светочувствительных элементов приёмника 7. Распределение интенсивности по изображению объекта вдоль горизонтальной оси (поперёк границы раздела чёрного и белого) регистрировалось светочувствительными элементами приёмника 7, сохранялось в памяти компьютера 8 и отображалось на его мониторе.

Изображения объекта регистрировались для разных типов дымов при различных их оптических плотностях в двух положениях приёмной оптической системы относительно источника подсветки объекта. Вблизи источника на расстоянии ≈ 150 мм, что соответствует, примерно, расстоянию от глаз пожарного-спасателя до фонаря подсветки, закреплённому на его каске, либо установленному на груди, и на удалении ≈ 800 мм, которое имитирует расстояние от глаз пожарного-спасателя до фонаря подсветки, находящегося в его руке.

Регистрация осуществлялась при двух ориентациях плоскости пропускания поляризатора 5, когда плоскость пропускания поляризатора была параллельна плоскости поляризации излучения подсветки объекта и когда она была перпендикулярна ей. Первый случай соответствовал фильтрации (блокировке) фона излучения, рассеянного частицами дыма в направлении «назад», второй – отсутствию его фильтрации.

Результаты экспериментального исследования контраста изображений бинарного объекта, формируемых в условиях задымления при поляризационной фильтрации помехи обратного рассеяния излучения подсветки и без фильтрации

Контрасты изображений бинарного объекта, регистрируемые при наличии дыма, вычислялись по формуле (2) и оценивались для точек изображений вблизи резкой границы перехода от светлой части объекта к тёмной на равноудалённых от границы расстояниях.

Во всех экспериментах объект находился на расстоянии от источника подсветки, равном 8,8 м.

На рисунке 3 представлены зависимости относительных (по отношению к контрасту изображения, зарегистрированного в отсутствие дыма K_0) контрастов K/K_0 изображений объектов от удельной оптической плотности D дыма, образуемого модельным очагом пожара ТП2 (пиролиз древесины)¹.

Оценка удельной оптической плотности D осуществлялась по формуле:

¹ Система стандартов пожарной безопасности. Системы пожарной сигнализации. Извещатели дымовые точечные. Общие технические условия: СТБ 11.16.03-2009.

$$D = \frac{10}{L} \log \frac{I_0}{I}, \quad (4)$$

где I_0 – величина сигнала, регистрируемого приёмником излучения в отсутствие дыма; L – длина пути излучения от источника до приёмника; I – величина сигнала, регистрируемого приёмником излучения при наличии дыма.

Зависимости получены при расстоянии от источника излучения до приёмной оптической системы ≈ 150 мм.

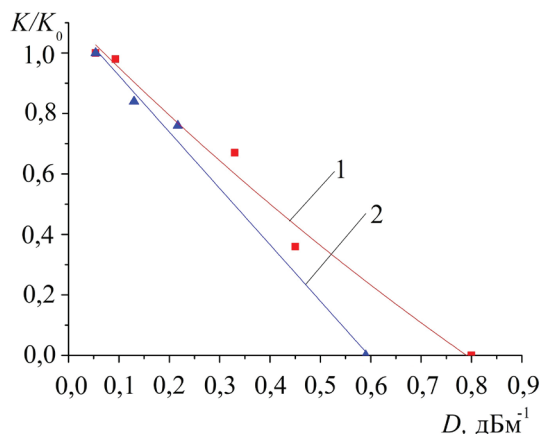


Рисунок 3 – Зависимости относительных контрастов K/K_0 изображений бинарного объекта, регистрируемых вблизи источника подсветки способом фильтрации рассеянного излучения (1) и без фильтрации (2), от удельной оптической плотности D дыма (пиролиз древесины)

Figure 3 – Dependence of relative contrasts of binary object images registered near the illumination source by filtering (1) and without filtration scattered radiation (2) on the specific optical density D of smoke (wood pyrolysis)

Кривая 1 отображает изменение контраста изображений с увеличением средней удельной оптической плотности дыма при фильтрации ПОР. Кривая 2 получена в отсутствие фильтрации ПОР. Видно, что с увеличением удельной оптической плотности дыма контраст изображений уменьшается. Однако скорость уменьшения контраста изображений, полученных при фильтрации ПОР, меньше, чем изменение его в изображениях, регистрируемых без фильтрации. Сравнение величин контрастов данных изображений для оптической плотности дыма, равной, например, $D = 0,4$ дБм⁻¹, показывает, что контраст изображения, формируемого с отсечкой ПОР, примерно в 2 раза выше контраста изображения, регистрируемого без фильтрации ПОР.

На рисунках 4 и 5 приведены изображения объекта, полученные при удельной оптической плотности дыма, равной $D = 0,5 \text{ дБм}^{-1}$, соответственно без фильтрации ПОР и её отсечке. Справа на изображениях объекта виден след излучения источника (длина волны излучения $\lambda = 650 \text{ нм}$), использовавшегося для контроля удельной оптической плотности дыма.

Из рисунка 5 видно, что контраст отфильтрованного изображения выше контраста изображения, полученного без фильтрации ПОР (помеха обратного рассеяния в виде яркого снопа лучей, накладывающаяся на изображение объекта (рисунок 4), практически полностью устранена). Однако яркость отфильтрованного изображения очень мала. Этот факт объясняется тем, что используемый в экспериментах поляризатор имел низкий коэффициент пропускания излучения $k = 0,56$.

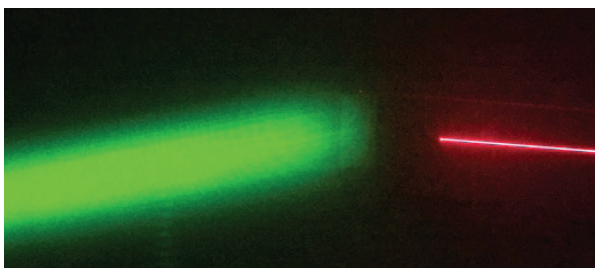


Рисунок 4 – Изображение бинарного объекта, зарегистрированное без фильтрации рассеянного излучения ($D = 0,5 \text{ дБм}^{-1}$) вблизи источника подсветки объекта

Figure 4 – Image of a binary object registered without filtering scattered radiation ($D = 0.5 \text{ dBm}^{-1}$) near the illumination source

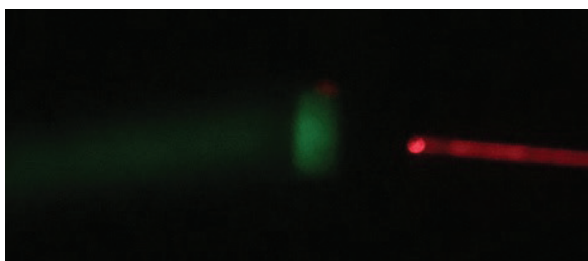


Рисунок 5 – Изображение бинарного объекта, зарегистрированное в условиях фильтрации рассеянного излучения ($D = 0,5 \text{ дБм}^{-1}$) вблизи источника подсветки объекта

Figure 5 – Image of a binary object registered by filtering scattered radiation ($D = 0.5 \text{ dBm}^{-1}$) near the illumination source

Представленные на рисунках 3–5 результаты получены в схеме регистрации, соответствующей

наблюдению объектов с подсветкой источником, расположенным на каске пожарного-спасателя либо его груди. Представляет интерес оценить контрасты изображений, формируемых при подсветке объекта источником, расположенным, например, в руке спасателя.

На рисунке 6 отображены зависимости контрастов изображений, полученных при расстоянии от источника излучения до приёмной оптической системы, равном $\approx 800 \text{ мм}$.

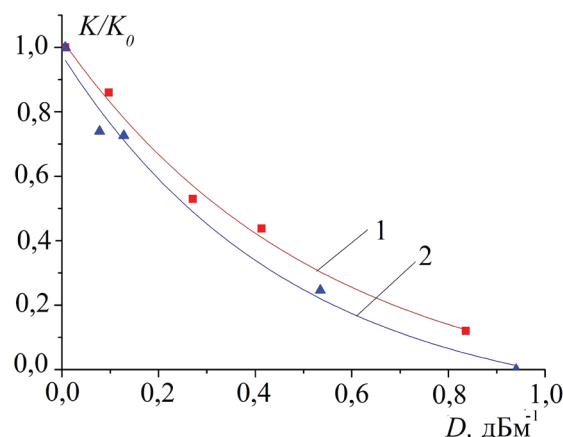


Рисунок 6 – Зависимости относительных контрастов K/K_0 изображений бинарного объекта, регистрируемых на удалении от источника подсветки способом фильтрации рассеянного излучения (1) и без фильтрации (2), от удельной оптической плотности D дыма (пиролиз древесины)

Figure 6 – Dependence of relative contrasts of binary object images registered at a distance from the illumination source by filtering scattered radiation (1) and without filtration (2) on the specific optical density D of smoke (pyrolysis of wood)

Видно, что основные особенности изменения контрастов в зависимости от удельной оптической плотности дыма сохраняются. В то же время сопоставление контрастов изображений объекта, полученных при отсечке ПОР (кривая 1) и без фильтрации (кривая 2), показывает, что они меньше отличаются друг от друга. При удельной оптической плотности дыма $D = 0,4 \text{ дБм}^{-1}$ отношение контрастов равно 1,3. Выравнивание качества изображений можно объяснить уменьшением мощности, регистрируемой ПОР, так как её часть не попадает в приёмный канал вследствие большого пространственного разнесения приёмника и источника излучения [10].

Исследование контраста изображений бинарного объекта, формируемых при двух режимах ре-

гистрации (через поляризационный фильтр и без него), проводилось также для дыма, выделяемого при тлении хлопка (модельный очаг пожара ТП3).

Данный тип дыма проявляется при возгорании хлопчатобумажных (волокнистых) материалов. Он, так же как и дым тлеющей древесины, относится к так называемым «светлым» дымам. Такие дымы состоят из твёрдых частиц с размерами от 5 до 10 мкм, хорошо рассеивающими свет.

На рисунке 7 отображены зависимости относительных контрастов K/K_0 изображений объектов, полученных при фильтрации ПОР (кривая 1) и в её отсутствие (кривая 2) от удельной оптической плотности D дыма тлеющего хлопка.

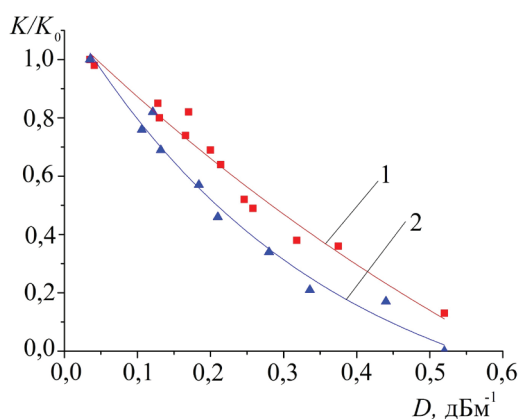


Рисунок 7 – Зависимости относительных контрастов K/K_0 изображений, регистрируемых способом фильтрации рассеянного излучения (1) и без фильтрации (2), от удельной оптической плотности D дыма (тление хлопка). Расстояние между регистрирующей оптической системой и источником подсветки объекта ≈ 150 мм

Figure 7 – Dependences of relative contrasts of images registered by filtering scattered radiation (1) and without filtration (2) on the specific optical density D of smoke (cotton smoldering). Distance between the recording optical system and the object illumination source ≈ 150 mm

Из динамики зависимостей, представленных на рисунке 7, следует, что контраст изображений, получаемых с отсечкой ПОР, выше контраста изображений, регистрируемых в отсутствие её фильтрации. Соотношение контрастов изображений, определённых при удельной оптической плотности дыма $D = 0,4$ дБм⁻¹, равно ≈ 2 .

На рисунке 8 представлены зависимости контрастов изображений, полученных при расстоянии от источника излучения до приёмной оптической системы ≈ 800 мм. Соотношение контрастов изображений, сформированных при отсечке и регистрации ПОР, на удельной оптической плотно-

сти дыма $D = 0,4$ дБм⁻¹ примерно такое же, как и в случае использования очага ТП2 и равно 1,2.

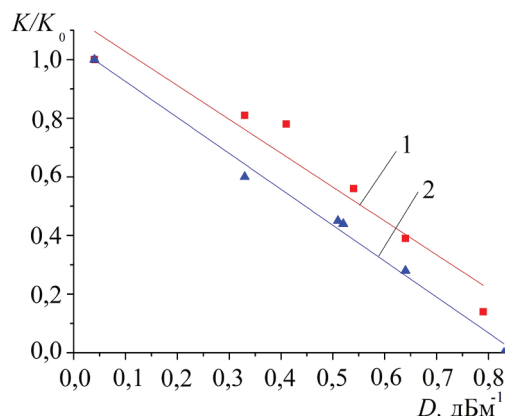


Рисунок 8 – Зависимости относительных контрастов K/K_0 изображений, регистрируемых способом фильтрации рассеянного излучения (1) и без фильтрации (2), от удельной оптической плотности D дыма (тление хлопка). Расстояние между регистрирующей оптической системой и источником подсветки объекта ≈ 800 мм

Figure 8 – Dependences of relative contrasts of images registered by filtering scattered radiation (1) and without filtration (2) on the specific optical density D of smoke (cotton smoldering). Distance between the recording optical system and the object illumination source ≈ 800 mm

На рисунках 9 и 10 приведены зависимости контрастов изображений бинарного объекта, регистрируемых в дымах, образуемых модельными очагами пожаров ТП4 (горение пенополиуретана) и ТП5 (горение *n*-гептана) от оптической плотности дымов.

Как и ранее, кривые 1 на рисунках 9 и 10 характеризуют динамику изменения с ростом удельной оптической плотности дыма контраста изображений, формируемых с фильтрацией ПОР, а кривые 2 – без фильтрации.

Из построенных зависимостей следует, что контрасты изображений, регистрируемых различными способами, практически не отличаются между собой. Это связано с тем, что дымы, выделяемые при горении синтетических материалов (пластмасс) и некоторых органических жидких соединений класса алканов, относятся к так называемым «чёрным» дымам. Они состоят в основном из частиц, поглощающих свет. Поэтому мощность ПОР, возникающей в данном случае, незначительна. Контраст изображений падает в основном вследствие уменьшения регистрируемого полезного сигнала от объекта (поглощения

частицами дыма излучения, отражённого от объекта) и накладывающегося на изображение фона излучения от пламени горящего вещества.

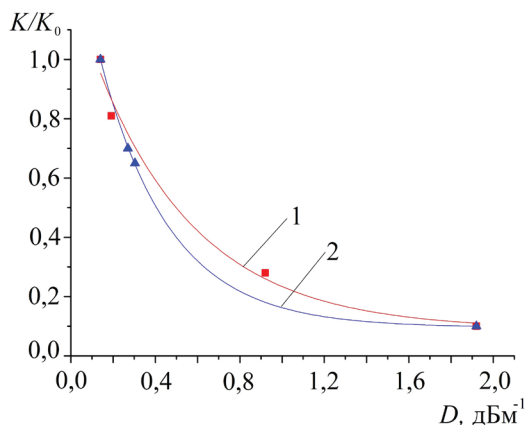


Рисунок 9 – Зависимости относительных контрастов K/K_0 изображений вблизи границы раздела бинарного объекта, регистрируемых способом фильтрации рассеянного излучения (1) и без фильтрации (2), от удельной оптической плотности D дыма (горение пенополиуретана). Расстояние между регистрирующей оптической системой и источником подсветки объекта ≈ 150 мм

Figure 9 – Dependences of relative contrasts of images registered by filtering scattered radiation (1) and without filtration (2) on the specific optical density D of smoke (burning foamex). Distance between the recording optical system and the object illumination source ≈ 150 mm

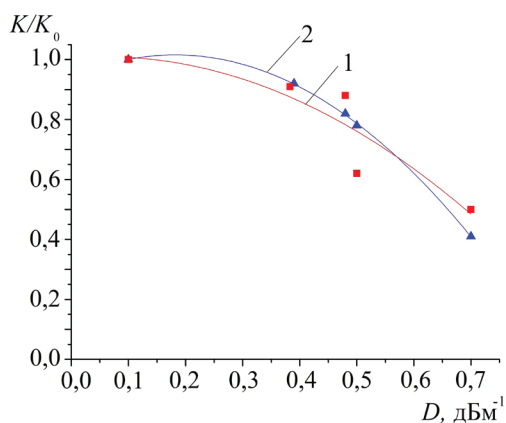


Рисунок 10 – Зависимости относительных контрастов K/K_0 изображений вблизи границы раздела бинарного объекта, регистрируемых способом фильтрации рассеянного излучения (1) и без фильтрации (2), от удельной оптической плотности D дыма (горение n -гептана). Расстояние между регистрирующей оптической системой и источником подсветки объекта ≈ 150 мм

Figure 10 – Dependences of relative contrasts of images registered by filtering scattered radiation (1) and without filtration (2) on the specific optical density D of smoke (burning n -heptane). Distance between the recording optical system and the object illumination source ≈ 150 mm

Исследование контрастов изображений в схеме регистрации, когда приёмная оптическая система располагается на удалении от источника подсветки объекта, не проводилось вследствие очевидности результатов, т. е. отсутствия отличий контрастов, поскольку мощность ПОР в данной схеме еще меньше, чем в рассмотренных выше.

Заключение

Установлено, что способ формирования изображения объекта с применением поляризационной фильтрации излучения помехи обратного рассеяния позволяет снизить скорость уменьшения контраста изображения с увеличением оптической плотности дыма в сравнении с регистрацией изображения без фильтрации помехи обратного рассеяния.

Существенная разница в контрастах изображений, регистрируемых с отсечкой помехи обратного рассеяния и в отсутствие фильтрации, наблюдается для «светлых» дымов (тление древесины, хлопка) на средних удельных оптических плотностях дыма. При удельной оптической плотности дымов, равной $D = 0,4$ дБм⁻¹, отношение контрастов в схеме регистрации вблизи источника подсветки объекта равно ≈ 2 , а при регистрации изображений на удалении от источника составляет $\approx 1,2$.

Выявлено, что при регистрации изображений бинарного объекта через так называемые «чёрные» дымы (горение пластмасс и некоторых органических жидкостей) разница в контрастах изображений, получаемых рассматриваемыми способами, практически отсутствует, что объясняется низким уровнем помехи обратного рассеяния, формируемым данным типом дыма.

Полученные результаты могут быть использованы при разработке оптических принадлежностей пожарного-спасателя, что позволит улучшить условия наблюдения объектов в неблагоприятных условиях видения: задымлении, парообразовании, тумане.

В настоящее время в НИИ ПБ и ЧС МЧС Беларуси ведутся проектные работы по разработке конструкции шлема пожарного с улучшенной функцией видения в аэрозольных средах и защитой глаз пожарного от воздействия излучений ультрафиолетового и инфракрасного диапазона длин волн на основе применения лазерного фонаря и термовлагостойкой поляризационной плёнки.

Список использованных источников

1. Тымкул, В.М. Опτικο-электронные приборы и системы. Теория и методы энергетического расчета / В.М. Тымкул, Л.В. Тымкул. – Новосибирск: СГГА, 2005. – 215 с.
2. Волков, В.Г. Активно-импульсные вертолетные очки ночного видения / В.Г. Волков // Вестник МГТУ имени Баумана. Серия «Приборостроение» – 2011. – С. 143–156.
3. Балоев, В.А. Анализ путей повышения эффективности наземных опτικο-электронных комплексов наблюдения / В.А. Балоев [и др.] // Оптический журнал. – 2012. – Т. 79, № 3. – С. 22–32.
4. Christopher, E. Combination head-protective helmet and thermal imaging apparatus. Patent EP0622030B1, publ. data 21.05.1997.
5. Kim Myung-hwan Smart fire fighting helmet. Patent KR101103516B1, publ. data 06.01. 2012.
6. Gilles Basson Gallet Sa Protective helmet and means for connection of an accessory. Patent CA2382804C, publ. data 05.01.2010.
7. Козлов, В.С. Исследование оптических свойств и дисперсного состава древесных дымовых аэрозолей / В.С. Козлов, М.В. Панченко // Физика горения и взрыва. – 1996. – Т. 32, № 5. – С. 122–133.
8. Агабеков, В.Е. Пленочные поляризаторы для жидкокристаллических устройств отображения информации / В.Е. Агабеков, Н.Г. Арико, Н.А. Иванова // Вести НАН Беларуси. Сер. хим. наук. – 2002. – № 4. – С. 98–112.
9. Сушко, Н.И. Получение и оптические свойства поляризационных пленок на основе нанокмпозитов поливиниловый спирт-гетерополикислота / Н.И. Сушко, С.А. Загорская, Т.В. Шевченко, О.И. Третинников // Полимерные материалы и технологии. – 2016. – Т. 2. – № 3. – С. 30–34.
10. Григорьевский, В.И. Устранение помехи обратного рассеяния лазерного излучения в квазинепрерывных лидарах / В.И. Григорьевский, Я.А. Тезадов, А.В. Элбакидзе // Современные проблемы дистанционного зондирования Земли из космоса. – 2018. – Т. 15, № 1. – С. 71–74.

References

1. Timkul V.M. *Optiko-elektronnye pribory i sistemy. Teoriya i metody energeticheskogo rascheta*. [Optoelectronic devices and systems. Theory and methods of energy calculation]. Novosibirsk, CGGA Publ., 2005, 215 p.
2. Volkov V.G. [The active – pulses helicopter glasses of night viewing]. *Vestnik MSTU imeni Baumana. Serya "Priborostroenie"* [Bulletin of the Moscow state technical University. Bauman's. "Instrumentation" Series], 2011, pp. 143–156 (in Russian).
3. Baloev V.A. [The analysis of ways to improve the effectiveness of overhead – based optical-electronic surveillance systems]. *Opticheskii jurnal* [Journal of optical], 2012, vol. 79, no. 3, pp. 22–32 (in Russian).
4. Christopher E. Combination head-protective helmet and thermal imaging apparatus. Patent EP0622030B1, publ. data 21.05.1997.
5. Kim Myung-hwan Smart fire fighting helmet. Patent KR101103516B1, publ. data 06.01. 2012.
6. Gilles Basson Gallet Sa Protective helmet and means for connection of an accessory. Patent CA2382804C, publ. data 05.01.2010.
7. Kozlov V.S., Panchenko M.V. [The investigation of optical properties and dispersed composition of wood smoke aerosols]. *Fizika gorennya i vzryva* [Physics of combustion and explosion], 1996, vol. 32, no. 5, pp. 122–133.
8. Agabekov V.E., Ariko N.G., Ivanova N.A. [Film polarizer's for liquid crystal display devices]. *Vesti NAN Belarus. Ser. Him. Nauk* [Vesti NAN of Belarus. Chem. Scien. Ser.], 2002, no. 4, pp. 98–112 (in Belarus).
9. Suchko N.I., Zagorskaya S.A., Shevchenko T.V., Tretinnikov O.I. [Preparation and optical properties of polarizing films based on nanocomposites polyvinyl alcohol-heteropolyacid]. *Polimernye materialy i tekhnologii* [Polymer materials and technologies], 2016, vol. 2, no. 3, pp. 30–34 (in Belarus).
10. Grigor'evski V.I., Tezadov Y.A., Elbakidze A.V. [The elimination of the interference of backscattering of laser radiation in quasicontinuous lidar]. *Sovremennye problemy distancionnogo zondirovaniya Zemli iz kosmosa* [Modern problems of remote sensing of the Earth and space], 2018, vol. 15, no. 1, pp. 71–74 (in Russian).

ПРАВИЛА ОФОРМЛЕНИЯ СТАТЕЙ

Статьи, направленные в редакцию журнала, должны удовлетворять требованиям «Инструкции о порядке оформления квалификационной научной работы (диссертации)...», утвержденной Постановлением ВАК РФ от 28.02.2014 г. № 3

1. Материал статьи должен соответствовать профилю журнала и излагаться предельно ясно.

2. Статья представляется на русском или английском языке и публикуется на языке представления.

3. Поступившие в редакцию статьи проходят двойное полуслепое рецензирование. Основные критерии целесообразности опубликования – актуальность тематики, информативность, научная новизна.

4. Статья представляется в распечатанном и в электронном виде в формате текстового редактора Word for Windows. Объем статьи не должен превышать 14 страниц, включая текст (шрифт Times New Roman, размер 12 п., интервал 1,5), таблицы, графический материал, всю необходимую информацию на английском языке.

5. На первой странице статьи указываются: индекс УДК, название статьи, фамилии авторов (фамилия автора, с которым следует вести переписку, отмечается звездочкой и указывается его адрес электронной почты), названия и почтовые адреса организаций (улица, номер дома, индекс, город, страна), в которых работают авторы, на русском и английском языках. Статья включает: аннотацию (в пределах 200–250 слов); ключевые слова (не более 5); введение, в котором делается краткий обзор сделанного в мире и конкретно формулируется цель работы; основную часть; заключение, в котором в сжатом виде сформулированы основные полученные результаты с указанием их новизны, преимуществ и возможностей применения; список использованных источников. Аннотация, ключевые слова, список использованных источников представляются на русском и английском языках.

6. Аннотация должна быть информативной (содержать «выжимку» из всех разделов статьи – введения с указанием цели работы, методики, основной части и заключения).

7. Графический материал должен быть контрастным и четким. Необходимо придерживаться единообразия техники исполнения однотипных иллюстраций. Изобразительный материал вставляется в текст статьи, а также даётся в виде отдельных файлов (**формат tif, jpg, разрешение не менее 300 dpi**). Текст на рисунках набирается основной гарнитурой; размер кегля соизмерим с размером рисунка (желательно 8 пунктов). Все рисунки нумеруются и сопровождаются подрисуночными подписями. Фрагменты рисунка обозначаются строчными курсивными латинскими буквами – «*a*», «*b*» и т. д. Надписи на рисунках и подписи к рисункам даются на русском и английском языках. Все сокращения и обозначения должны быть расшифрованы в подрисуночной подписи. Рисунки желательно предоставлять в цвете. На рисунках должны быть указаны оси с обозначением приводимых величин и масштабов. На графиках

не нужно давать координатную сетку, если это не осциллограмма.

8. Полутонные фотографии приборов или их частей представляются при публикации в тех случаях, когда они несут существенную информацию, которую нельзя выразить иным способом. Фотографии должны быть высококачественными, контрастными, с хорошо различимыми деталями.

9. Таблицы не должны дублировать графики. Каждая таблица имеет заголовок. На все таблицы и рисунки следует давать ссылки в тексте. Название и содержание таблиц представляется на русском и английском языках.

10. Обозначения и сокращения, принятые в статье, расшифровываются непосредственно в тексте.

11. Размерность всех величин, принятых в статье, должна соответствовать Международной системе единиц измерений (СИ).

12. Многострочные формулы должны быть набраны в редакторе MathType, номера формул – по правому краю. Нумеруются лишь формулы, на которые есть ссылки в тексте. Отдельные строчные буквы и специальные символы набираются в тексте гарнитурой Symbol **без использования редактора формул**. При наборе формул и буквенных обозначений необходимо учитывать следующие правила: **русский алфавит не используется**; греческие буквы, математические символы (grad, div, ln, min, max и др.), символы химических элементов (в т. ч. в индексе) набираются **прямо**; латинские буквы – переменные и символы физических величин (в т. ч. в индексе) набираются **курсивом**; векторы – жирным шрифтом (стрелки вверх не ставятся).

13. Список использованных источников составляется в порядке упоминания ссылок по тексту, должен содержать полные библиографические данные и приводится в конце статьи. Не рекомендуется давать ссылки на материалы конференций, статьи из электронных журналов без идентификатора DOI, учебные пособия, интернет-ресурсы. Ссылки на неопубликованные работы не допускаются. Желательно, чтобы количество ссылок было не менее 10; самоцитирование – не более 20 %.

14. Авторы на отдельной странице предоставляют о себе следующие сведения: фамилия, имя, отчество, ученая степень и звание, место работы и занимаемая должность, адрес электронной связи.

15. Статьи, излагающие результаты исследований, выполненных в учреждениях, должны иметь соответствующее разрешение на опубликование в открытой печати.

16. При необходимости в конце основного текста указываются наименование фонда, оказавшего финансовую поддержку, или уровень и наименование программы, в рамках которой выполнена работа, на русском и английском языках.

AUTHOR GUIDELINES

1. Article materials should correspond to the journal profile and be clearly written.
 2. An article should be submitted in Russian or English and will be published in its original language.
 3. Articles received by the Editorial Board will be reviewed by 2 specialists. The main criteria of acceptance are theme actuality, information value, and scientific novelty.
 4. All materials should be submitted in two hard copies together with electronic file in the Word for Windows format (97/2000/2003). The paper should not exceed 14 pages of the typewritten text (Times New Roman, 12 points, 1.5-space).
 5. The article should contain UDC number, Title (printed in capitals), Authors' names (the corresponding author name should be marked with asterisk), full Address of organization(s) in which the author(s) work, Abstract (200–250 words), Keywords (not more than 5 words), Introduction, the Text of the paper with tables, diagrams and figures (if there are any), Conclusion with clearly stated inferences, List of References, List of Symbols and Abbreviations (if it is necessary). Title, Authors' names and affiliation(s), Abstract, Keywords should be presented both in English and Russian languages.
 6. The abstract should be informative (contain «squeeze» from all sections of the article – the introduction stating the purpose of the work, methods, main part and conclusion).
 7. Figures should be black-and-white, represented in graphical formats tif, attached with Excel or MS Graph and added with captions. All symbols in figures should be described.
 8. Tables should be placed directly in the article body. Diagrams and tables should not contain the same information. Each table should have the title. All tables, diagrams and figures should be referenced in the text.
 9. Symbols and abbreviations which are used in articles should be deciphered directly in the text and also (if necessary) taken out on a separate page.
 10. Dimensions of all quantities used in the article should correspond to International System of Units.
 11. Formulas should be typed in MathType.
 12. List of References is to be placed at the end of the article with full bibliographic information. Order of references should correspond to the order of their occurrence in the text. It is not recommended to refer to conference proceedings, papers from electronic journals without *DOI* number, textbooks, internet resources. References on unpublished works are prohibited. It is recommended to refer to not less than 10 references, self-citations – not more than 20 %/
 13. The following information about every co-author should be presented: family name, first name, patronymic (or second) name (if there are any), scientific degree and title, organization and position, full address with the postal code for correspondence, office or mobile phone numbers, fax, e-mail.
 14. Articles containing investigation results obtained in organizations should have a corresponding permission for publication.
 15. Names of Foundations or Programs financially granted the research may be acknowledged in the end of the text.
 16. Authors are responsible for submitting articles previously published or accepted by other publisher.
 17. Articles not meeting the requirements of the Editorial Board would not be accepted and may be returned to the authors. The date of receipt is considered to be the day when the Editorial Board receives the author's original paper.
 18. Authors conducting postgraduate (graduate studies, doctoral studies) have a priority in publishing their articles out of queue in the year of completion. Authors do not pay for publishing scientific articles. The Editorial Board can shorten and/or change the text if it does not strain the meaning of the article.
-

Индексы:
74835; 748352